

NEW INSIGHTS INTO THE REGULATION OF SERINE
PALMITOYLTRANSFERASE

By

Nivedita Sengupta

Thesis submitted to the Faculty of the
Molecular and Cell Biology Graduate Program
Uniformed Services University of the Health Sciences
In partial fulfillment of the requirements for the degree of
Doctor of Philosophy 2014.



UNIFORMED SERVICES UNIVERSITY, SCHOOL OF MEDICINE GRADUATE PROGRAMS
Graduate Education Office (A 1045) 4301 Jones Bridge Road, Bethesda MD 20814



APPROVAL OF THE DOCTORAL DISSERTATION IN THE
MOLECULAR AND CELL BIOLOGY GRADUATE PROGRAM

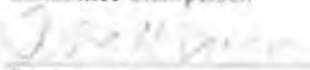
Title of Dissertation: "New Insights into the Regulation of Serine Palmitoyltransferase"

Name of Candidate: Nivedita Sengupta
Doctor of Philosophy Degree
February 7, 2014

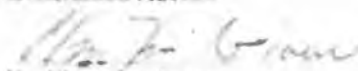
DISSERTATION AND ABSTRACT APPROVED:


Dr. Jeffrey Harmon
DEPARTMENT OF PHARMACOLOGY
Committee Chairperson

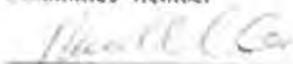
DATE
2/7/14


Dr. Teresa Dunn
DEPARTMENT OF BIOCHEMISTRY
Dissertation Advisor

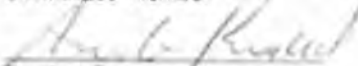
2/7/14


Dr. Chiao-Lin Guan
DEPARTMENT OF MICROBIOLOGY AND IMMUNOLOGY
Committee Member

2/7/14


Dr. Rachel Cox
DEPARTMENT OF BIOCHEMISTRY
Committee Member

2/7/14


Dr. Ann Rosenwald
DEPARTMENT OF BIOLOGY - Georgetown University
Committee Member

2/7/14



UNIFORMED SERVICES UNIVERSITY, SCHOOL OF MEDICINE GRADUATE PROGRAMS
Graduate Education Office (A 1045), 4301 Jones Bridge Road, Bethesda, MD 20814



FINAL EXAMINATION/PRIVATE DEFENSE FOR THE DEGREE OF DOCTOR OF PHILOSOPHY
IN THE MOLECULAR AND CELL BIOLOGY GRADUATE PROGRAM

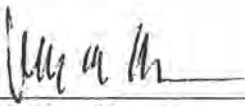

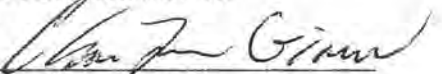
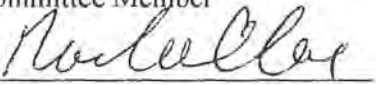
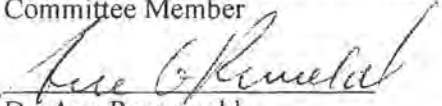
Name of Student: Nivedita Sengupta

Date of Examination: February 7, 2014

Time: 9:30 am

Place: B4046

DECISION OF EXAMINATION COMMITTEE MEMBERS:

	PASS	FAIL
 Dr. Jeffrey Harmon DEPARTMENT OF PHARMACOLOGY Committee Chairperson	<input checked="" type="checkbox"/>	<input type="checkbox"/>
 Dr. Teresa Dunn DEPARTMENT OF BIOCHEMISTRY Dissertation Advisor	<input checked="" type="checkbox"/>	<input type="checkbox"/>
 Dr. Chou-Zen Giam DEPARTMENT OF MICROBIOLOGY AND IMMUNOLOGY Committee Member	<input checked="" type="checkbox"/>	<input type="checkbox"/>
 Dr. Rachel Cox DEPARTMENT OF BIOCHEMISTRY Committee Member	<input checked="" type="checkbox"/>	<input type="checkbox"/>
 Dr. Ann Rosenwald DEPARTMENT OF BIOLOGY – Georgetown University Committee Member	<input checked="" type="checkbox"/>	<input type="checkbox"/>

ACKNOWLEDGMENTS

First and foremost, I would like to express my sincere thanks and gratitude to my mentor Dr. Teresa M Dunn, chair, Department of Biochemistry, who has guided me and provided me with all the resources needed to finish my doctoral dissertation in her laboratory. Her expert mentoring helped me in logical thinking and careful designing of experiments. This dissertation would not have been possible without her constant help and support. The great support and invaluable scientific advice from my dissertation committee chair Dr. Jeffery Harmon, chair, Department of Pharmacology, has helped me a lot in completing my research work for which I am very grateful to him. I would also like to thank my thesis committee members Dr. Rachel Cox, Dr. Chou-Zen Giam and Dr. Ann Rosenwald for their constructive criticism and thoughtful suggestions which enabled me to effectively design my experiments for better conclusions of my thesis project.

Dr. Saibal Dey was my mentor during the first two years of my graduate studies. He was immensely supportive at both a personal and professional level. His advice was very helpful in selecting the laboratories for rotation. I would also like to express my sincere thanks to Kenneth Gable without whom I would not have been able to complete my experiments. He helped me right from the first day from teaching me laboratory techniques, helping me to do chromatography, SPT assays and many other techniques and was always a person I could approach for help anytime. I would also like to thank my other laboratory colleagues, Dr. Gongshe Han, Dr. Sita Gupta and Saurav Majumdar for their help and support throughout the course of my work. I also very much appreciate the help I received from Dr. Niranjana Kumari Somashekarappa and Dagmar Bacikova from the Department of Pharmacology.

My thanks also go to Dr. Orna Cohen-Fix, National Institutes of Health, Bethesda, for her help in performing the next generation sequencing for my research project. The support from her laboratory helped in the timely completion of the experiments and data analysis. I am also grateful to Dr. Clifton Dalgard, Anatomy, Physiology and Genetics, USUHS, for his suggestions and help in analyzing the next generation sequencing data.

The USUHS graduate office has always been of tremendous help to me, from processing visa papers, providing course work materials and helping with other necessary paper work. I would especially like to thank our former graduate office secretary Ms. Janet Anastasi for her personal and professional support during the beginning of my graduate studies.

I would also like to acknowledge the biomedical instrumentation center (BIC) for their timely service with oligo synthesis and sequencing needs which was immensely helpful. I also thank the people in the office of Department of Biochemistry and especially Ms. Karen William for always taking care of our laboratory supply needs.

All this would not have been possible without the constant support and encouragement from my parents who have always loved me. I want to express my deep and heartiest respect to my parents for helping me to finish my PhD. I also thank my parent-in-laws for their constant support and encouragement. I would like to mention specifically my husband Manish Bhomia who has done everything possible for me so that I can pass this phase of my life successfully.

Last but not the least I would like to thank the Uniformed Services University of the Health Sciences for providing me with the graduate research fellowship to complete my thesis.

DEDICATION

I dedicate this dissertation work to my loving and caring parents, my father Bikas Kumar Sengupta and my mother Ranjana Sengupta. Their love and support was always there with me when needed, and because of which I was able to successfully finish my dissertation.

The author hereby certifies that the use of any copyrighted material in the thesis manuscript entitled:

“New Insights into the Regulation of Serine Palmitoyltransferase”

is appropriately acknowledged and, beyond brief excerpts, is with the permission of the copyright owner.

Nivedita Sengupta 4/4/2014

Nivedita Sengupta
MCB, Department of Biochemistry
Uniformed Services University
Date 04/04/2014

ABSTRACT

NEW INSIGHTS INTO THE REGULATION OF SERINE PALMITOYLTRANSFERASE

Nivedita Sengupta, PhD, 2014

Thesis directed by: Dr. Teresa M. Dunn, PhD, Chair, Department of Biochemistry.

Sphingolipid biosynthesis starts with condensation of an acyl-CoA chain with L-serine to form 3-ketosphingosine. This committed and rate limiting step is catalyzed by the enzyme serine palmitoyltransferase (SPT) which is present in all eukaryotes and even in some prokaryotes. The *S. cerevisiae* SPT is comprised of three ER-associated transmembrane proteins, Lcb1p, Lcb2p and Tsc3p. The Lcb1p and Lcb2p subunits interact directly with each other to form the catalytically active SPT heterodimer. However, the activity of the heterodimer is low, sufficient only to support growth of *S. cerevisiae* at low (e.g., 26 °C) but not at high (e.g., 37 °C) temperature where more sphingolipid is essential for survival. The activity of the heterodimer is enhanced several fold by the Tsc3p subunit, allowing growth at 37 °C. Tsc3p directly binds to the heterodimer and also alters its preference for the acyl-CoA substrate. The Orm proteins are negative regulators of SPT which also directly bind to SPT and down regulate its enzymatic activity. In this study, it has been shown that TMD1 of Lcb1p is essential for the binding of the Orms to SPT. It was also shown that the Orms have an inhibitory effect on the basal activity of the Lcb1p-Lcb2p heterodimer. The *orm1Δorm2Δtsc3Δ* mutant grows modestly at 37 °C but gives rise to suppressors which are not bypassing

sphingolipid biosynthesis and grow as well as wild type yeast at 37° C, suggesting the presence of other proteins that regulate sphingolipid biosynthesis. In an attempt to identify other regulatory components of SPT, suppressors of the *orm1Δorm2Δtsc3Δ* mutant were isolated and a recessive suppressor mutant (*Sup4*) that allowed growth similar to that of wild type yeast at 37 °C was characterized. Studies showed that the *tsc3ΔSup4* mutant exhibited increased myriocin resistance and enhanced *in vivo* SPT activity compared to the *tsc3Δ* mutant. Genetic analysis revealed that two unlinked recessive mutations (*Sup4^{m1}*, *Sup4^{m2}*) are responsible for the *Sup4* phenotype; the *Sup4^{m1}* mutation alone weakly suppresses the *tsc3Δ* mutant, while the *Sup4^{m2}* mutation alone has no effect. A comparison of the genomic sequences of *tsc3ΔSup4^{m1m2}* with *tsc3Δ* using next generation sequencing identified several candidate mutations and genetic linkage analysis revealed that *Sup4^{m2}* is a mutation in the ORF of the *CHA4* gene resulting in a truncated non-functional protein. Cha4p is a DNA binding transcriptional activator which regulates genes involved in serine metabolism. One of the transcriptional targets of Cha4p is *CHA1*, which encodes L-serine deaminase, a mitochondrial enzyme responsible for degradation of L-serine and failure to transcriptionally upregulate *CHA1* in the *cha4* mutant results in increased levels of intracellular L-serine, a substrate of SPT. Despite 700-fold coverage of the entire genome, the sequencing data analyses failed to identify the *Sup4^{m1}* mutation, suggesting that it might be an insertion or deletion. However, the *tsc3ΔSup4^{m1}* mutant and the *tsc3ΔLCBI-ΔTMD1* mutants have similar myriocin resistance and growth at 37 °C. Moreover, *CHA4* deletion enhanced the suppressor phenotypes of both the mutants. The *Sup4^{m1}* mutation does not play any role in serine uptake. Together these studies show

that the *Sup4^{m1}* mutation allows better serine utilization and its effect is similar to that of deleting TMD1 of Lcb1p. In the course of analyzing candidate mutations for their role in suppression, it was found that deletion of *VMA13* blocks the *Sup4^{m1m2}* mediated suppression of *tsc3Δ* at 37 °C. As *VMA13* encodes a small subunit of the vacuolar proton ATPase (V-ATPase), an electrogenic proton pump which directly and indirectly affects the vesicular transport, this result raises the possibility that appropriate intracellular transport of serine may be important for regulating SPT activity.

TABLE OF CONTENTS

LIST OF TABLES	xiv
LIST OF FIGURES	xv
LIST OF ABBREVIATIONS.....	xvii
CHAPTER 1: Introduction	1
Sphingolipids:	1
Importance of sphingolipids:	1
Physiological significance of sphingolipids:	3
Sphingolipidoses	3
Neuronal disorders	4
Genetic defects of sphingolipid biosynthesis.....	4
Cancer	5
Cardiovascular disorders.....	5
Obesity and diabetes	6
Infectious diseases	6
Sphingolipid metabolism:	6
Serine Palmitoyltransferase (SPT):.....	8
<i>Saccharomyces cerevisiae</i> SPT:	9
Human SPT:.....	10
Regulation of sphingolipid biosynthesis:.....	11
CHAPTER 2: TMD1 of Lcb1p is required for Orm protein mediated negative regulation of enzymatic activity of the SPT heterodimer.	13
Abstract	13
Background:	13
Materials and methods:	14
Strains:	14
Growth media:	14
Plasmids:.....	14
Primers:	15
Yeast transformation:.....	15
Yeast plasmid and genomic preparation:.....	15
Serial dilution cell spotting assay:	15
Microsome preparation:	16
Western blot:.....	16
Free long chain base extraction for analysis by HPLC:.....	17
Total long chain base extraction for analysis by HPLC:	17
Immunoprecipitation of TAP-tagged proteins:.....	18
Results:.....	19

The first transmembrane domain of Lcb1p is required for Orm binding and regulation.	19
The Orm proteins inhibit the basal catalytic activity of the Lcb1p-Lcb2p heterodimer.	24
Discussion:.....	29
CHAPTER 3: Identification and characterization of recessive suppressors involved in enhancement of sphingolipid biosynthesis in the absence of Tsc3p.....	32
Abstract:.....	32
Background:.....	32
Materials and Methods:.....	33
Strains:.....	33
Growth media:.....	33
Plasmids:.....	33
Glycosylation reporter cassette:.....	34
Primers:.....	34
Tetrad dissection and analysis of products of meiosis:.....	34
Yeast transformation:.....	34
Yeast plasmid and genomic preparation:.....	34
Genomic DNA isolation and library preparation for Next Generation Sequencing:.....	35
Serial dilution cell spotting assay:.....	35
Microsome preparation:.....	35
Western blot:.....	35
Total long chain base extraction for analysis by HPLC:.....	35
Free long chain base extraction for analysis by HPLC:.....	35
Free long chain base extraction for analysis by mass spectrometry:.....	36
Measurement of intracellular amino acids:.....	37
SPT assay:.....	37
Serine labelling of long chain bases:.....	38
Serine uptake assay:.....	39
Results:.....	40
Screening performed to isolate recessive suppressors of <i>orm1Δ orm2Δ tsc3Δ</i>	40
<i>Sup4</i> , the best recessive suppressor of the temperature sensitive phenotype of <i>tsc3Δ</i> , has two unlinked mutations and both are required for good suppression.....	42
The <i>tsc3ΔSup4^{m1m2}</i> mutant has elevated <i>in vivo</i> SPT activity.....	47
The <i>Sup4^{m1m2}</i> neither increases basal <i>in vitro</i> SPT activity nor does it abolish sphingolipid degradation.....	52
<i>Sup4^{m2}</i> has a mutation in the <i>CHA4</i> gene.	56
Deletion of the <i>CHA1</i> , a transcriptional target of <i>CHA4</i> , enhances suppression by <i>Sup4^{m1}</i> equivalently to <i>cha4Δ</i>	61
The <i>CHA4</i> deletion results in increased serine uptake.....	63
Deletion of <i>CHA4</i> influences the <i>Sup4^{m1}</i> mutation and the Lcb1p-ΔTMD1 equivalently but loss of the <i>ORMs</i> is not similar to the <i>Sup^{m1}</i> mutation.....	68
Vma13p is needed for the <i>Sup4^{m1m2}</i> mediated regulation of sphingolipid biosynthesis.	72
Discussion:.....	77

CHAPTER 4: Topological characterization of the small subunits of human SPT,	92
Abstract:	92
Background:	92
Materials and methods:	93
Strains:	93
Growth media:	94
Plasmids:	94
Primers:	96
Yeast transformation:	96
Yeast plasmid and genomic preparation:	96
Site-directed mutagenesis:	96
Microsome preparation:	96
Western blot:	96
Split-ubiquitin yeast two-hybrid assay:	96
Right-side-out vesicle preparation:	97
Protease protection assay:	98
Results:	98
The ssSPTs have single TMD with the N-termini in the cytosol and the C-termini in the ER lumen.....	98
Candidate ssSPT interacting proteins were identified using the split-ubiquitin yeast two-hybrid system.....	101
Discussion:	105
REFERENCES	109

LIST OF TABLES

Table 1. List of strains used in chapter 2.	31
Table 2. List of strains used in chapter 3.	83
Table 3. List of primers used in chapter 3.	85
Table 4. List of candidate mutations identified in the <i>tsc3ΔSup4^{m1m2}</i> and not in the <i>tsc3Δade2-101</i> by next generation sequencing and linkage analysis with <i>Sup4^{m1}</i> and <i>Sup4^{m2}</i>	87
Table 5. Table showing list of genes not linked to <i>Sup4^{m1}</i> and <i>Sup4^{m2}</i>	89
Table 6. List of precursors/products ion mass/charge (m/z) ratio's, associated collision energy, and dwell time used for MRM detection of individual molecular species of free LCBs and LCB-Ps.	90
Table 7. List of candidates found in split-ubiquitin based two-hybrid screen using LexA- Cub-ssSPTa as bait.	103
Table 8. Interaction of the 10 candidate proteins with either LCB1, LCB2a, LCB2b, ssSPTa, ssSPTb, or Elo3 as determined by split-ubiquitin yeast two-hybrid assay.	104
Table 9. List of strains used in chapter 4.	107
Table 10. List of primers used in chapter 4.	108

LIST OF FIGURES

Figure 1-1. The Sphingolipid biosynthesis and salvage pathway in <i>Saccharomyces cerevisiae</i> .	7
Figure 1-2. Topology of <i>S. cerevisiae</i> SPT subunits (Lcb1p, Lcb2p, and Tsc3p).	9
Figure 2-1. A. Cartoon depicting the proposed model of interaction between Lcb1p and Ormp. B. Deletion of TMD1 from Lcb1p results in phenotypes similar to those of the <i>orm1Δorm2Δ</i> mutant.	21
Figure 2-1C. Deletion of TMD1 of Lcb1p results in high levels of long chain bases (LCBs).	22
Figure 2-1D. TMD1 of Lcb1p is required for the Orm-SPT interaction.	23
Figure 2-2A. Orms interact with the SPT heterodimer in the absence of Tsc3p.	26
Figure 2-2B. Deletion of Orm or the TMD1 of Lcb1p enabled the <i>tsc3Δ</i> mutant to grow at 37°C.	27
Figure 2-2C. The Orm proteins regulate the Lcb1p-Lcb2p heterodimer.	28
Figure 3-1. Screen to identify recessive suppressors of <i>orm1Δ orm2Δ tsc3Δ</i> .	41
Figure 3-2. <i>Sup4</i> , the best recessive suppressor of the temperature sensitive phenotype of the <i>tsc3Δ</i> , has two unlinked mutations and both are required for good suppression.	44
Figure 3-3. Tetrad analysis performed to confirm <i>Sup4</i> as two gene (<i>Sup4^{m1}</i> , <i>Sup4^{m2}</i>) mutation.	45
Figure 3-4. <i>Sup4^{m1}</i> and <i>Sup4^{m2}</i> are two unlinked recessive mutations.	46
Figure 3-5. The <i>Sup4^{m1m2}</i> is not a bypass suppressor.	49
Figure 3-6. The <i>tsc3ΔSup4^{m1m2}</i> mutant is resistant to myriocin.	50
Figure 3-7. The <i>tsc3ΔSup4^{m1m2}</i> has elevated <i>in vivo</i> LCB synthesis.	51
Figure 3-8. <i>Sup4^{m1m2}</i> does not increase <i>in vitro</i> SPT activity.	54
Figure 3-9. <i>Sup4^{m1}</i> is not a mutation in the <i>DPL1</i> or <i>LCB4</i> gene.	55
Figure 3-10. Loss of <i>ADE2</i> function does not have any effect on the <i>tsc3ΔSup4^{m1m2}</i> phenotype.	58
Figure 3-11. <i>Sup4^{m2}</i> is a mutation in the <i>CHA4</i> .	59
Figure 3-12. Deletion of the <i>CHA1</i> , a transcriptional target of Cha4p, enhances suppression by <i>Sup4^{m1}</i> equivalently to <i>cha4Δ</i> .	62
Figure 3-13. In the absence of the <i>Sup4^{m1}</i> mutation, addition of serine rescues the growth of <i>cha4Δtsc3Δ</i> on SD at 37 °C.	65
Figure 3-14. <i>CHA4</i> deletion results in increased serine uptake and high intracellular serine levels.	66
Figure 3-15. In the absence of the <i>Sup4^{m1}</i> mutation, deletion of <i>CHA1</i> also rescued the temperature sensitivity of <i>tsc3Δ</i> at 37 °C on minimal media at serine concentrations similar to <i>cha4Δtsc3Δ</i> .	67
Figure 3-16. Deletion of <i>CHA4</i> influences the <i>Sup4^{m1}</i> mutation and the Lcb1p-ΔTMD1 equivalently but the <i>Sup4^{m1}</i> mutation does not behave like an <i>orm1Δorm2Δ</i> mutant.	70
Figure 3-17. The <i>tsc3ΔSup4^{m1m2}vma13Δ</i> mutant failed to grow at 37 °C and the phenotype was reversed by wild type Vma13p.	74
Figure 3-18. Deletion of the <i>VMA13</i> does not interfere with serine uptake of <i>tsc3ΔSup4^{m1m2}</i> .	75

Figure 4. The ssSPTs have a single TMD and are oriented with their N-termini in the cytosol.....	100
--	-----

LIST OF ABBREVIATIONS

3KDS – 3-ketodihydrosphinganine

Cer –Ceramide

Cer1P – Ceramide – 1 – phosphate

dH₂O – Deionized water

DHS – Dihydrosphinganine

ER – Endoplasmic reticulum

GlcCer – Glucosyl ceramide

HDL - High density lipoprotein

HPLC – High performance liquid chromatography

hr – Hour

HSN1 - Hereditary sensory neuropathy I

IPC - Inositol phosphorylceramide

KAN – Kanamycin

LacCer – Lactosyl ceramide

LCB – Long chain base

LCB-P - Long chain base phosphates

M – Molar

M(IP)₂C - Mannosyldiinositol phosphorylceramide

Min – Minute

MIPC - Mannosylinositol phosphorylceramide

NATR – Nourseothricin

OD – Optical density

ORF – Open reading frame
PHS – Phytosphingosine
P.O.M – Products of meiosis
SIP - Sphingosine-1-phosphate
SC – Sodium citrate
SD – Synthetic dextrose
SPH – Sphingosine
SPT – Serine palmitoyltransferase
Sup17 – Suppressor 17
Sup4 – Suppressor 4
SUR2 - Sphinganine C4-hydroxylase
TEA – Triethylamine
V – Volts
V-ATPase - Vacuolar proton ATPase
YPD – Yeast extract peptone dextrose

CHAPTER 1: Introduction

SPHINGOLIPIDS:

Sphingolipids are a diverse class of lipids. The simplest sphingolipids are the long chain bases which are amino alcohols with a hydrocarbon chain. The long chain bases are acylated at the amino group to generate ceramides which are further modified by attachment of different head groups at the C1-OH to generate complex sphingolipids. In humans, complex sphingolipids are very diverse because of the wide array of different head groups. For example, sphingomyelin has a phosphorylcholine head group, the cerebrosides have either glucose or galactose, and the gangliosides have oligosaccharide chains consisting of many sugars along with one or more sialic acids. In contrast, *Saccharomyces cerevisiae* has only three complex sphingolipids, inositolphosphorylceramide (IPC) containing an inositolphosphate head group added to ceramide, mannosylinositolphosphorylceramide (MIPC) with a mannose added to IPC, and mannosyldiinositolphosphorylceramide $M(IP)_2C$ with a second inositolphosphate added to MIPC (54).

IMPORTANCE OF SPHINGOLIPIDS:

Sphingolipids mediate diverse cellular functions which can be broadly classified into two categories. First, sphingolipids have important structural roles based on their molecular shapes and chemical properties. They are important components of membranes, predominantly found in the plasma membrane in contrast to the intracellular membranes which have less sphingolipids (87). The chemical properties of the sphingolipids modulate the physical properties of membrane bilayers such as insulation and barrier functions of myelin (71) and skin (42). Sphingolipids also affect vesicular

transport by influencing membrane curvature. Along with phospholipids and cholesterol, sphingolipids form distinct microdomains (lipid rafts) which are sites of protein aggregation and interaction (56). For example, gangliosides on axons interact with the myelin associated glycoprotein (MAG) present on the innermost myelin sheath, resulting in optimal axon-myelin cell-cell interactions which provide axon stability and help in regeneration (77). Also, glycosphingolipids, along with cholesterol and sphingomyelin, influence membrane structure resulting in modification of the activity of several glycosylphosphatidylinositol anchored proteins and receptors such as the insulin receptor and epidermal growth factor receptor (22).

The second major function of sphingolipids and their metabolites is as signaling molecules to regulate the activity of various proteins including enzymes and receptors. For instance, sphingolipid metabolites such as sphingosine-1-phosphate (S1P) and ceramide are involved in signal transduction pathways where they act as second messengers for regulating cell cycle progression, apoptosis and other cellular functions. Studies have shown that S1P derived from sphingosine binds to G-protein-coupled receptors and mediates signaling, inhibiting apoptosis and activating mitosis resulting in cell growth (24) (74). Ceramides, on the other hand, promote cell differentiation and apoptosis (4). Ceramides also regulates calcium ion homeostasis (51) and perturbation in ceramide level disrupts calcium ion homeostasis resulting in improper nutrient delivery within the cell (51). Lysosphingolipids and S1P as components of high density lipoprotein (HDL) (76) release nitric oxide and inhibit production of reactive oxygen species and monocyte accumulation within the blood vessels thus mediating protection against atherosclerosis and coronary heart disease (70). S1P also plays a role in cardiac

development, migration of osteoclasts, and in formation and function of vasculature (45). Moreover, LCB and its derivatives are involved in mediating heat shock response (19).

PHYSIOLOGICAL SIGNIFICANCE OF SPHINGOLIPIDS:

Diseases resulting from improper sphingolipid metabolism highlight both the critical roles that sphingolipids play in normal cellular function and the importance of properly regulating their synthesis and turnover.

Sphingolipidoses

The sphingolipidoses, a group of inherited diseases resulting from improper sphingolipid degradation, are relatively common, occurring 1 in 5000/7000 live births (84). With the exception of the X-linked Fabry disease, most of these diseases are autosomal recessive disorders and the affected enzymes normally reside in the lysosome where degradation of sphingolipids occurs. Patients suffering from sphingolipidoses display varied phenotypic defects because of accumulation of different species of sphingolipid intermediates in different cell types (91, 92). For example, in Krabbe's disease, the myelin forming cells are primarily affected because of inappropriate processing of the galactosylceramide. Gaucher disease is characterized by anemia and enlargement of liver and spleen due to the lack of a mannose receptor which is needed for transport of the enzyme glucocerebrosidase to the lysosome for degradation of intracellular lipids (6). In all the sphingolipidoses, high levels of intracellular sphingolipids causes inflammation, oxidative stress, ER stress, and disturbed autophagy (40).

Neuronal disorders

In neurons complex gangliosides are the predominant sphingolipids and defects in ganglioside degradation result in damage to the central nervous system (86). In many neurodegenerative diseases including Alzheimer's, Parkinson's and Huntington's, aberrant lysosomal degradation of sphingolipids is observed (64). Sphingolipids also play a role in development of multiple sclerosis (93). It has also been observed that drug use, over time, results in improper sphingolipid accumulation causing neuronal disorder (3). Cationic amphiphilic drugs, because of their chemical properties get trapped in lysosomes resulting in elevation of the pH and mislocalization of the enzymes needed for sphingolipid degradation (17). For example, treatment of humans with tricyclic antidepressants over a long period results in sphingomyelin accumulation (44) (50).

Genetic defects of sphingolipid biosynthesis

Genetic disorders resulting from defective sphingolipid biosynthesis are rare, but mutations in either the LCB1 or LCB2 subunit of SPT are responsible for the most common inherited autosomal dominant peripheral neuropathy, hereditary sensory neuropathy I (HSAN1). (16). The mutant enzyme has an altered substrate preference and uses L-alanine as substrate resulting in accumulation of non-degradable products, deoxysphingolipids, which are toxic to cells (69). The mutations also result in increased levels of ceramides which cause neuronal apoptosis (16). Besides HSAN1, other rare genetic disorders occur because of mutations in lactosylceramide α -2,3-sialyltransferase, which causes an autosomal recessive epilepsy syndrome (82) and mutations in fatty acid 2-hydroxylase cause leukodystrophy, spasticity, dystonia, (21) and neuro degeneration (52).

Cancer

Sphingolipid levels are dysregulated in many cancers and there is evidence that the balance between SIP and ceramides is a determining factor in the development of various cancers (57). SIP is considered a tumor promoting factor because of its mitogenic effects whereas ceramide is regarded as tumor suppressing because of its pro-apoptotic effects. For example, ceramides influence the apoptosis of cancer cells in response to radiation and chemotherapy (63). In human prostate cancer, increased expression of acid ceramidase is observed which reduces ceramide and elevates sphingosine levels (78). Moreover, studies indicate that the intake of dietary sphingomyelin inhibits colon carcinoma (20).

Cardiovascular disorders

Sphingomyelinase activity positively correlates with endothelial dysfunction and development of atherosclerosis. Sphingomyelinase activity in cardiovascular cells results in release of ceramides which signals contraction of cardiac myocytes (68). It has been reported that inhibition of sphingomyelinase prevents cardiovascular diseases like atherosclerosis and thrombosis by reducing the production of ceramides (66). Ceramide is also implicated in dilated lipotoxic cardiomyopathy. In a mouse model of this disease, reduction of the ceramide content specifically in the heart by heterozygous deletion of the LCB1 subunit of the SPT enzyme resulted in improved cardiac function (66). The antiproliferative effects of ceramide have been used to develop stents coated with a ceramide analog to reduce stenosis (65).

Obesity and diabetes

Ceramides are implicated in obesity and diabetes. Saturated fatty acids are one of the major causes of obesity and diabetes (12) (9). Excess dietary palmitate enhances SPT activity resulting in production of more sphingolipids containing saturated fatty acids. This results in apoptosis of the pancreatic β -cells causing insulin resistance, leading to diabetes. This effect can be reversed by inhibiting SPT by myriocin which causes improved insulin sensitivity (80). Other than SPT, ceramide synthase and glucoceramide synthase are also implicated in insulin resistance and type 2-diabetes (41) (1).

Infectious diseases

Sphingolipids play a major role in transmission of infectious diseases. Glycosphingolipids act as receptors for many bacterial toxins, viruses and fungi and mediate entry of pathogens into cells. For example sialic acids are the components of binding sites for influenza virus entry into the host cells (88). Studies have shown that ceramides generated from degradation of sphingomyelin impacts bacterial infection; for example, *Neisseria gonorrhoeae* need cellular sphingomyelinase activity for infection (38). Further it has been shown that increased dihydrosphingomyelin levels prevent HIV-1 infection by rigidifying membranes (90). Some of the post infectious autoimmune diseases are known to be caused by cross reactive sphingolipid species. In Guillain-Barre-syndrome, antibodies directed against lipooligosaccharide of *C. jejuni* also bind with the host gangliosides resulting in degradation and pathogenesis (47).

SPHINGOLIPID METABOLISM:

Sphingolipids are synthesized either by *de novo* biosynthesis or by recycling of the intermediates formed within the salvage pathway. *De novo* sphingolipid synthesis is

initiated on the cytoplasmic side of the endoplasmic reticulum (ER) by the eukaryotic sphingolipid biosynthetic enzymes which are integral membrane proteins (19). In both *Saccharomyces cerevisiae* and humans, the first step of sphingolipid synthesis is the condensation of an acyl-CoA chain (usually palmitoyl-CoA) with serine to form 3-ketosphinganine (3-KDS). This committed and rate limiting step is catalyzed by serine

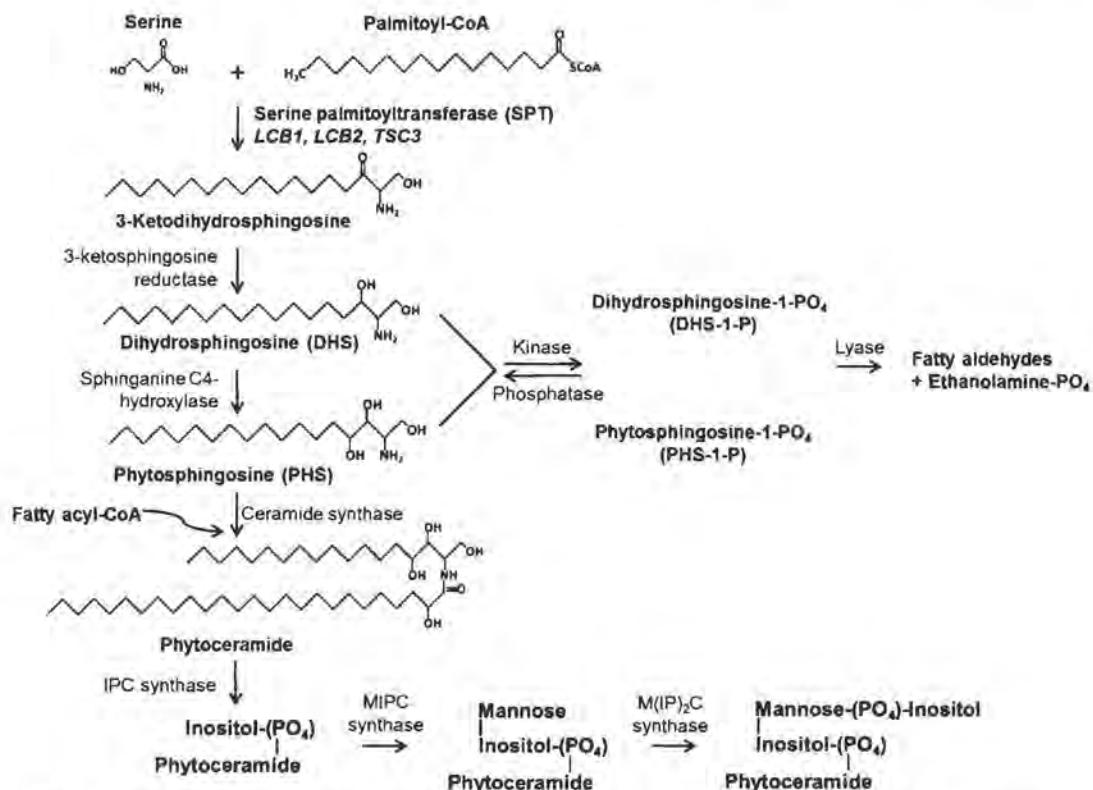


Figure 1-1. The Sphingolipid biosynthesis and salvage pathway in *Saccharomyces cerevisiae*.

(14)

palmitoyltransferase (SPT) which is present in all eukaryotes and even in some prokaryotes. 3-KDS is rapidly reduced to dihydrosphingosine (DHS) which is hydroxylated at C4 to form phytosphingosine (PHS) in yeast. Phytoceramide is formed by N-linked acylation of PHS or by hydroxylation of dihydroceramide and attachment of inositol phosphate generates inositolphosphorylceramide (IPC) which is further modified

by mannosylation to form mannosylphosphorylceramide (MIPC) and a second inositol phosphorylation generates mannosyldiinositolphosphorylceramide (MIP₂C). In mammals, DHS is first acylated to form dihydroceramide which is desaturated at C4 to form ceramide (36). The ceramides are then transported to the Golgi either by vesicular transport or by the ceramide transport protein (CERT). CERT transports ceramide from the ER to Golgi (35) and, the four phosphate adaptor protein 2 (FAPP2) mediates transport of glucosylceramide within the Golgi (15). Within the Golgi ceramides undergo addition of different head groups, which are simpler in the case of *S. cerevisiae* but highly diverse and complex in the case of mammals (18). In certain cell types, like neurons, sphingolipids are also obtained from the salvage pathway by recycling of the long chain base phosphates (LCB-P) (72). The LCB-P, synthesized by phosphorylation of LCB by a LCB kinase, can either be recycled by the LCB-P-phosphatase or degraded by a LCB-P-lyase that cleaves the C2-C3 bond to form an aldehyde and ethanolamine phosphate.

SERINE PALMITOYLTRANSFERASE (SPT):

As the rate limiting enzyme of sphingolipid biosynthesis, regulation of SPT activity is important for maintaining cellular sphingolipid homeostasis. SPT is highly conserved and found in all eukaryotic organisms. It is a multi-subunit enzyme and a member of the subfamily of pyridoxal-5'-phosphate-dependent enzymes known as the α -oxoamine synthases. All members of this family of enzymes catalyze the decarboxylative condensation of the α -carbon of an amino acid with an acyl-CoA (2). Bacterial SPT is a soluble homodimer (94), but the eukaryotic SPTs are multimeric membrane-associated proteins.

***Saccharomyces cerevisiae* SPT:**

Yeast SPT is composed of three different ER membrane spanning subunits, Lcb1p, Lcb2p and Tsc3p (8). Lcb1p subunit has three trans-membrane domains (TMDs) with its N-terminus in the ER lumen and C - terminus in the cytosol (30). Unpublished

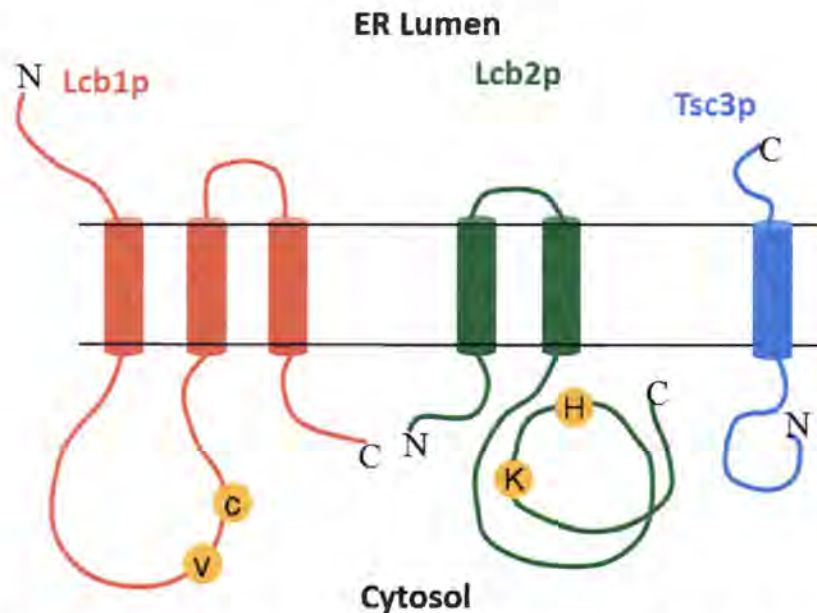


Figure 1-2. Topology of *S. cerevisiae* SPT subunits (Lcb1p, Lcb2p, and Tsc3p).

studies from our laboratory indicate that Lcb2p has two TMDs with both the N and C-termini in the cytosol. The Lcb1p interacts directly with the Lcb2p to form the basal catalytically active heterodimer. Residues involved in catalysis are present on both the Lcb1p and Lcb2p subunits, and modeling studies using the bacterial SPT indicate that the active site is at the heterodimeric interface (60) (33). The third subunit, Tsc3p, is a small protein that is unstable in the absence of Lcb2p. Deletion of either *LCB1* or *LCB2* abolishes SPT activity completely whereas deletion of *TSC3* decreases enzymatic activity 20-100 fold (26).

Human SPT:

Human SPT also has three subunits similar to yeast SPT. There is a single gene encoding LCB1, the human homolog of yeast Lcb1p (34) whereas there are two genes encoding two different LCB2 isoforms, LCB2a and LCB2b, which are homologs of yeast Lcb2p. LCB1 and LCB2b are stably expressed in absence of other partners whereas LCB2a is unstable in the absence of LCB1. The two human LCB2 isoforms interact directly with LCB1 forming catalytically active human SPT heterodimers. There are two functional orthologs of Tsc3p in mammals, ssSPTa and ssSPTb, which were identified by functional screening of a human cDNA library. Similar to Tsc3p, these small proteins do not have any intrinsic catalytic activity but interact directly with the LCB1-LCB2a/b heterodimers and increase their activity several fold (31). The ssSPTa and ssSPTb have a highly conserved central core and more divergent N- and C-terminal domains. The ssSPTs confer distinct acyl-CoA selectivity, with ssSPTa showing a preference for palmitoyl (C16)-CoA and ssSPTb for stearoyl (C18)-CoA. It was shown that this difference is conferred by a single amino acid residue that resides just N-terminal to the conserved central domain (37). In fact, with the two isoforms of LCB2 and of the ssSPTs, it is now clear that there are four different human SPT isozymes, and each has been found to have distinct acyl-CoA substrate specificity. ssSPTa and ssSPTb are stable and localize to the ER in the absence of LCB1 or LCB2a/b. Given that they influence both SPT activity and acyl-CoA substrate preference, the small proteins are attractive candidates for regulating sphingolipid biosynthesis.

REGULATION OF SPHINGOLIPID BIOSYNTHESIS:

Given the important functions of sphingolipids, it is expected that their metabolism is tightly controlled and that the regulation will be mediated by multiple pathways. Regulation of sphingolipid metabolism occurs both during biosynthesis and also during export and uptake (48). Recent studies have imparted considerable understanding of the regulation of biosynthesis. Sphingolipid biosynthesis is regulated in response to heat-induced changes in substrate availability (13). It has been shown that an increase in endogenous fatty acid synthesis as well as stimulation in serine uptake occurs in response to heat. *De novo* sphingolipid synthesis is also feedback regulated by intermediates and the end products of the biosynthetic pathway. The most compelling evidence for feedback regulation of sphingolipid is seen in the CERT-mediated ceramide transfer (35). As mentioned above, CERT is a soluble transporter protein which mediates transfer of ceramide from the ER to the Golgi. It has been found that when ceramides are abundant, CERT is phosphorylated, resulting in inhibition of ceramide transport (53). The phosphorylation-induced inhibition of CERT is reversed when sphingolipid biosynthesis is reduced, for example, upon treatment with myriocin; CERT is dephosphorylated, resulting in increased transport. As myriocin blocks SPT, the source of ceramide for increased transport is still not clear. Another new insight in feedback regulation comes from the Orm protein-mediated regulation of sphingolipid synthesis. The Orms are ER-localized proteins which interact directly with the subunits of SPT. Deletion of the *ORM* genes results in increased production of LCB and sphingolipids implicating the Orm proteins as negative regulators of sphingolipid synthesis (7). The yeast protein kinases, Ypk1p and Ypk2p, themselves regulated by TORC2, phosphorylate the Orm proteins at

the N-terminus and relieve inhibition of SPT in response to intracellular sphingolipid levels; for example, treatment with myriocin, an inhibitor of SPT results in increased phosphorylation of the Orms (73). In addition, it has also been reported that phosphorylated Orm proteins stimulate complex sphingolipid synthesis. In addition to Ypk1/2, Npr1 kinase (also regulated by TORC1) also mediates positive phosphorylation of the Orm proteins, but these phosphorylations apparently stimulate complex sphingolipid synthesis downstream of SPT (81). These findings have contributed enormously to the understanding of the molecular regulation of sphingolipid biosynthesis in response to cellular need. However, a lot remains to be elucidated for a complete understanding of the regulatory mechanisms. For example, the exact mechanism of Orm mediated regulation and the specific binding sites required for Orm and SPT interaction are unclear. Moreover, it is as yet undetermined whether the SPT heterodimer is under the influence of Orm mediated regulation, or whether the Orms act by antagonizing activation by the small subunits.

CHAPTER 2: TMD1 of Lcb1p is required for Orm protein mediated negative regulation of enzymatic activity of the SPT heterodimer.

ABSTRACT

The Orm proteins directly interact with the SPT and negatively regulate its activity. However, the site of Orm-SPT interaction is unknown. By genetic and biochemical studies it has been shown that the first transmembrane domain (TMD1) of Lcb1p is required for the interaction of the Orm proteins with the SPT for regulation. Moreover, it was observed that deletion of either the *ORMs* or TMD1 of Lcb1p results in increased *in vivo* SPT activity, which enables the *tsc3Δ* mutant to grow at 37 °C suggesting that the Orm proteins act directly on the heterodimer and do not simply antagonize Tsc3p-mediated activation of the heterodimer.

BACKGROUND:

The Orm gene family encodes ER-localized transmembrane proteins which negatively regulate SPT activity. An *orm1Δorm2Δ* mutant is characterized by its extremely high levels of *in vivo* LCBs and sphingolipids providing evidence in support of Orms as negative regulators of SPT activity (7). In *S. cerevisiae*, there are two Orm homologs, Orm1p and Orm2p which interact directly with SPT subunits to form the SPOTS complex (7). The N-termini of the Orm proteins have serine and threonine residues which are phosphorylated by the YPK kinases (73). Upon phosphorylation, the Orms have reduced ability to inhibit SPT activity resulting in increased LCBs and sphingolipid synthesis. The Lcb1p-Lcb2p heterodimer has low basal activity that is stimulated by Tsc3p, raising the possibility that the Orms may regulate SPT by antagonizing the interaction of Tsc3p with the Lcb1p-Lcb2p heterodimer. Lcb1p, Lcb2p,

and Tsc3p co-purify with the Orm proteins showing that the mechanism of Orm protein-mediated regulation is not by displacing Tsc3p from the SPT complex. However, it does not rule out the possibility that the Orm proteins can still prevent or reduce the ability of Tsc3p to activate the heterodimer. Previous studies from our laboratory have shown that TMD1 (amino acid residues 50-85) of Lcb1p is not essential for catalytic activity of the SPT heterodimer or for its activation by Tsc3p (30). Moreover the Lcb1- Δ TMD1p subunit is properly localized to and oriented in the ER membrane along with the Lcb2p and the Tsc3p subunit. Also Han et al. have shown that the Orm proteins can bind to Lcb1p in absence of Lcb2p (32). Finally, some organisms have a single fusion SPT in which the LCB1 domain is joined to the C terminus of the LCB2 domain and these single chain SPTs lack a counterpart of Lcb1-TMD1 (29). Interestingly, these organisms also lack ORM homologs. Taken together these observations suggest that TMD1 of Lcb1p may be important for regulation of SPT activity by the Orms.

MATERIALS AND METHODS:

Strains:

All strains are in the BY4741 background and are listed in Table 1.

Growth media:

The media used in this study were YPD or SD supplemented with the indicated concentrations of tunicamycin. Media was prepared by following standard protocols (79).

Plasmids:

LCB1- Δ TMD1-pGH315 – The yeast *LCB1* gene with its own promoter and terminator sequence was cloned into the pRS315 plasmid to generate pGH315. The

TMD1 (amino acid residues 50-85) of *LCB1* was deleted in pGH315 vector by introducing *NheI* sites after codon 49 and before 86 by site directed mutagenesis followed by restriction digestion and religation (31).

Primers:

Primers used in this study:

2TSC3 – 5'-GGGCCCCTCGAGGGCAAGTAGTGCATCCAG-3'

1TSC3 – 5'-GGGCCCCGATCCTTTATGTATTGTGTGTA- 3'

L1XF 5'-GAATTCCTCGAGATAGGGGCATATTGCTGCGGT-3'

L1XR 5'-GGCCGGATCCTCGAGCGCATTCTCTGGGCGCCGTG-3'

Yeast transformation:

All yeast transformations were done using the standard yeast transformation protocol (79).

Yeast plasmid and genomic preparation:

Yeast plasmid and genomic DNA were isolated using the Zymoprep I TM Kit (Zymo Research, Inc) according to the manufacturer's instructions.

Serial dilution cell spotting assay:

S. cerevisiae cells growing in logarithmic phase were suspended in dH₂O at an OD₆₀₀ of 0.5 in a 96 well microtiter plate, and 10 fold serially diluted six times. The serially diluted cell suspensions were spotted onto the desired agar plates and incubated at the appropriate temperatures.

Microsome preparation:

S. cerevisiae strains were grown overnight in liquid YPD media to an OD₆₀₀ of approximately 1. Cells were pelleted by centrifugation for 5 min, washed once with dH₂O and once with TEGM buffer (50 mM Tris-HCl pH 7.5, 1 mM EGTA, and 1 mM β -mercaptoethanol). The pellets were suspended in TEGM buffer containing 1 mM PMSF, 2 mg/ml pepstatin A, 1 mg/ml leupeptin, and 1 mg/ml aprotinin. Glass beads were added to the meniscus and the cells were disrupted by vortexing (4 times for 1 min and 2 times for 30 sec) with 1 min cooling on ice in between each cycle of vortexing. The cell lysates were transferred to eppendorf tubes, and centrifuged at 8000 x g for 10 min at 4 °C to remove beads, unbroken cells and debris. The supernatant was transferred to an ultracentrifuge tube and centrifuged at 100,000 x g for 30 min at 4 °C. The pellet was homogenized, suspended in TEGM buffer and a second centrifugation at 100,000 x g at 4 °C for 30 min was performed. The final pellet was suspended in TEGM buffer containing 30% glycerol and flash frozen in liquid nitrogen before storing in – 80 °C (25).

Western blot:

Microsomal proteins were mixed with SDS sample buffer (Life Technologies, Inc) and reducing agent (Life Technologies, Inc) according to the manufacturer's protocol and heated at 70 °C for 10 min. Proteins were resolved on a 4-12% Bis-Tris gel (Life Technologies, Inc) using 1X MOPS running buffer (Life Technologies, Inc) at 190V and transferred to nitrocellulose membrane at 75V for 90 min. The blots were blocked in TTBS (0.1 M Tris pH 7.5, 0.15 M NaCl, 0.1% Tween 20) containing 5% dry milk for 2 hrs followed by incubation with appropriate antibodies diluted in TTBS containing 2% dry milk for 1 hr. Finally, the blots were washed 3 times with TTBS and

the bound antibodies were detected using the enhanced chemiluminescence detection system (Perkin Elmer).

Free long chain base extraction for analysis by HPLC:

S. cerevisiae strains were grown overnight to an OD₆₀₀ of 0.5-1. 30 OD₆₀₀ units of cells were harvested, washed with dH₂O and suspended in 0.1 ml of 2 M NH₄OH followed by 2 ml of chloroform:methanol (1:2) containing 0.5 µM C17-SPH (internal control). Glass beads were added to the meniscus and vortexed 4 times for 1 min and 2 times for 30 sec for cell lysis. Cell lysates were pelleted and the supernatant was collected avoiding glass beads and cellular debris. 1.5 ml of chloroform was added to the supernatant and mixed followed by addition of 3 ml of 0.5 M NH₄OH. The solution was mixed, centrifuged for 5 min and the top layer was discarded. The remaining solution was washed 3 times with 3 ml dH₂O containing 0.06 M KCl and the upper phase was discarded. The samples were dried under N₂ and 80 µl of methanol:190 mM TEA (20:3) and 20 µl AccQ•Fluor™ reagent (6-aminoquinolyl-N-hydroxysuccinimidyl carbamate, or AQC) were added and incubated for 60 min at 25 °C. 0.01 ml of 1 M KOH was added to the samples and incubated at 37 °C for 30 min. The samples were neutralized by addition of 0.01 ml of 1 M acetic acid in methanol and analyzed by HPLC (25).

Total long chain base extraction for analysis by HPLC:

10 OD₆₀₀ equivalents of logarithmically growing yeast cells were harvested in screw cap tubes. The cells were washed once with dH₂O and dried under N₂. 1 ml of 1 M HCl-methanol containing the 0.5 µM C17-sphingosine (internal standard) was added to the dried cells boiled for 30 min and cooled on ice. 1 ml of 1% NaCl was added, followed by addition of 2 ml of hexane:ether (1:1). The solution was vortexed and centrifuged for

~1 min. The top layer was aspirated; 0.25 ml of 10 N NaOH was added, and mixed. Finally, 1.75 ml of hexane was added and the solution was centrifuged briefly for ~1 min. The top layer was transferred to an HPLC vial and dried under N₂. 80 µl of methanol:190 mM triethylamine (TEA) (20:3) and 20 µl AccQ•Fluor™ reagent (6-aminoquinolyl-N-hydroxysuccinimidyl carbamate, or AQC) was added and the samples were analyzed by HPLC (25).

Immunoprecipitation of TAP-tagged proteins:

Microsomal proteins (~1mg) were resuspended in 1 ml immunoprecipitation buffer (50 mM HEPES-KOH, pH 6.8, 150 mM potassium acetate, 2 mM magnesium acetate, 1 mM CaCl₂, 15% glycerol) with 0.1% digitonin (Gold Biotechnology, Inc.) and supplemented with protease and phosphatase inhibitors (Research Products International Corporation). Membrane proteins were solubilized by nutating lysates at 25 °C for 1 hr. Unsolubilized material was removed by centrifugation at 100,000 x g, for 35 min at 25 °C and the soluble fraction was incubated with IgG coated sepharose beads (25 ml bed volume) for 2.5 hrs at 4 °C. The beads were pelleted by spinning for 30 sec at 8200 x g, then washed four times with 1 ml immunoprecipitation buffer containing 0.1% digitonin and were suspended in LDS-sample buffer and reducing agent (Life Technologies, Inc).

RESULTS:

The first transmembrane domain of Lcb1p is required for Orm binding and regulation.

Studies from our laboratory have shown that the expression of Tsc3p is dependent on the presence of Lcb2p (30) and Han et al. have shown that the Orm proteins can interact with the Lcb1p in the absence of Lcb2p (32). These data together suggested that the primary interaction sites between the Orms and the SPT complex are present in the Lcb1p. A series of deletion experiments performed with Lcb1p to determine its catalytically active region indicated that the first transmembrane domain (TMD1) is dispensable for the catalytic activity of the SPT holoenzyme (30) raising the possibility that the role of TMD1 of Lcb1p might be to mediate interaction with the Orms (**Figure 2-1A**). To investigate this possibility, whether deletion of TMD1 of Lcb1p conferred phenotypes similar to those displayed by the *orm1Δorm2Δ* mutant was tested. The *orm1Δorm2Δ* mutant is cold and tunicamycin sensitive because of high levels of intracellular LCBs and sphingolipids. It was found that the *LCB1-ΔTMD1* mutant was also cold and tunicamycin sensitive similar to the *orm1Δorm2Δ* (**Figure 2-1B**). Moreover the *LCB1-ΔTMD1* mutant displayed increased levels of *in vivo* LCBs similar to the levels seen in the *orm1Δorm2Δ* mutant and levels were not further elevated by *ORM* deletion (**Figure 2-1C**). The slightly lower level of LCBs in the *LCB1-ΔTMD1* mutant compared to the *orm1Δorm2Δ* mutant is most likely due to reduced expression of the Lcb1p-ΔTMD1 protein (**Figure 2-1C**). These data indicate that the Orms fail to regulate SPT activity in the *LCB1-ΔTMD1* mutant. To investigate this further, co-immunoprecipitation study were performed to determine whether the Orms fail to interact with the SPT subunits in the absence of TMD1 of Lcb1p. The results showed that full length Lcb1p

and Lcb2p co-purified with C-terminally TAP-tagged Orm2p whereas the interaction between the Lcb1p- Δ TMD1 (and Lcb2p) with Orm2p-TAP was significantly reduced (**Figure 2-1D**). Elo1p, a component of the ER-associated fatty acid elongase complex that does not interact with SPT, also failed to co-purify with the Orm2p-TAP. This negative control further confirmed that the failure of Lcb1p- Δ TMD1 to copurify with the Orms reflects the loss of a specific interaction due to TMD1 deletion. These results show that TMD1 is needed for the interaction of the Orm proteins with the SPT heterodimer.

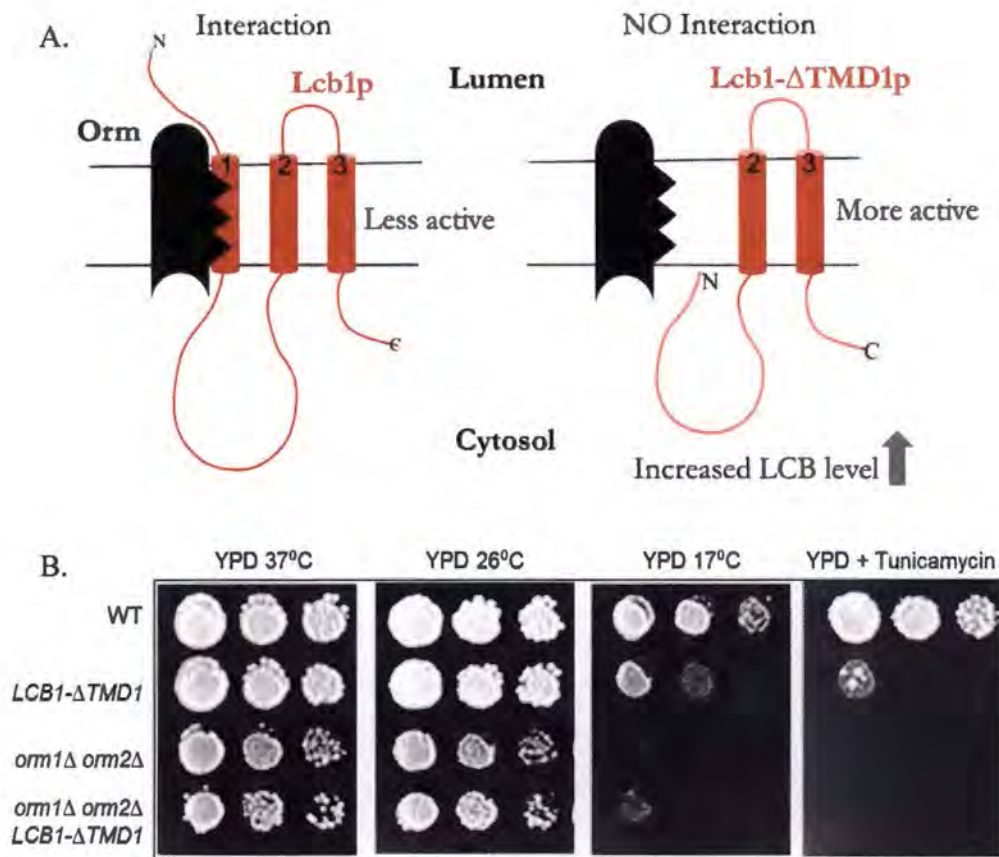


Figure 2-1. **A.** Cartoon depicting the proposed model of interaction between Lcb1p and Ormp. **B.** Deletion of TMD1 from Lcb1p results in phenotypes similar to those of the *orm1Δorm2Δ* mutant.

A serial dilution cell spotting assay was performed to assess the growth on YPD plates at 37 °C, 26 °C, 17 °C and on YPD at 26 °C with 1 μg/ml tunicamycin. Unlike the WT, the *LCB1-ΔTMD1* mutant grew poorly at 17 °C or on tunicamycin plates mimicking the phenotypes exhibited by the *orm1Δorm2Δ* mutant

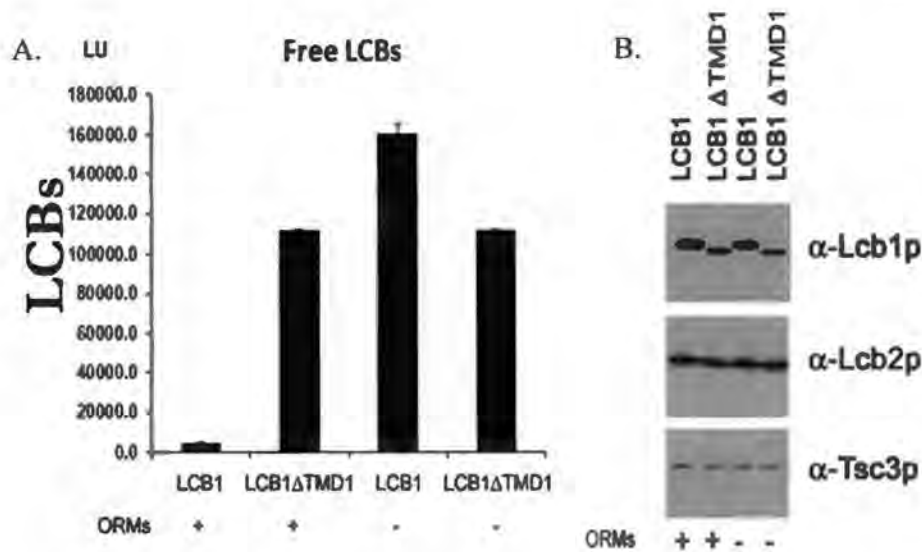


Figure 2-1C. Deletion of TMD1 of Lcb1p results in high levels of long chain bases (LCBs).

A. Free *in vivo* LCBs were extracted from logarithmically growing WT, *LCB1-ΔTMD1*, *orm1Δorm2Δ*, and *orm1Δorm2ΔLCB1-ΔTMD1* mutant cells. Free LCB levels in the *LCB1-ΔTMD1* are comparable to an *orm1Δorm2Δ* and were not further elevated by *ORM* deletion. **B.** Western blots showing expression of Lcb1p, Lcb2p and Tsc3p in the WT, *LCB1-ΔTMD1*, *orm1Δorm2Δ*, and *orm1Δorm2ΔLCB1-ΔTMD1* mutants. Lcb1p-ΔTMD1 is expressed at lower levels than Lcb1p, likely accounting for the slightly lower levels of LCBs in the *LCB1-ΔTMD1* and the *orm1Δorm2ΔLCB1-ΔTMD1* mutants compared to the *orm1Δorm2Δ* mutant.

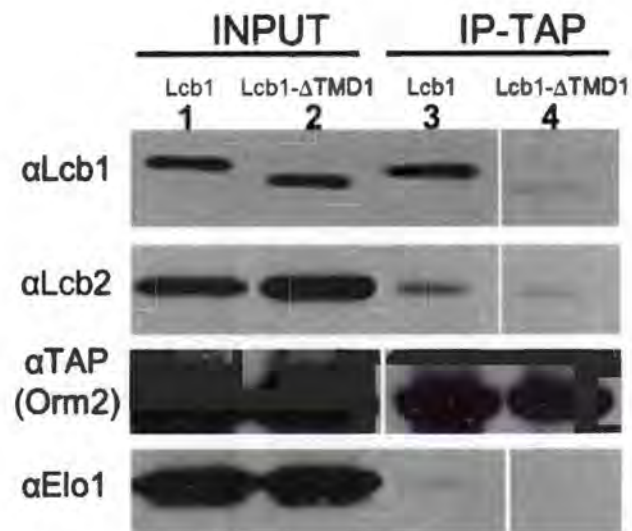


Figure 2-1D. TMD1 of Lcb1p is required for the Orm-SPT interaction.

The strains used for preparing microsomal membranes were *ORM2-TAP* and the *lcb1ΔORM2-TAP* expressing the Lcb1p-ΔTMD1. Microsomal membranes were solubilized with 0.1% digitonin. After incubation with the supernatant, IgG-sepharose beads were washed five times prior to boiling in SDS buffer. Proteins were detected by immunoblotting. Elo1 was used as a negative control.

The Orm proteins inhibit the basal catalytic activity of the Lcb1p-Lcb2p heterodimer.

As mentioned above, all three SPT subunits copurify with the Orm proteins indicating that the Orms do not simply displace Tsc3p from the Lcb1p-Lcb2p heterodimer (7). Furthermore, equivalent amounts of Lcb1p and Lcb2p copurified with Orm2p-TAP from solubilized microsomes prepared from either the *tsc3Δ* mutant or from the wild-type cells (**Figure 2-2A**). These results verify that the binding of the Orms to SPT is not dependent on the Tsc3p, but do not address whether the Orms inhibit the heterodimer directly or simply prevent Tsc3p from activating it.

To investigate whether the Orms inhibit the basal activity of the Lcb1p-Lcb2p heterodimer, *ORM1* and *ORM2* were deleted in the *tsc3Δ* mutant. If the Lcb1p-Lcb2p heterodimer is inhibited by the Orms, then deletion of the *ORMs* might rescue the temperature sensitivity of the *tsc3Δ* mutant at 37 °C. The ability of the *orm1Δorm2Δtsc3Δ* mutant to grow on YPD at 37 °C, albeit modestly, indicates that the basal activity of the Lcb1p-Lcb2p heterodimer is inhibited by the Orms (**Figure 2-2B**). This was further supported by the observation that deletion of TMD1 of Lcb1p rescued the growth of the *tsc3Δ* mutant on YPD at 37 °C. In fact, deletion of TMD1 suppresses much better than deletion of the Orms; on YPD at 37 °C the growth of the *LCB1-ΔTMD1tsc3Δ* was clearly evident after 2 days whereas the growth of *orm1Δorm2Δtsc3Δ* was barely detectable even after 5 days (**Figure 2-2B**). It is possible that the poorer growth of the *orm1Δorm2Δtsc3Δ* mutant is because, in addition to inhibiting SPT, the Orms play a positive regulatory role in the synthesis of complex sphingolipids (81). Perhaps in the *orm1Δorm2Δtsc3Δ* mutant the LCBs are less efficiently channeled into the downstream sphingolipids leading to the modest growth at 37 °C. However the total *in*

vivo LCB levels were found to be higher in the *LCB1-ΔTMD1tsc3Δ* mutant compared to the *orm1Δorm2Δtsc3Δ* mutant, which had total LCB levels very similar to the *tsc3Δ* mutant (Figure 2-2C). This does not support the idea that the Orms play a positive role in the *LCB1-ΔTMD1* mutant, because if the reason the *orm1Δorm2Δtsc3Δ* do not suppress as well as *LCB1-ΔTMD1tsc3Δ* were due to reduced conversion of free LCBs into complex sphingolipids, then the *ORM* deletion and the *TMD1* deletion mutants would be expected to have the same level of total LCBs, which was not the case. Perhaps the *LCB1-ΔTMD1/LCB2* heterodimer has intrinsically higher catalytic activity, than the wild-type heterodimer, resulting in production of more LCBs. Alternatively; *TMD1* may mediate interaction with other negative regulators which can be another reason for more LCB production. Nonetheless, taken together these results suggest that the Orms directly inhibit the basal activity of the *Lcb1p-Lcb2p* heterodimer and do not simply antagonize activation by *Tsc3p*.

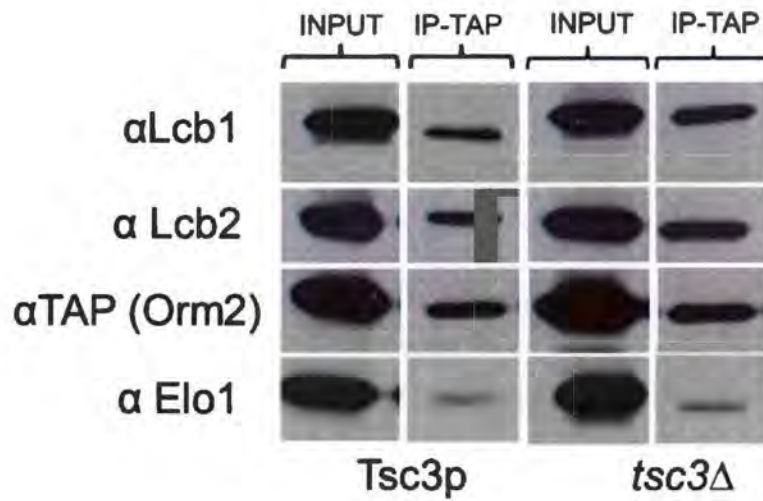


Figure 2-2A. Orms interact with the SPT heterodimer in the absence of Tsc3p.

Co-immunoprecipitation performed using the Orm2-TAP. Microsomal membranes were solubilized with 0.1% digitonin. After incubation with the supernatant, IgG-sepharose beads were washed five times prior to boiling in SDS buffer. Proteins were detected by immunoblotting. Elo1 is used as a negative control.

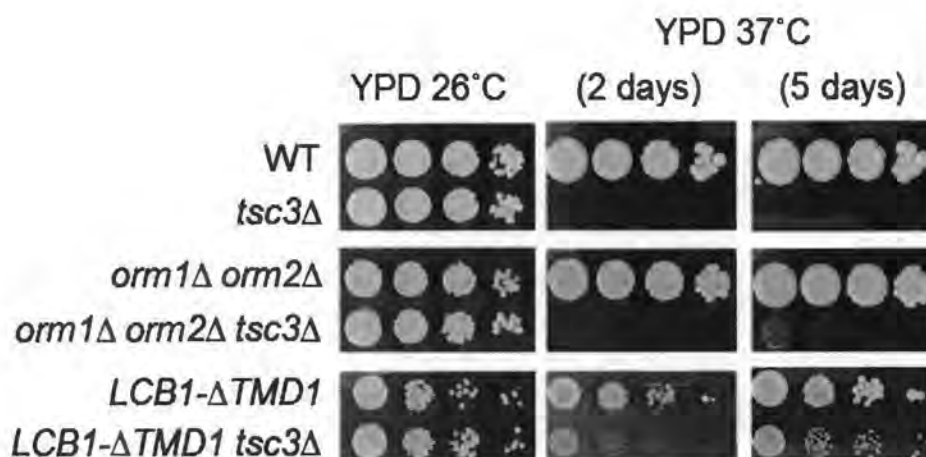


Figure 2-2B. Deletion of Orm or the TMD1 of Lcb1p enabled the *tsc3Δ* mutant to grow at 37°C.

Serial dilution cell spotting assay showing growth on YPD plates at 26°C and 37°C. The *LCB1-ΔTMD1* was chromosomally integrated at the *LCB1* locus by homologous recombination. All strains were spotted at an initial concentration of 0.5 and serially diluted 10 folds. Photographs were taken after 3 days of growth. The *LCB1-ΔTMD1tsc3Δ* grows more efficiently at 37 °C compared to the *orm1Δorm2Δtsc3Δ* mutant.

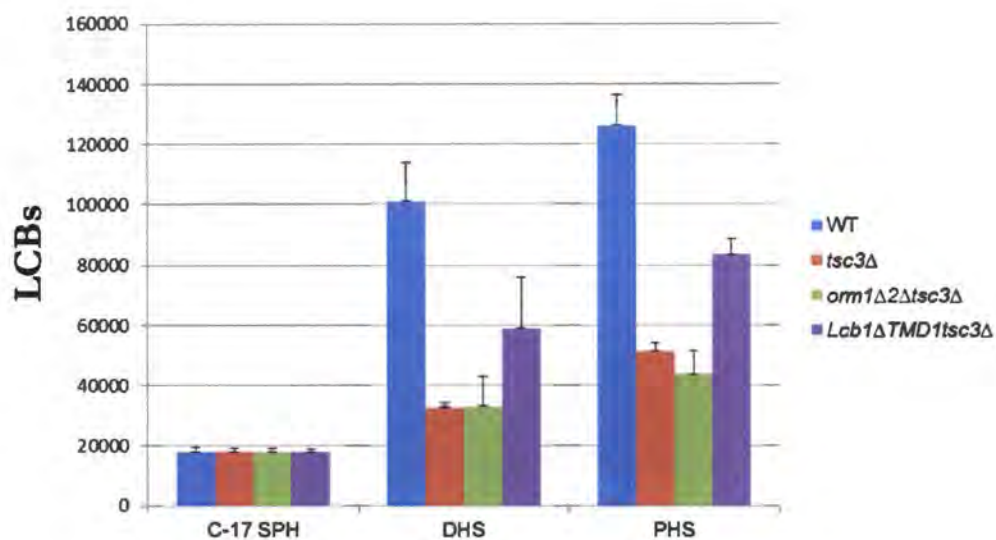


Figure 2-2C. The Orm proteins regulate the Lcb1p-Lcb2p heterodimer.

The *LCB1-ΔTMD1* was chromosomally integrated at the *LCB1* locus by homologous recombination. The *LCB1-ΔTMD1tsc3Δ* has high levels of total LCBs compared to the *tsc3Δ* and the *orm1Δorm2Δtsc3Δ*. Logarithmically growing WT, *tsc3Δ*, *orm1Δorm2Δtsc3Δ* and *LCB1-ΔTMD1tsc3Δ* strains were harvested and total LCBs were extracted and analyzed by HPLC.

DISCUSSION:

The Orms are shown to be interacting directly with Lcb1p and TMD1 is necessary for the binding. Our studies show that the *LCB1-ΔTMD1* mutant has unregulated SPT activity causing accumulation of high levels of LCBs *in vivo* which results in cold and tunicamycin sensitivity similar to that displayed by the *orm1Δorm2Δ* mutant. The unregulated SPT activity of the *LCB1-ΔTMD1* mutant results from loss of interaction between the Orms and SPT. These data confirm that the TMD1 of Lcb1p is necessary for Orm mediated SPT regulation but does not rule out the possibility that there are other interaction sites between Lcb1p and the Orms, or even between the Orms and Lcb2p or Tsc3p. Deletion of the *ORMs* supported very modest growth of the *tsc3Δ* mutant at 37 °C whereas expressing Lcb1p-ΔTMD1 in the *tsc3Δ* resulted in better growth at 37 °C compared to the *orm1Δorm2Δtsc3Δ*. Further experiments showed that the growth of the *LCB1-ΔTMD1tsc3Δ* mutant at 37 °C results from increased intracellular LCBs levels compared to the *tsc3Δ* mutant. Additional data in support of Orm mediated regulation of SPT heterodimer were derived from the observation that, the *ypk1Δtsc3Δ* mutant fails to grow at 35 °C unlike the *tsc3Δ* mutant (Unpublished data Dr. Gongshe Han). Deletion of *YPK1* results in constitutive dephosphorylation of the Orms resulting in inhibition of SPT (73). Because of this, in the *ypk1Δtsc3Δ* mutant the SPT is in a more repressed state compared to that in the *tsc3Δ*. Moreover, overexpression of Orms lacking the Ypk1 phosphorylation sites under the galactose inducible promoter is lethal for the *tsc3Δ* mutant (Unpublished data Dr. Gongshe Han). All this data suggests that the Orms are directly regulating the Lcb1p-Lcb2p heterodimer rather than acting by antagonizing activation of the heterodimer by Tsc3p. Moreover, it can be concluded that although

TMD1 is required for Orm interaction, deletion of TMD1 is not equivalent to loss of Orm proteins. This is in accordance with the findings (81) that the Orms have a positive regulatory role in complex sphingolipid synthesis and also raises the possibility that the TMD1 of Lcb1p may integrate other regulatory signals besides those mediated by the Orm proteins.

Table 1. List of strains used in chapter 2.

NAME	STRAIN	GENOTYPE
TDY4B	WT	<i>Mata his3Δ leu2Δ ura3Δ lys2Δ</i>
TDY4071	<i>tsc3Δ</i>	<i>Mata tsc3Δ::clonNATr his3Δ leu2Δ ura3Δ lys2Δ</i>
KGY1001	<i>orm1Δorm2Δ</i>	<i>Mata orm1Δ::clonNATr orm2Δ::HIS3 ura3Δ leu2Δ lys2Δ</i>
KGY1105	<i>orm1Δorm2Δ tsc3Δ</i>	<i>Mata tsc3Δ::URA3^{mut} orm1Δ::clonNATR orm2Δ::HIS3 ura3Δ leu2Δ met15Δ his3Δ</i>
TDY1035	<i>ORM2-TAP</i>	<i>Mata his3Δ leu2Δ ura3Δ met15Δ lcb1Δ::KAN</i>
TDY1036	<i>lcb1ΔORM2-TAP</i>	<i>Mata his3Δ leu2Δ ura3Δ met15Δ</i>
TDY1120	<i>LCB1-ΔTMD1</i>	<i>Mata his3Δ leu2Δ ura3Δ met15Δ lys2Δ lcb1Δ::LCB1-ΔTMD1</i>
TDY1126	<i>LCB1-ΔTMD1 tsc3Δ</i>	<i>Mata his3Δ leu2Δ ura3Δ met15Δ lys2Δ tsc3Δ::URA3 lcb1Δ::LCB1-ΔTMD1</i>

CHAPTER 3: Identification and characterization of recessive suppressors involved in enhancement of sphingolipid biosynthesis in the absence of Tsc3p.

ABSTRACT:

The *orm1Δorm2Δtsc3Δ* mutant shows modest growth at 37 °C but it gives rise to recessive suppressors which grow much better at 37 °C. By suppressor screening, a recessive suppressor (*Sup4*) of *orm1Δorm2Δtsc3Δ* was isolated which grows as well as wild type yeast at 37 °C. Genetic analysis revealed that the *Sup4* mutant has two unlinked mutations which are henceforth named as *Sup4^{m1}* and *Sup4^{m2}*. To identify the genes, next generation sequencing of *Sup4^{m1m2}* was performed. The *Sup4^{m2}* mutation was found to be in the *CHA4* gene, which encodes a transcription factor that regulates serine synthesis through Ser3p and degradation through Cha1p. It was found that the Cha4p regulates sphingolipid synthesis by activation of the deaminase Cha1p. Moreover, deletion of *CHA4* resulted in increased serine uptake indicating involvement of *CHA4* in serine transport. Deletion of either the TMD1 of Lcb1p or the *ORMs* has an additive effect on the myriocin resistance and growth at 37 °C of *tsc3ΔSup4^{m1}cha4Δ*, suggesting that *CHA4* and *Sup4^{m1}* regulate sphingolipid biosynthesis in a way which is independent of Orm protein mediated regulation.

BACKGROUND:

The *orm1Δorm2Δtsc3Δ* mutant grows modestly at 37 °C implying that the Orms are not simply antagonizing activation of the Lcb1p-Lcb2p heterodimer by the Tsc3p subunit, but rather that the Orms directly exert their regulatory effects on the SPT heterodimer. Interestingly, the *orm1Δorm2Δtsc3Δ* mutant gives rise to recessive suppressors which grow well at 37 °C. In a previous attempt to identify negative

regulators of SPT, only dominant mutations in Lcb2p that increased catalytic activity of the SPT heterodimer and thereby suppressed the temperature sensitive phenotype of *tsc3Δ* were identified (60). As the suppressors of *orm1Δorm2Δtsc3Δ* mutant were recessive, it indicated a loss of function mutation in gene(s) other than the *ORMs* and suggested that the basal catalytic activity of the heterodimer is under the influence of regulatory mechanisms independent of the Orms.

MATERIALS AND METHODS:

Strains:

All strains are in the BY4741 background. The strains used in this study are listed in Table 2.

Growth media:

The media used in this study were YPD or SD supplemented with the indicated concentrations of myriocin, phytosphingosine or serine, and standard yeast sporulation media. Media was prepared by following standard protocols (79).

Plasmids:

DPL1-pRS315 – The *DPL1* gene was PCR amplified with 400 base pair upstream and 125 base pair downstream of the coding sequence using the *DPL1* forward and reverse primers. The PCR amplicon having *Bam*HI and *Xho*I ends was ligated to the *Bam*HI and *Sal*I digested pRS315 to generate the *DPL1*-pRS315.

LCB4-pRS315 - The *LCB4* gene was PCR amplified with 500 base pair upstream and 300 base pair downstream of the coding sequence using the *LCB4* forward and

reverse primers. The PCR amplicon having *NotI* and *XhoI* ends was ligated to the *NotI* and *XhoI* digested pRS315 to generate the *LCB4*-pRS315.

Glycosylation reporter cassette:

The glycosylation reporter cassette consists of a 53-amino acid domain comprising amino acid residues from 80 to 133 of invertase (Suc2p). It contains three NX(S/T) sites which are known to undergo asparagine-linked glycosylation in Suc2p. The 53-amino acid glycosylation domain was inserted at the 4th codon of the *Lcb1p* to generate the GC@4 *Lcb1p*- pRS315 plasmid. Insertion of the GC cassette at the 4th codon did not interfere with the function or the topology of the *Lcb1p* protein (30).

Primers:

Primers used in this study are listed in Table 3.

Tetrad dissection and analysis of products of meiosis:

Yeast mating and sporulation was done according to the standard protocols (79).

Yeast transformation:

All yeast transformations were done using the standard yeast transformation protocol (79).

Yeast plasmid and genomic preparation:

Yeast plasmid and genomic DNA were isolated using the Zymoprep I TM Kit (Zymo Research, Inc) according to the manufacturer's protocol.

Genomic DNA isolation and library preparation for Next Generation Sequencing:

The genomic DNA was isolated using the MasterPure™ Yeast DNA Purification Kit from Epicentre (Illumina) according to the manufacturer's protocol. The library for next generation sequencing was kindly prepared by our collaborator Dr. Harold Smith at NIDDK, NIH, using Truseq DNA sample preparation kit v2 (Illumina, Inc). The sequences were analyzed by Otogenetics and viewed using the DNANEXUS visualization platform. Additional analyses were done using the open web based platform, Galaxy, in collaboration with Dr. Clifton Dalgard (Department of Anatomy, Physiology and Genetics, USUHS).

Serial dilution cell spotting assay:

As described in the materials and methods, chapter 2.

Microsome preparation:

As described in the materials and methods, chapter 2.

Western blot:

As described in the materials and methods, chapter 2.

Total long chain base extraction for analysis by HPLC:

As described in the materials and methods, chapter 2.

Free long chain base extraction for analysis by HPLC:

As described in the materials and methods, chapter 2.

Free long chain base extraction for analysis by mass spectrometry:

10 OD₆₀₀ of logarithmically growing cells were harvested in glass tubes, washed with water and the pellet was extracted 3 times using 1 ml of water:ethanol:diethyl ether:pyridine:NH₄OH (15:15:5:1:0.018) at 65 °C for 15 min (each time). 125 pmol per tube of Avanti Polar Lipid MS standards (LM-6002) were added to the samples before the first extraction. The extracts were pooled and dried under N₂, re-dissolved in 1 ml chloroform with bath sonication, 1 ml butanol was added and phospholipids were hydrolyzed for 30 min at 37 °C after the addition of 0.2 ml of 1 M KOH (in methanol). After hydrolysis, the extract was neutralized by the addition of 0.2 ml 1 M acetic acid (in methanol). 1 ml butanol saturated water was added, centrifuged to separate the phases and the upper aqueous layer was removed by aspiration, being careful not to disrupt the precipitate at the interface. This was repeated two more times after which the remaining lower phase was dried under N₂. The dried lipid was re-dissolved in 0.5 ml LC/MS buffer A with bath sonication, spun to pellet insoluble material and then transferred to MS analysis vials. Typically 40 µl was injected. The LCBs and ceramides were resolved in a binary gradient with the following solvents (MS buffer A: tetrahydrofuran:methanol:dH₂O (30:20:50) with 5 mM ammonium formate and 0.2% formic acid, MS buffer B: tetrahydrofuran:methanol:dH₂O (70:20:10) with 5 mM ammonium formate and 0.2% formic Acid). The samples were analyzed on a Supelco Discovery Bio Wide Pore C18 (15 cm x 4.6 mm, 5 µm column at 40 °C (50 mm) using an Agilent 1200 Series HPLC coupled to ABSciex QTRAP 4000 MS. The LCBs and the LCB-Ps elution gradient was 0% solvent B at 2 min; 25% solvent B at 5 min, 100% solvent B at 8 min held until 12 min; then returned to 0% B after 4 min. The LCBs and

the LCB-Ps were detected in MRM mode. The MRM parameters are listed in Table 6 (59).

Measurement of intracellular amino acids:

0.5 OD₆₀₀ of exponentially growing cells in YPD were harvested, washed once with dH₂O, and suspended in 100 µl of dH₂O. 100 µl of 100% methanol at -40 °C was added to the cell suspension. The cell suspension was immediately frozen in liquid nitrogen for 10 min and quickly thawed at 42 °C. The cell suspension was again frozen in liquid nitrogen for 10 min and thawed on ice. The thawed samples were centrifuged at 20000 x g for 2 min at 25 °C. 20 µl of the supernatant was collected into HPLC vials and derivatized by addition of 60 µl borate buffer (AccQ-Fluor™ Reagent Kit, Waters) and 20 µl AccQ-Fluor™ reagent (6-aminoquinolyl-N-hydroxysuccinimidyl carbamate, or AQC). The sample was heated at 50 °C for 10 min. 10 µl of the sample was injected into the HPLC column (Genesis C18 4 µM 250 mm, 25 °C) for analysis. The amino acids were resolved using a binary gradient at 1 ml/min with the following solvents (Solvent A – 25 mM potassium phosphate buffer (pH 5.4) and 3% acetonitrile, Solvent B – 25mM potassium phosphate buffer (pH 5.4) and 60% acetonitrile). The elution gradient was 33% solvent B at 32 min; 100% solvent B at 40 min, held for 5 min; 0% B at 50 min, held for 10 min. The derived amino acids were detected by fluorescence (excitation: 244 nm/emission: 398 nm).

SPT assay:

Microsomes from the indicated strains were used to measure SPT activity. For the enzymatic assay, a reaction containing (SPT activity was assayed in a 300-µl volume

containing 50 mM HEPES, pH 8.1, 50 mM pyridoxal phosphate, 2 mM serine (10 μ Ci/ml) 20 μ M BSA, 0.2 mg of microsomal membranes and with varying acyl-CoA concentration, was incubated at 37 °C for 10 min. The reaction was stopped by addition of chloroform. The products were extracted and quantified following the total LCB extraction protocol (31).

Serine labelling of long chain bases:

Yeast cells growing logarithmically were harvested and suspended in YPD media at a concentration of 1 OD₆₀₀/ml. 10 μ Ci/ml of ³H L-serine was added to the culture and incubated in a 26 °C water bath. 2 ml of cells were harvested (5, 10, 20, 60 and 120 min) and 1 ml of 1 M HCl-methanol containing 100 μ M C17-sphingosine (internal standard) was immediately added, boiled for 30 min and cooled on ice. 1 ml of 1% NaCl was added to the mixture and vortexed followed by addition of 2 ml of hexane:ether (1:1). The solution was vortexed and centrifuged for ~1 min. The top layer was aspirated; 0.25 ml of 10 N NaOH was added, and mixed. Finally, 1.75 ml of hexane was added, mixed and the solution was centrifuged briefly for ~1 min. The top layer was transferred to a fresh vial and dried under N₂. The dried samples were resuspended in 40 μ l hexane containing DHS as a loading standard followed by loading on a TLC plate along with the non-radiolabelled PHS, DHS, and 3KDS standards. The TLC plate was run twice in a chamber containing chloroform:methanol:NH₄OH (2N) (80:20:2). The radioactive LCBs were imaged by X-ray film and visualized using a phosphoimager whereas the non-radioactive LCBs were visualized by ninhydrin staining.

Serine uptake assay:

Yeast cells were grown overnight in YPD to an OD₆₀₀ of <1. 50 mM sodium citrate (pH 5.5) containing 2% D-glucose (SC buffer) was freshly prepared. The cells were harvested, washed with dH₂O and suspended in SC buffer at a concentration of 2 OD₆₀₀/ml. 0.45 µm filter papers (Millipore) were placed on the millipore filter chambers and equilibrated with SC buffer. A mixture of ³H L-serine (5 mCi/ml) to cold serine (2 mM) was prepared in a ratio of 1:1 (v/v), added to the cell suspension at a concentration of 0.01 mM and the tubes were placed in a shaker for constant agitation. 200 µl of the culture was pipetted out onto the filter (at 2.5, 5, 10 and 20 min) and immediately washed 2 times with SC buffer. The filter papers containing the cells were dried under heat in scintillation vials. 5 ml of Bio-safe II scintillation fluid (Research Products International Corp.) was added to the vials containing the dried filters and the radioactivity was measured using a Perkin Elmer Tri-Carb 2800TR liquid scintillation counter. For the measurement of the total counts, 10 µl of the culture containing the mixture of hot and cold serine was added to vials containing scintillation fluid and measured using the above mentioned scintillation counter (13).

RESULTS:

Screening performed to isolate recessive suppressors of *orm1Δ orm2Δ tsc3Δ*.

To gain more insight into the regulation of SPT, spontaneously arising suppressors of the *orm1Δorm2Δtsc3Δ* mutant that displayed significantly improved growth at 37 °C were isolated (**Figure 3-1A**). Previous *tsc3Δ* suppressor screens performed in our laboratory identified several point mutations in Lcb2p which increased the activity of the Lcb1p-Lcb2p heterodimer in the absence of Tsc3p. These point mutations were dominant (60). This screen focused on the recessive suppressors as loss-of-function mutations in negative regulators are expected to be recessive. The suppressors arose in an *orm1Δorm2Δtsc3Δ* mutant, eliminating the possibility of loss of function mutations in *ORM1* or *ORM2*. Among the 38 suppressor mutants that were analyzed, 12 suppressors were found to be recessive by backcrossing with the parent *orm1Δorm2Δtsc3Δ* mutant. Pairwise crossing of the 12 recessive suppressor mutants isolated from parent strains (in both *Mata* and *Mata*), revealed the presence of two complementation groups (**Figure 3-1B**). Among these groups, the suppressor having the best growth rate, called “Suppressor 4 (*Sup4*)”, was chosen for further studies (**Figure 3-1C**).

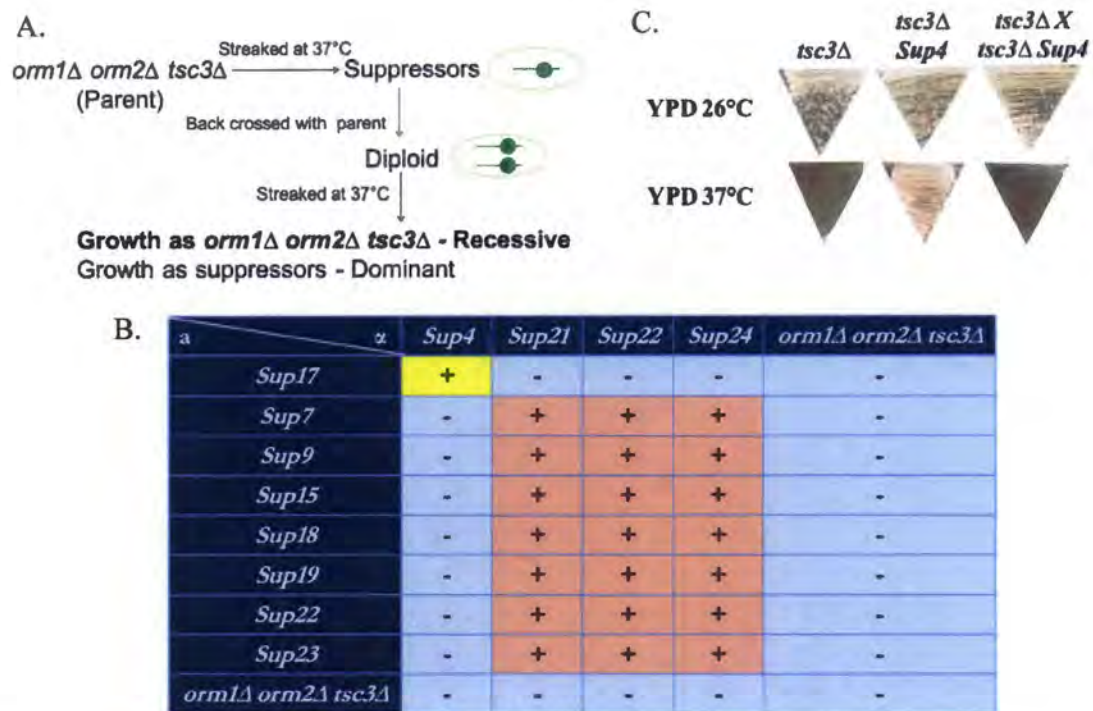


Figure 3-1. Screen to identify recessive suppressors of *orm1Δ orm2Δ tsc3Δ*.

A. Schematic representation of the screening strategy. **B.** Table showing complementation analysis of the recessive suppressors. The recessive suppressors were pairwise crossed for complementation analysis. *Sup4* and *Sup17* are in the same complementation group. **C.** *Sup4* is a recessive mutation. The *tsc3ΔSup4* mutant was crossed with the *tsc3Δ* to generate the diploid. The diploid and the parental haploids were streaked on YPD 26 °C and 37 °C. Photographs were taken after 3 days.

***Sup4*, the best recessive suppressor of the temperature sensitive phenotype of *tsc3Δ*, has two unlinked mutations and both are required for good suppression.**

Sup4 and *Sup17* were the two suppressor mutants in the first complementation group. Surprisingly the growth of these two suppressor mutants was different on YPD at 37 °C. *Sup4* exhibited significantly better growth than *Sup17* (Figure 3-2A), and the diploid generated by crossing the two mutants displayed weak suppression similar to *Sup17*, raising the possibility that *Sup4* may not be a single gene mutation. Indeed, genetic analysis revealed that two unlinked mutations are responsible for the *Sup4* phenotype (Figure 3-2B). If *Sup4* had been a single gene mutation then crossing a *tsc3ΔSup4* with *tsc3Δ* followed by tetrad dissection would have yielded two temperature resistant (*tsc3ΔSup4*) and two temperature sensitive (*tsc3Δ*) products of meiosis in each tetrad. However, analysis of the tetrads showed that only 25% of the tetrads yielded two products of meiosis that grew like *tsc3ΔSup4* (strongly suppressed) and two products of meiosis that grew like *tsc3Δ* (not suppressed). 50% of the tetrads yielded one product of meiosis that was strongly suppressed (like *tsc3ΔSup4*), one product of meiosis that was weakly suppressed (poor growth compare to *tsc3ΔSup4*), and two products of meiosis that were not suppressed (like *tsc3Δ*). The other 25% of tetrads gave two weakly suppressed products of meiosis and two unsuppressed products of meiosis (like *tsc3Δ*). These results are consistent with the presence of one mutation (*Sup4^{m1}*) that weakly suppresses *tsc3Δ* and a second unlinked mutation (*Sup4^{m2}*) that does not itself suppress *tsc3Δ*, but that enhances the suppression of *tsc3Δ* by *Sup4^{m1}* (Figure 3-2C). To confirm this two gene model a *tsc3ΔSup4^{m1}* (weakly growing product of meiosis) haploid was crossed with a *tsc3ΔSup4^{m2}* (non-growing product of meiosis) haploid and the diploid was sporulated. Following tetrad dissection and analysis, it was observed that 25% of all

the products of meiosis were strongly growing at 37 °C like *tsc3ΔSup4*. This result further confirmed the model that one of the mutations (*Sup4^{m1}*) supports weak growth of *tsc3Δ* at 37 °C whereas another unlinked mutation (*Sup4^{m2}*) can only enhance the effect of the *Sup4^{m1}* (**Figure 3-3**). To verify that *Sup4^{m1}* is a single gene mutation, tetrads from the *tsc3ΔSup4^{m1}* X *tsc3Δ* diploid were analyzed. As expected, all the tetrads showed 2:2 ratio of weakly growing to non-growing products of meiosis on YPD at 37 °C confirming *Sup4^{m1}* as a single gene mutation. The *Sup4^{m2}* was also confirmed as a single gene mutation by analyzing tetrads obtained from the *tsc3ΔSup4^{m1}* X *tsc3ΔSup4^{m1m2}* diploid. All the tetrads from this cross showed a 2:2 ratio of weakly growing to strongly growing products of meiosis on YPD at 37 °C verifying *Sup4^{m2}* as a single gene mutation (**Figure 3-4A**).

Though *Sup4^{m1}* was recessive, there was the possibility that *Sup4^{m2}* is a dominant mutation because it does not support any growth on its own and its effect can only be seen in the presence of *Sup4^{m1}*. However, as mentioned above, the *Sup4* X *Sup17* diploid showed a weak suppressor phenotype like *Sup17*, indicating that *Sup4^{m2}* is recessive. However, to further confirm *Sup4^{m2}* as recessive, *tsc3ΔSup4^{m1}* was crossed with the *tsc3ΔSup4^{m1m2}*. The diploid showed a weak growth like *tsc3ΔSup4^{m1}* on YPD at 37 °C confirming that *Sup4^{m2}* is a recessive mutation (**Figure 3-4B**). It was also observed that the diploid *tsc3ΔSup4^{m1}* X *tsc3Δ* failed to grow on YPD at 37 °C reconfirming *Sup4^{m1}* as a recessive mutation (**Figure 3-4B**).

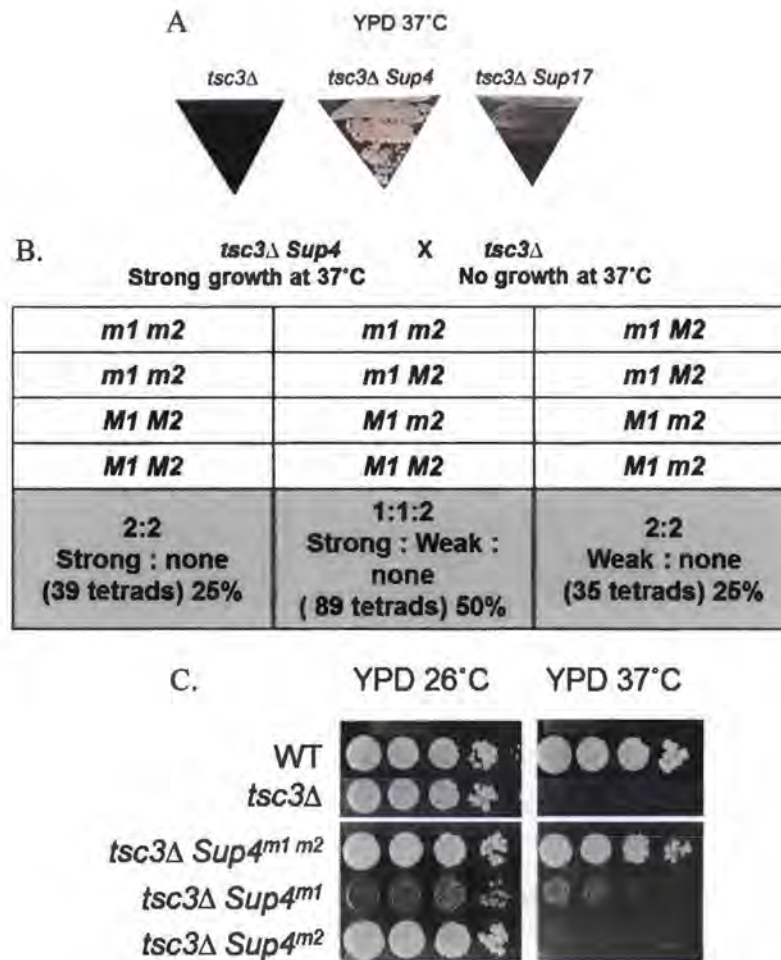


Figure 3-2. *Sup4*, the best recessive suppressor of the temperature sensitive phenotype of the *tsc3Δ*, has two unlinked mutations and both are required for good suppression.

A. The *tsc3ΔSup17* grows weakly compared to *tsc3ΔSup4* on YPD at 37 °C.
B. *Sup4* is a two gene mutation. The *tsc3ΔSup4* mutant was crossed with the *tsc3Δ* mutant to generate diploid for sporulation and tetrad analysis. Analysis of the tetrads revealed spores growing weakly or strongly on YPD at 37 °C.
C. Growth of the WT, *tsc3Δ*, *tsc3ΔSup4^{m1 m2}*, *tsc3ΔSup4^{m1}* *ade2-101* and *tsc3ΔSup4^{m2}* mutants were compared on YPD at 26 °C and 37 °C. All strains were spotted at an initial OD₆₀₀ of 0.5 and serially diluted 10 fold. Photographs were taken after 3 days.

<i>tsc3Δ Sup4^{m1}</i> Weak growth at 37°C	X	<i>tsc3ΔSup4^{m2}</i> No growth at 37°C
<i>m1 M2</i>	<i>m1 m2</i>	<i>m1 m2</i>
<i>m1 M2</i>	<i>m1 M2</i>	<i>m1 m2</i>
<i>M1 m2</i>	<i>M1 m2</i>	<i>M1 M2</i>
<i>M1 m2</i>	<i>M1 M2</i>	<i>M1 M2</i>
2:2 Weak : none (4 tetrads) 25%	1:1:2 Strong : Weak : none (8 tetrads) 50%	2:2 Strong : none (4 tetrads) 25%

Figure 3-3. Tetrad analysis performed to confirm *Sup4* as two gene (*Sup4^{m1}*, *Sup4^{m2}*) mutation.

Table showing number and percentage of types of spores recovered from dissection of tetrads generated by sporulation of the *tsc3ΔSup4^{m1}* X *tsc3ΔSup4^{m2}* diploid.

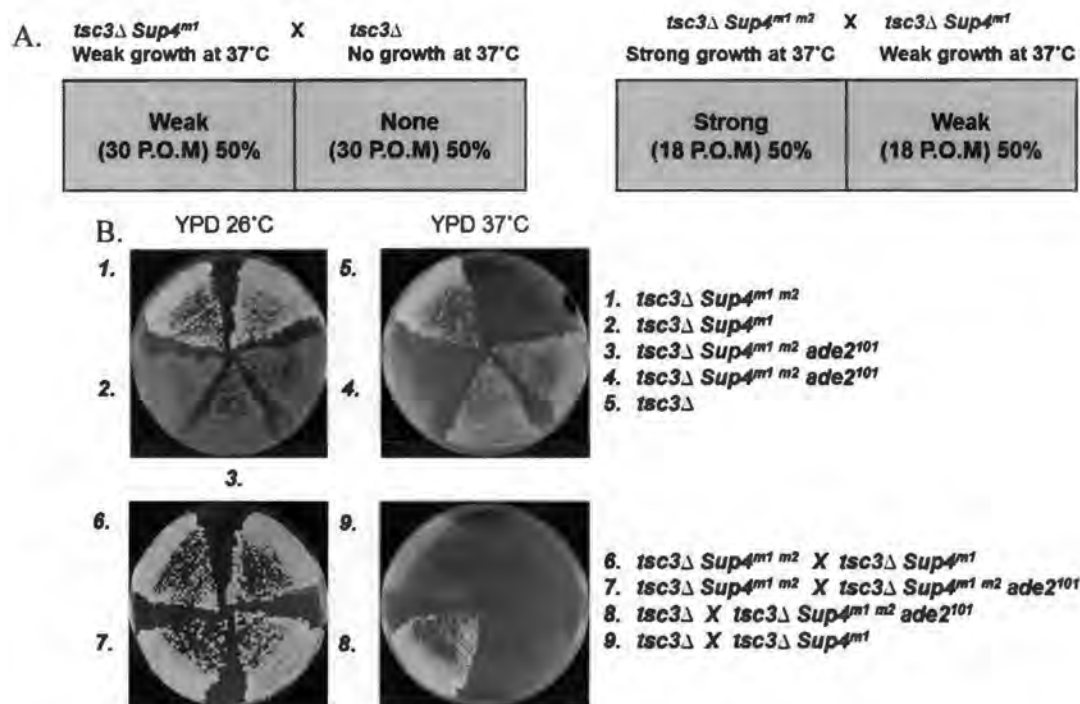


Figure 3-4. *Sup4^{m1}* and *Sup4^{m2}* are two unlinked recessive mutations.

A. Tables showing the results of backcrosses done to establish that the *Sup4^{m1}* and the *Sup4^{m2}* are single gene mutations. B. Both *Sup4^{m1}* and *Sup4^{m2}* were recessive. The diploids and the respective haploids were streaked on YPD at 26 °C and 37 °C and the growth was compared after 3 days.

The *tsc3ΔSup4^{m1m2}* mutant has elevated *in vivo* SPT activity.

In a previous study by Lester et al. (55), a suppressor mutant 'slc' was isolated that enabled *S. cerevisiae* completely lacking SPT to survive by bypassing the requirement for sphingolipids. To test whether the *Sup4^{m1m2}* is bypassing the need for sphingolipids, *LCB1* was deleted in the *tsc3ΔSup4^{m1m2}* mutant. The resulting strain did not grow unless the media was supplemented with a sphingoid base like an *lcb1Δtsc3Δ* (**Figure 3-5**) and thus it is clear that the *Sup4^{m1}* and *Sup4^{m2}* mutations are not bypassing the requirement for SPT.

Growth of *tsc3ΔSup4^{m1m2}* at 37 °C suggests an increase in *in vivo* LCB and sphingolipid levels. Hence the *tsc3ΔSup4^{m1m2}* was tested for resistance to myriocin, a specific inhibitor of the SPT enzyme. In a serial dilution cell spotting assay done on YPD at 26 °C, the *tsc3Δ* mutant survived only up to a concentration of 270 ng/ml whereas the *tsc3ΔSup4^{m1m2}* mutant was highly resistant displaying growth at high concentrations (1080 ng/ml) similar to WT (**Figure 3-6**). However, the *tsc3ΔSup4^{m2}* single mutant showed myriocin resistance comparable to the *tsc3ΔSup4^{m1m2}* mutant which was surprising since it alone cannot rescue *tsc3Δ* at 37 °C (**Figure 3-6**). These data suggest that the *tsc3ΔSup4^{m1m2}* mutant has increased levels of *in vivo* LCBs and sphingolipids.

To directly investigate whether the *tsc3ΔSup4^{m1m2}* mutant has higher rates of *in vivo* LCB synthesis than *tsc3Δ*, cells were incubated with ³H serine for increasing times and LCBs were extracted and quantitated. To reduce the complexity of measuring all the different species of LCBs and sphingolipids, *tsc3ΔSup4^{m1m2}sur2Δ* and *tsc3Δsur2Δ* strains were generated. Sur2p, the sphinganine C4-hydroxylase catalyzes the conversion of dihydrosphingosine (DHS) to phytosphingosine (PHS). Although the *sur2Δ* mutant

makes no PHS, DHS is acylated to form dihydroceramides and the downstream complex sphingolipids at rates similar to WT (28). To convert any 3-ketodihydrosphinganine that is present in the *sur2Δ* mutant to DHS, the extracted LCBs were treated with sodium borohydride after extraction of the LCBs (**Figure 3-7A**). The *tsc3ΔSup4^{m1m2}sur2Δ* and *tsc3Δsur2Δ* strains were pulsed with ³H serine and an equal number of cells were harvested at 5, 10, 20, 60 and 120 min. Following addition of C-17 sphingosine (a non *S. cerevisiae* LCB, added as an internal control), total LCBs were extracted and treated with sodium borohydride. Cold DHS was added to the extracts prior to TLC analysis as loading control. The results showed that radioactively labeled DHS accumulated faster and to higher levels in the *tsc3ΔSup4^{m1m2}sur2Δ* mutant compared to *tsc3Δsur2Δ* and the levels dropped with addition of myriocin (**Figure 3-7B**). Mass spectrometric analyses confirmed the presence of higher levels of LCBs and ceramides in the *tsc3ΔSup4^{m1m2}* than in the *tsc3Δ* mutant (**Figure 3-7C**).

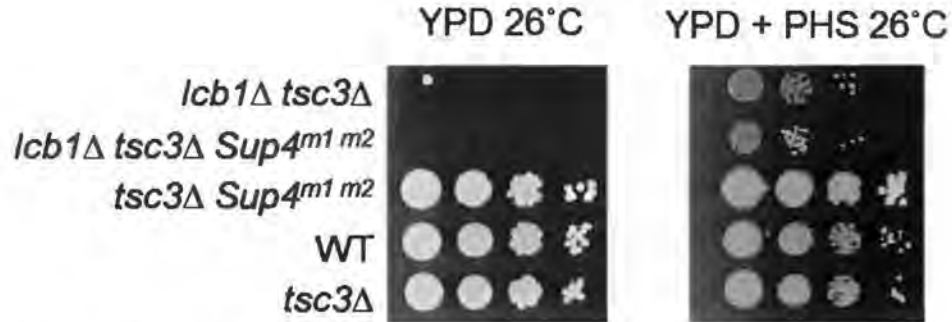


Figure 3-5. The *Sup4^{m1m2}* is not a bypass suppressor.

The *lcb1Δtsc3ΔSup4^{m1m2}* mutant was obtained by replacing the *LCB1* in the *tsc3ΔSup4^{m1m2}* with the kanamycin cassette by homologous recombination. The *lcb1Δtsc3ΔSup4^{m1m2}* mutant failed to grow on YPD 26 °C like the control *lcb1Δtsc3Δ*, unless the media was chemically supplemented with phytosphingosine (PHS). The growth of *lcb1Δ tsc3ΔSup4^{m1m2}* was compared with *lcb1Δtsc3Δ*, *tsc3ΔSup4^{m1m2}*, WT, and *tsc3Δ* on YPD at 26 °C with and without PHS. All strains were spotted at an initial OD₆₀₀ of 0.5 and serially diluted 10 fold. Photographs were taken after 3 days.

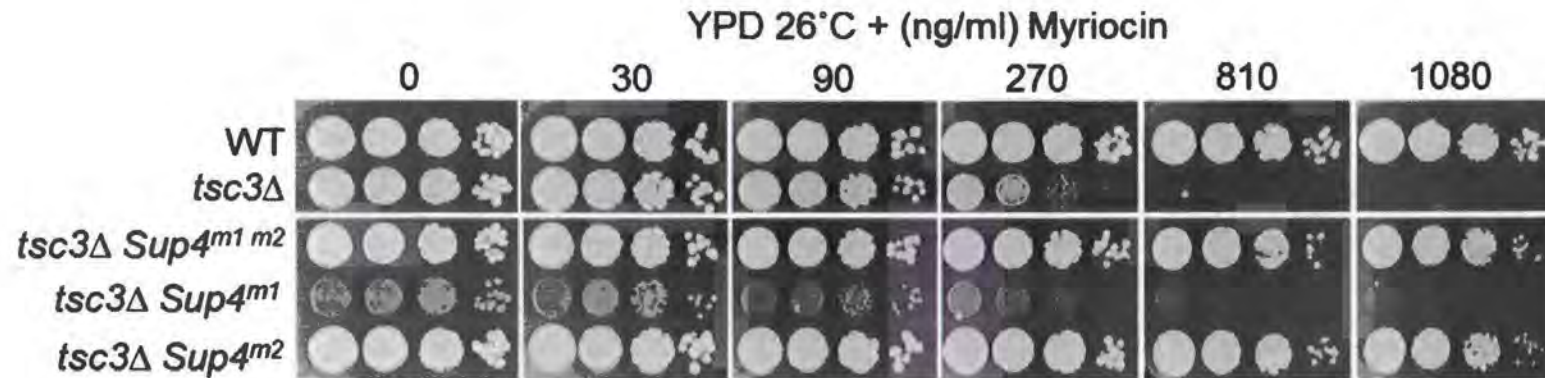


Figure 3-6. The *tsc3ΔSup4^{m1m2}* mutant is resistant to myriocin.

tsc3ΔSup4^{m1m2} is as resistant to myriocin as WT. Growth of the WT, *tsc3Δ*, *tsc3ΔSup4^{m1m2}*, *tsc3ΔSup4^{m1}ade2-101*, *tsc3ΔSup4^{m2}* was compared on YPD 26 °C containing increasing concentration of myriocin. All strains were spotted at an initial OD₆₀₀ of 0.5 and serially diluted 10 fold. Photographs were taken after 3 days.

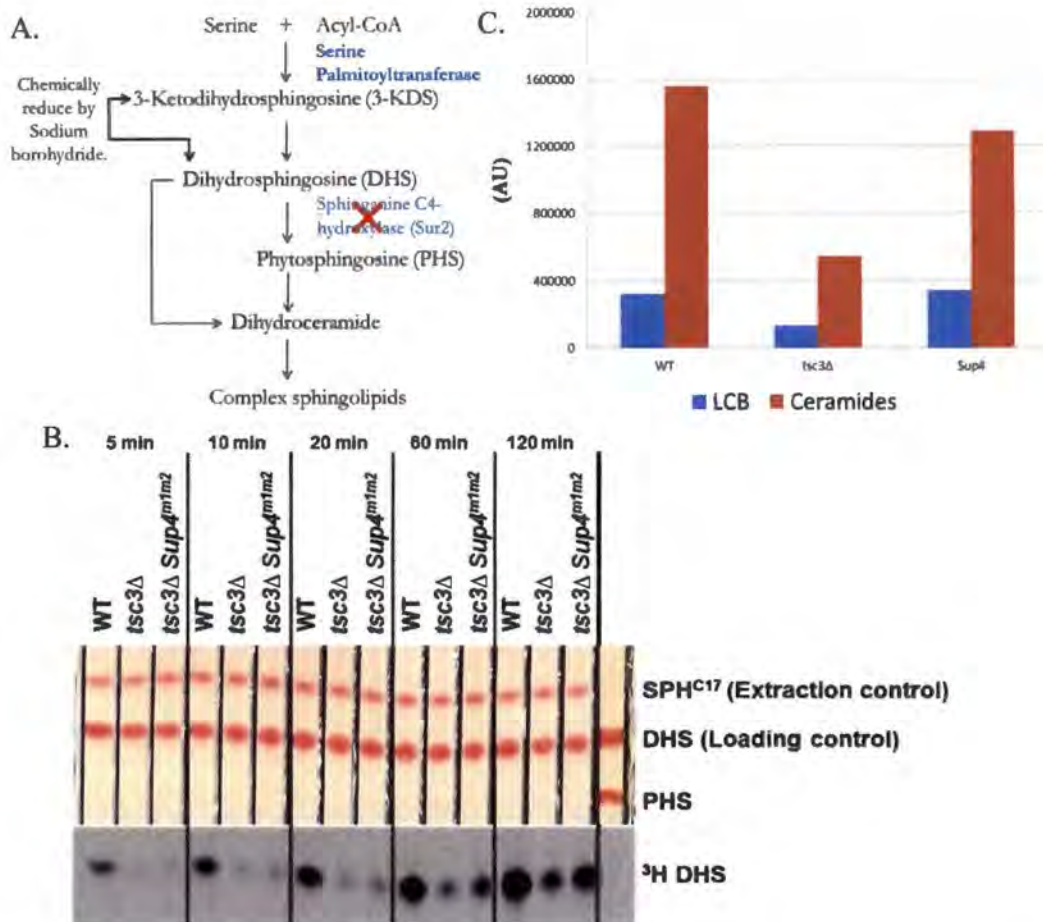


Figure 3-7. The *tsc3ΔSup4^{m1m2}* has elevated *in vivo* LCB synthesis.

A. Cartoon of the sphingolipid biosynthetic pathway showing the manipulations done to generate products with only the DHS backbone. **B.** The *tsc3ΔSup4^{m1m2}* accumulates more LCBs overtime compared to *tsc3Δ*. All the strains were in the *sur2ΔKAN* background. Logarithmically growing WT, *tsc3Δ* and *tsc3ΔSup4^{m1m2}* strains were harvested and incubated at 26 °C after pulsing with radioactive serine. Cells were harvested from each strain at 5, 10, 20, 60 and 120 min. Following harvesting, total LCBs were extracted immediately using C17 SPH as an internal standard and then reduced chemically by sodium borohydride. The sample was dried under N₂ and resuspended in 40 μl hexane before loading on a TLC plate. The TLC plate was run twice in chloroform:methanol:2N NH₄OH (80:20:2) along with the standards PHS and DHS. **C.** LCBs and ceramides were extracted from the WT, *tsc3Δ* and *tsc3ΔSup4^{m1m2}* mutant strains and analyzed by mass spectrometry. All the species of LCBs and complex sphingolipids were summed before plotting as LCB and ceramides.

The *Sup4^{m1m2}* neither increases basal *in vitro* SPT activity nor does it abolish sphingolipid degradation.

There is the possibility that the increased LCBs and sphingolipids exhibited by the *tsc3ΔSup4^{m1m2}* mutant result from increased expression of one or both of the subunits of the Lcb1p/Lcb2p heterodimer or from a change in the intrinsic enzymatic activity of the heterodimer due, e.g., to a posttranslational modification(s). To investigate levels of expression of the Lcb1p and Lcb2p subunits, microsomes were prepared from the WT, *tsc3Δ* and the *tsc3ΔSup4^{m1m2}* mutants and the Lcb1p and Lcb2p subunits were detected by immunoblotting. The results show that Lcb1p and Lcb2p were expressed at similar levels in the *tsc3ΔSup4^{m1m2}*, *tsc3Δ*, and WT strains (**Figure 3-8B**). Moreover, the suppressor mutations do not appear to change the intrinsic activity of the Lcb1p/Lcb2p heterodimer because the *in vitro* SPT activity of microsomes prepared from *tsc3ΔSup4^{m1m2}* is similar to that in microsomes prepared from *tsc3Δ*. Moreover, SPT activity from both strains displayed the same substrate inhibition profile as the concentration of myristoyl (C14)-CoA in the assay was increased (**Figure 3-8A**). Hence it was concluded that the *Sup4^{m1m2}* mutant does not have elevated Lcb1p-Lcb2p expression nor intrinsically higher SPT activity.

Another possible explanation for the elevated *in vivo* LCBs in the *Sup4^{m1m2}* mutant could be reduced degradation, for example due to mutation in Lcb4p or Dpl1p, the enzymes required for degradation of LCBs. Lcb4p is a long-chain base kinase which generates long-chain base phosphates (62, 75). Dpl1p is the LCB-P lyase that irreversibly cleaves LCB-Ps to ethanolamine phosphate and hexadecanal (75). Deletion of these genes results in increased levels of sphingolipids *in vivo*, allowing very weak suppression of the *tsc3Δ* mutant at 37 °C (**Figure 3-9A**). Thus, *LCB4* or *DPL1* are plausible *Sup4^{m1}*

candidates. To test this, the *tsc3ΔSup4^{m1m2}* mutant was transformed with plasmids expressing wild type Lcb4p or Dpl1p and tested for growth at 37 °C. In each case, the transformants retained their ability to grow at 37 °C similar to the empty vector control (**Figure 3-9B**). Since *Sup4^{m1}* is recessive, these results demonstrate that the *Sup4^{m1}* mutation is not in Lcb4p or Dpl1p and argue that the increase in LCBs and sphingolipids in the *tsc3ΔSup4^{m1m2}* mutant is not because of altered sphingolipid degradation.

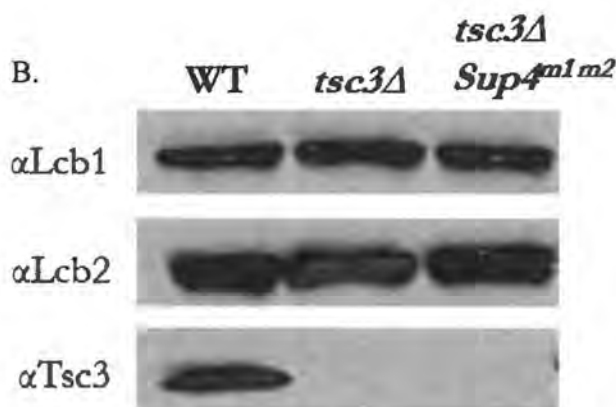
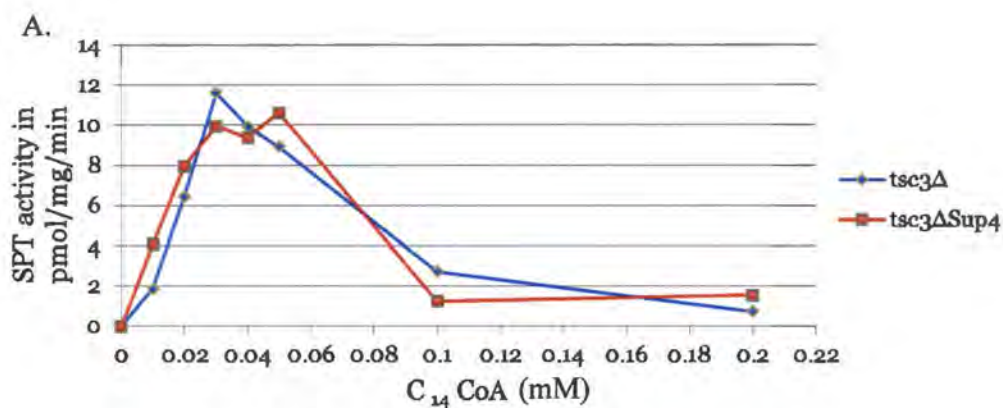


Figure 3-8. *Sup4^{m1m2}* does not increase *in vitro* SPT activity.

A. Microsomes were prepared from the *tsc3Δ* and the *tsc3ΔSup4^{m1m2}* strains and the *in vitro* SPT activity was measured using varying concentrations of C₁₄-CoA (the preferred substrate for the Lcb1p/Lcb2p heterodimer) and 0.2 mg of microsomal protein. B. Lcb1p and Lcb2p were equivalently expressed in the *tsc3Δ* and the *tsc3ΔSup4^{m1m2}* mutants. Logarithmically growing WT, *tsc3Δ* and *tsc3ΔSup4^{m1m2}* mutants were harvested followed by microsome preparation and proteins were resolved by SDS-PAGE. The Lcb1p, Lcb2p, and Tsc3p were detected by immunoblotting with their respective antibodies.

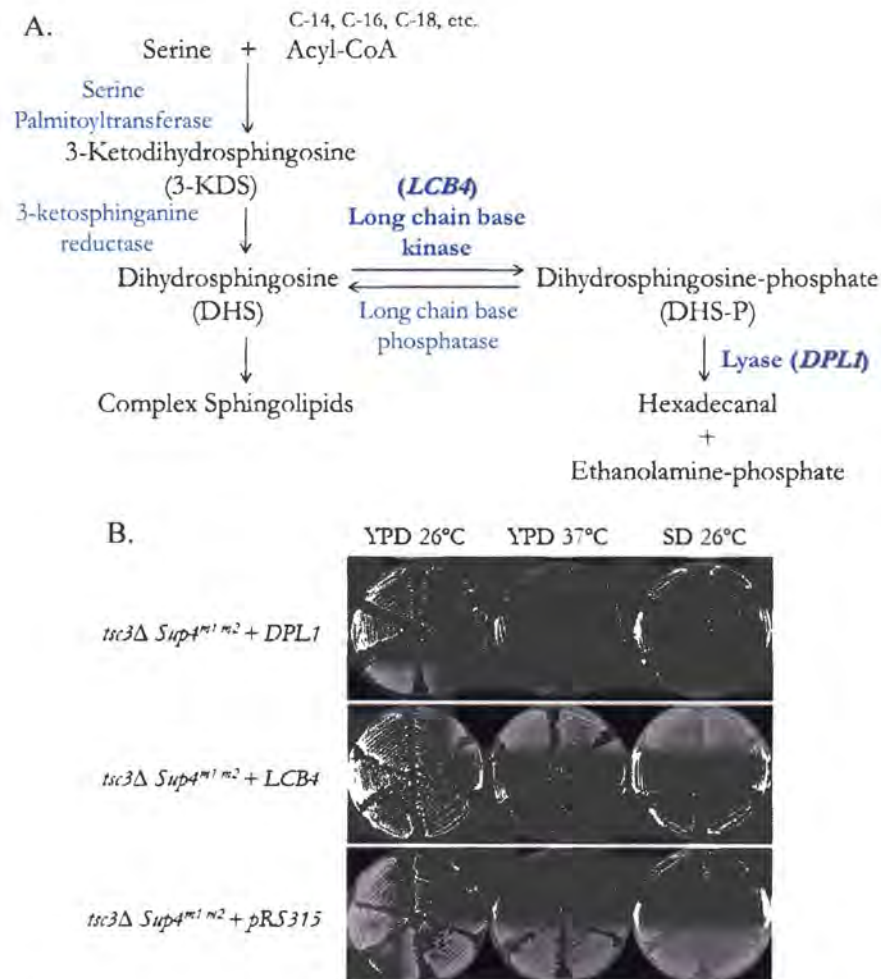


Figure 3-9. *Sup4^{m1}* is not a mutation in the *DPL1* or *LCB4* gene.

A. Cartoon of the sphingolipid degradative pathway showing the steps catalyzed by Lcb4p and Dpl1p. **B.** The *tsc3ΔSup4^{m1m2}* transformants harbouring plasmids expressing either wild type *DPL1* or *LCB4* were streaked on SD-Leu 26 °C, YPD 26 °C, YPD 37 °C and photographed after 3 days.

***Sup4^{m2}* has a mutation in the *CHA4* gene.**

Attempts to identify the wild type *Sup4^{m1}* and *Sup4^{m2}* gene by conventional cloning strategies failed. Hence next generation sequencing was adopted to identify the mutated genes. Specifically, a study was undertaken to compare the genomic sequences of *tsc3ΔSup4^{m1m2}* with *tsc3Δ*. As a positive control, a point mutation (the *ade2-101* allele with a C→T mutation (27)) was introduced in the *tsc3ΔSup4^{m1m2}* mutant by homologous recombination. The *tsc3ΔSup4^{m1m2}ade2-101* did not have any effect on the *Sup4^{m1m2}* phenotype (Figure 3-10). The *tsc3ΔSup4^{m1m2}ade2-101* mutant was crossed with *tsc3Δ* to generate a diploid that was sporulated for tetrad dissection. 30 products of meiosis for each sample (*tsc3ΔSup4^{m1m2}ADE2* and *tsc3Δade2-101*) were obtained. The sample size was 30 to reduce the noise created as a result of spontaneous mutations accumulated during the growth of yeast prior to isolation of genomic DNA. For each DNA pool, the 30 spore colonies were independently inoculated into 5 ml of YPD and grown up to an OD₆₀₀ of 2. Genomic DNA was prepared from 5 ml of each of the 30 cultures and pooled together to prepare the library for sequencing.

Analysis of the sequencing data validated the presence of the control C to T mutation in the ORF of the *ADE2* gene. This mutation was present in 100% of the sequencing reads obtained from the *tsc3Δade2-101* pool and was never present in the sequencing reads from the *tsc3ΔSup4^{m1m2}* pool. In addition, the average number of reads per loci was greater than 700 establishing that the depth of sequencing should be sufficient to identify the *Sup4^{m1}* and the *Sup4^{m2}* mutations. Sequence analysis of the data identified several candidate mutations (present in *tsc3ΔSup4^{m1m2}* and missing in *tsc3Δ*) which are listed in Table 4. These candidates were tested for linkage with the *Sup4^{m1}* and *Sup4^{m2}* mutations using standard meiotic linkage analysis. One candidate displaying

linkage to *Sup4^{m1m2}* had an 'A' deletion in the ORF of the *CHA4* gene. This mutation was present in the *tsc3ΔSup4^{m1m2}* reads >90% of the time and not in reads from *tsc3Δade2-101*. Sanger sequencing of the *CHA4* locus using genomic DNA isolated from the *tsc3ΔSup4^{m1m2}* and the *tsc3Δade2-101* confirmed the presence of the 'A' deletion in the *tsc3ΔSup4^{m1m2}* mutant. The deletion mutation resides in codon 267 of the AAA codon of *CHA4* ORF and results in a truncated non-functional protein (**Figure 3-11A**).

CHA4 was deleted in *tsc3ΔSup4^{m1}* and *tsc3Δ* respectively to test whether the deletion of 'A' in the *CHA4* ORF is the *Sup4^{m1}* or the *Sup4^{m2}* mutation. Deletion of *CHA4* did not allow growth of *tsc3Δ* mutant at 37 °C but enhanced the growth of the *tsc3ΔSup4^{m1}* mutant to similar levels as were seen for the *tsc3ΔSup4^{m1m2}* mutant (**Figure 3-11B**). Moreover, the *tsc3Δcha4Δ* mutant generated suppressors at a higher rate than the *tsc3Δ* single mutant, and similar to the previously observed *tsc3ΔSup4^{m2}* mutant. This suggested that *CHA4* is allelic to *Sup4^{m2}*. To confirm that *CHA4* and *Sup4^{m2}* are allelic, *tsc3ΔSup4^{m1}cha4Δ* was crossed with *tsc3ΔSup4^{m1m2}* and the resulting diploid was tested for growth at 37 °C. As this diploid was homozygous for *tsc3Δ* and *Sup4^{m1}*, if *CHA4* is the wild type allele of *Sup4^{m2}*, then the diploid (*cha4Δ/Sup4^{m2}*) should grow like *tsc3ΔSup4^{m1m2}* at 37 °C. This was the case; the diploid grew like the *tsc3ΔSup4^{m1m2}* mutant at 37 °C (**Figure 3-11C**). Finally, this diploid was sporulated and dissected, and all 4 products of meiosis in every tetrad displayed good growth at 37 °C. Thus it was concluded that the *Sup4^{m2}* mutation resides in the *CHA4* ORF (**Figure 3-11D**).

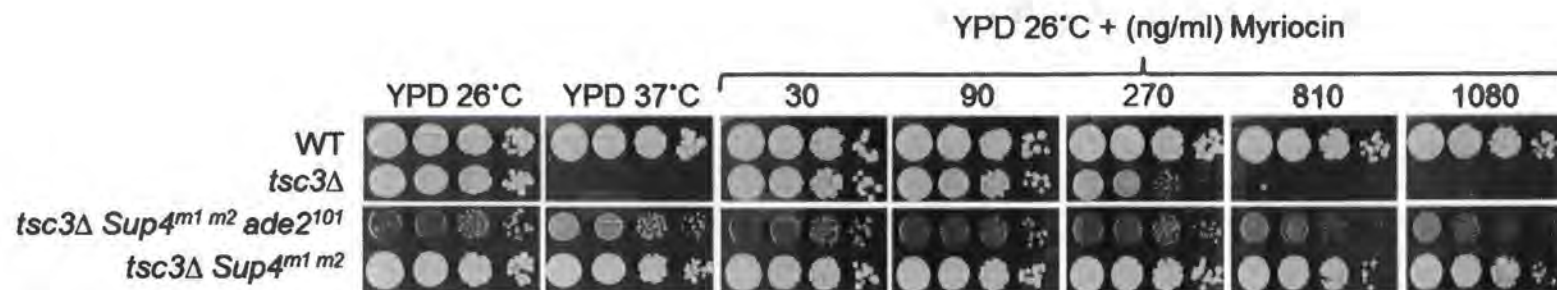


Figure 3-10. Loss of *ADE2* function does not have any effect on the *tsc3ΔSup4^{m1m2}* phenotype.

The growth of *tsc3ΔSup4^{m1m2}ade2-101* was compared with the WT, *tsc3Δ*, and *tsc3ΔSup4^{m1m2}* on YPD 26 °C, YPD 37 °C and YPD 26 °C with increasing concentrations of myriocin. All strains were spotted at an initial OD₆₀₀ of 0.5 and then serially diluted 10 fold. Photographs were taken after 3 days.

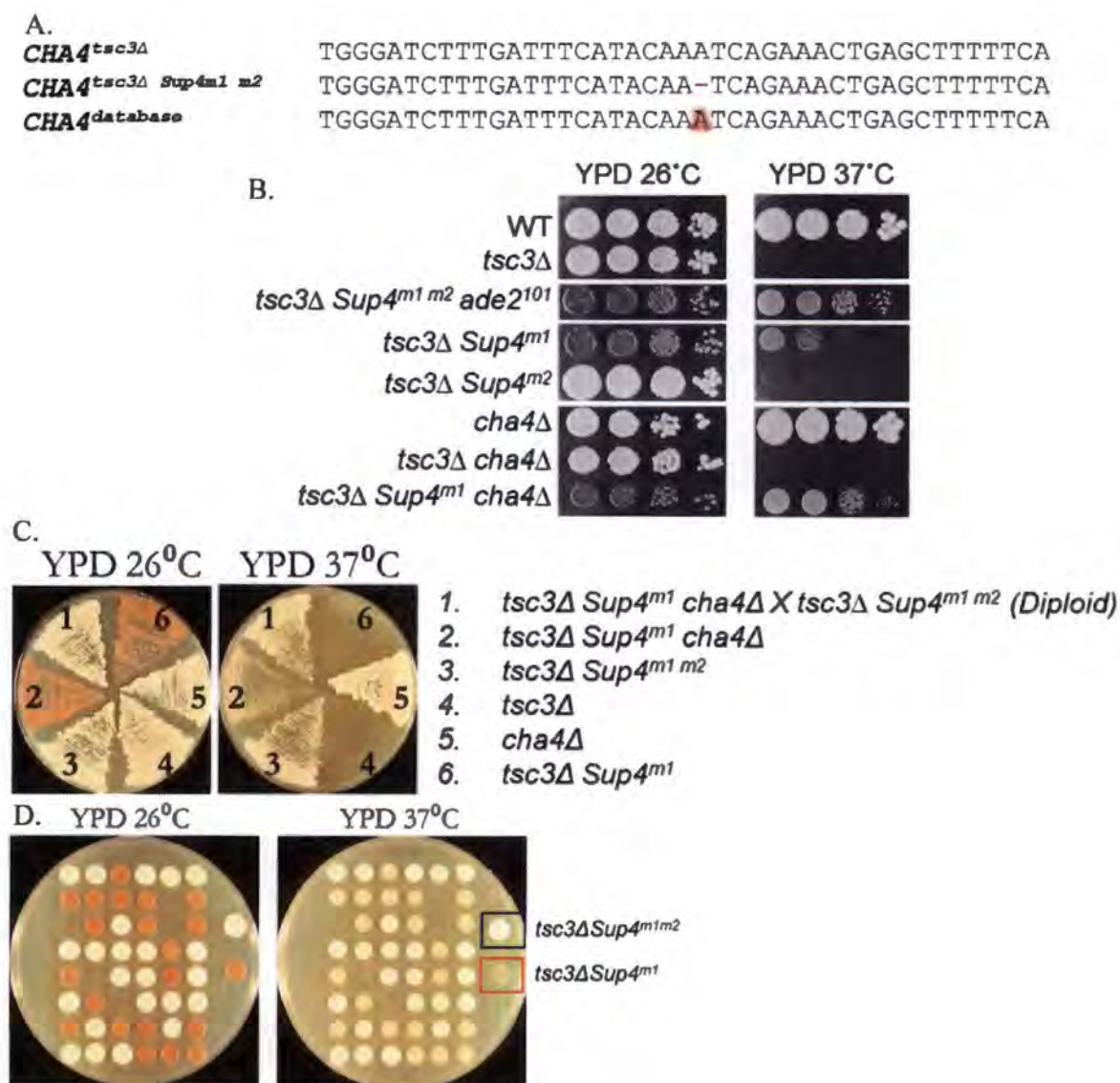


Figure 3-11. *Sup4^{m2}* is a mutation in the *CHA4*.

A. Alignment of the Sanger sequencing data of the “*CHA4*” locus. Genomic DNA was obtained from the *tsc3Δ* and the *tsc3ΔSup4^{m1 m2}*, and the sequencing showed the deletion of an “A” in the ORF of *CHA4* in the *tsc3ΔSup4^{m1 m2}* and not in the *tsc3Δ*. **B.** Deletion of *CHA4* enhanced the growth of *tsc3ΔSup4^{m1}*. The *CHA4* ORF was replaced by the kanamycin marker in *tsc3Δ* and also in the *tsc3ΔSup4^{m1}ade2-101* mutant. The growth of WT, *tsc3Δ*, *tsc3ΔSup4^{m1 m2}ade2-101*, *tsc3ΔSup4^{m1}ade2-101*, *tsc3ΔSup4^{m2}*, *cha4Δ*, *tsc3Δcha4Δ*, and *tsc3ΔSup4^{m1}cha4Δade2101* mutants was compared on YPD at 26 °C and 37 °C. All strains were spotted at an initial OD₆₀₀ of 0.5 and then serially diluted 10 fold. Photographs were taken after 3 days. **C.** *CHA4* is allelic to the *Sup4^{m2}* mutation. The *tsc3ΔSup4^{m1 m2}* was crossed with

the *tsc3ΔSup4^{m1}cha4Δade2-101* and growth of the diploid on YPD at 37 °C. The growth of the diploid was similar to the *tsc3ΔSup4^{m1m2}* mutant at 37 °C. The diploid along with the parental haploids was streaked on YPD 26 °C and 37 °C and photographed after 3 days. **D.** The above mentioned diploid was sporulated and following tetrad dissection and analysis, all the products of meiosis were found to grow strongly on YPD at 37 °C.

Deletion of the *CHA1*, a transcriptional target of *CHA4*, enhances suppression by *Sup4^{mi}* equivalently to *cha4Δ*.

Cha4p is a DNA binding transcriptional activator which activates expression of the *CHA1* gene encoding a mitochondrial L-serine deaminase that is responsible for serine catabolism (5) (43). Due to the mutation in *CHA4*, *CHA1* expression is reduced resulting in increased L-serine levels *in vivo* (61). The high serine levels might thereby provide increased substrate which can be utilized by SPT to increase sphingolipid biosynthesis. Hence, it was investigated whether the loss of Cha1p in *cha4Δ* mutant is sufficient to allow suppression of *tsc3ΔSup4^{mi}* at 37 °C or whether Cha4p might have an additional target(s) that are important for the elevated sphingolipid synthesis in the *tsc3ΔSup4^{mi/m2}* mutant. A *tsc3ΔSup4^{mi}cha1Δ* was generated by knocking out the *CHA1* gene by homologous recombination in the *tsc3ΔSup4^{mi}* mutant. In a serial dilution cell spotting assay on YPD plates at 37 °C, the *tsc3ΔSup4^{mi}cha1Δ* mutant behaved similarly to the *tsc3ΔSup4^{mi}cha4Δ* and *tsc3ΔSup4^{mi/m2}* mutants (**Figure 3-12A**). This indicated that the loss of Cha1p expression due to *CHA4* deletion is indeed sufficient for suppression of *tsc3ΔSup4^{mi}* by *cha4Δ*. However, it is worth noting that the *cha4Δtsc3Δ* mutant showed significantly higher myriocin resistance than the *cha1Δtsc3Δ* mutant (**Figure 3-12B**). This suggests that the *CHA4* deletion may impact intracellular serine more than does simple loss of Cha1p function. As Cha4p is also a negative regulator of *SER3*, a gene involved in serine biosynthesis, deletion of *CHA4* also elevates serine biosynthesis (43) which may account for the higher myriocin resistance of the *cha4Δtsc3Δ* mutant compared to the *cha1Δtsc3Δ* mutant.

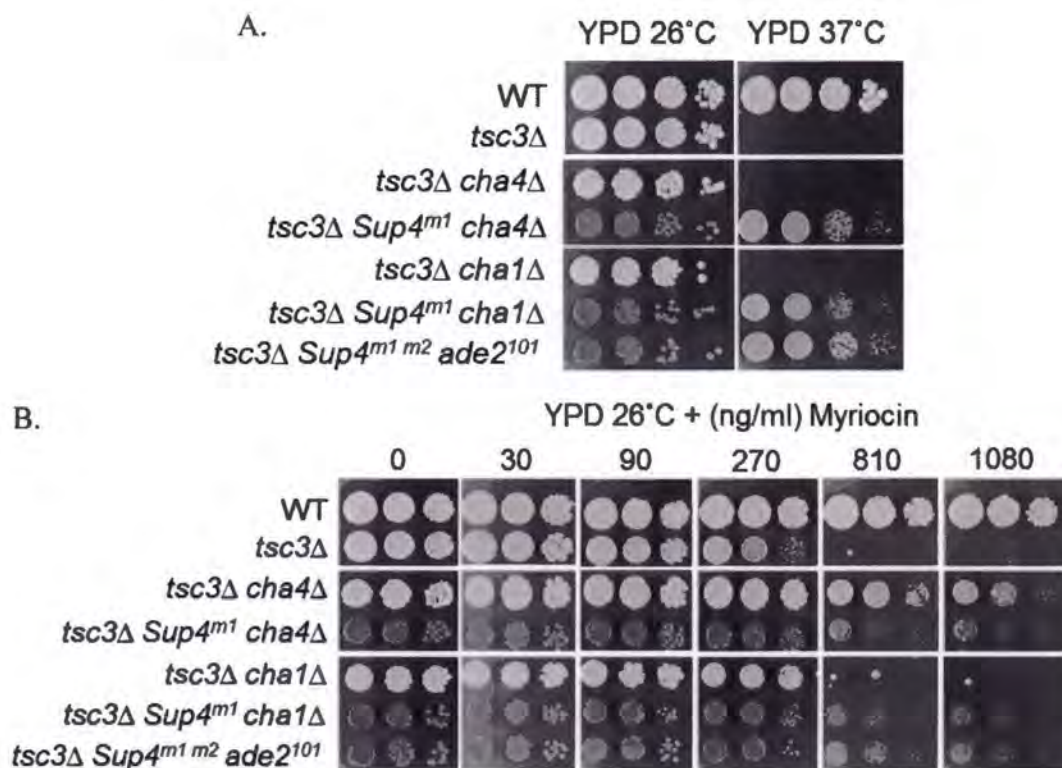


Figure 3-12. Deletion of the *CHA1*, a transcriptional target of Cha4p, enhances suppression by *Sup4^{m1}* equivalently to *cha4Δ*.

A. Deletion of *CHA1* increased the growth rate of *tsc3ΔSup4^{m1}* on YPD at 37 °C. **B.** The *tsc3ΔSup4^{m1}cha4Δ* and the *tsc3ΔSup4^{m1}cha1Δ* have similar levels of myriocin resistance. The WT, *tsc3Δ*, *tsc3Δcha4Δ*, *tsc3ΔSup4^{m1}cha4Δade2-101*, *tsc3Δcha1Δ*, *tsc3ΔSup4^{m1}cha1Δade2-101*, and the *tsc3ΔSup4^{m1 m2}ade2-101* mutants were tested for growth on YPD at 26 °C and 37 °C as well as on YPD at 26 °C with increasing concentrations of myriocin. All strains were spotted at an initial OD₆₀₀ of 0.5 and then serially diluted 10 fold. Photographs were taken after 3 days.

The *CHA4* deletion results in increased serine uptake.

It was observed that though the *tsc3ΔSup4^{m1m2}* mutant grows robustly at 37 °C on rich media, it fails to do the same on minimal media. This result, together with the observation that the *CHA1* deletion alters intracellular serine (13), raised the possibility that extracellular serine (higher in rich media (YPD) than in minimal media (SD)) might explain the difference. Indeed, extracellular serine rescued the temperature sensitivity of the *tsc3Δ* mutant and the rescue was enhanced in the presence of the *Sup4^{m1m2}* mutations. Moreover, addition of serine to minimal media eliminated the need for *Sup4^{m1}* and allowed growth of the *tsc3Δcha4Δ* at 37 °C at the same rate as the *tsc3ΔSup4^{m1m2}* mutant (**Figure 3-13**). This suggested that the *Sup4^{m1}* mutation might be involved in serine uptake. To investigate this further, serine uptake using ³H serine was measured in the *tsc3Δcha4Δ*, *tsc3ΔSup4^{m1}*, *tsc3ΔSup4^{m1m2}*, and *tsc3Δ* mutants. It was found that *tsc3ΔSup4^{m1m2}* has the highest serine uptake rate followed by *tsc3Δcha4Δ* whereas *tsc3ΔSup4^{m1}* and *tsc3Δ* have comparable serine uptake levels providing evidence that deletion of *CHA4* and not *Sup4^{m1}* results in increased uptake of serine for suppression of *tsc3Δ* on serine supplemented minimal media at 37 °C (**Figure 3-14A**). This result was further validated by measuring and comparing the intracellular serine levels in the WT, *tsc3Δ*, *tsc3ΔSup4^{m1m2}*, *tsc3ΔSup4^{m1}* and the *tsc3Δcha4Δ* mutant. The intracellular free serine level was high in the *tsc3ΔSup4^{m1m2}* and the *tsc3Δcha4Δ* whereas in the WT, *tsc3Δ*, and *tsc3ΔSup4^{m1}*, the levels were low (**Figure 3-14B**), confirming that deletion of *CHA4* and not *Sup4^{m1}* results in the high intracellular serine accumulation that apparently accounts for the better suppression of *tsc3ΔSup4^{m1}* at 37 °C. These data also show that Tsc3p influences serine uptake by *cha4Δ* suggesting that low SPT activity causes reduced serine uptake. Taken together, these studies suggest that suppression of *tsc3Δ* at 37 °C by

the *Sup4^{m1m2}* mutations involves both higher uptake and decreased turnover of serine. The rescue of the temperature sensitivity of *ts3Δ* on minimal media at 37 °C by deletion of *CHA1* at the same serine concentrations (**Figure 3-15**) provides additional evidence in support of Cha4p-Cha1p mediated regulation of sphingolipid biosynthesis.

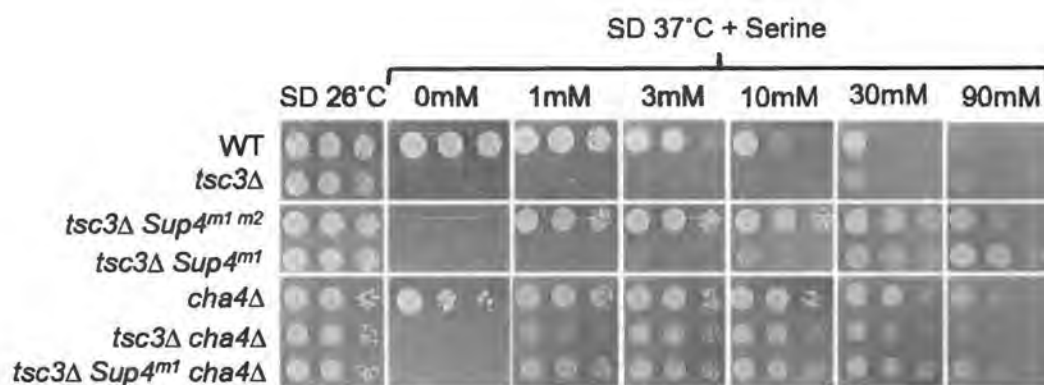


Figure 3-13. In the absence of the *Sup4^{m1}* mutation, addition of serine rescues the growth of *cha4Δtsc3Δ* on SD at 37 °C.

The WT, *tsc3Δ*, *tsc3ΔSup4^{m1 m2}ade2-101*, *tsc3ΔSup4^{m1}ade2-101*, *cha4Δ*, *tsc3Δcha4Δ*, and the *tsc3ΔSup4^{m1}cha4Δade2-101* mutants were tested for growth on SD at 26 °C and 37 °C, and on SD at 37 °C with increasing concentrations of serine. All strains were spotted at an initial OD₆₀₀ of 0.5 and then serially diluted 10 fold. Photographs were taken after 3 days.

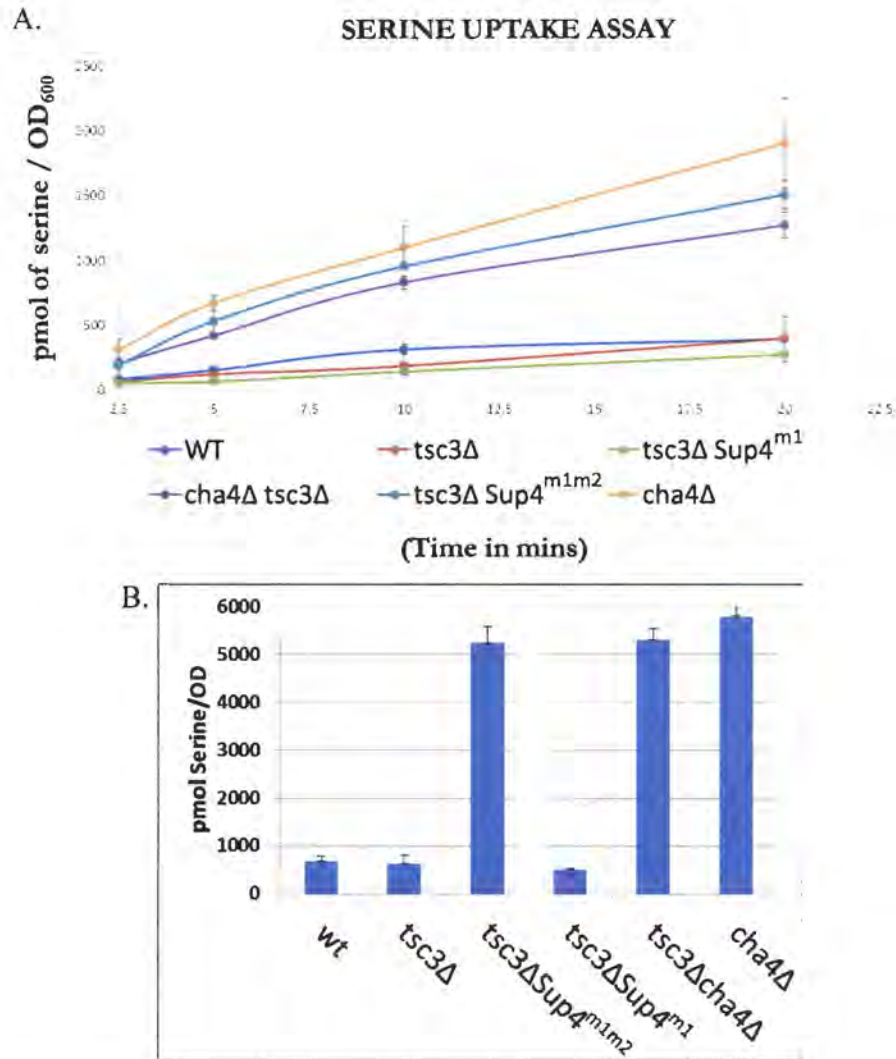


Figure 3-14. *CHA4* deletion results in increased serine uptake and high intracellular serine levels.

A. Serine uptake was measured using WT, *tsc3Δ*, *tsc3ΔSup4^{m1}ade2-101*, *tsc3Δcha4Δ*, *tsc3ΔSup4^{m1m2}*, and *cha4Δ* mutants. 10 OD₆₀₀ units of logarithmically growing cells were harvested and washed with dH₂O and 50 mM Sodium Citrate (SC) buffer. Cells were suspended in the SC buffer at a concentration of 2 OD₆₀₀/ml and a mixture of cold and radioactive ³H serine was added. Equal amounts of culture were taken at 2.5, 5 10, and 20 min and the cells were recovered by filtration and washed 2 times with the SC buffer. The filter papers were dried and the radioactivity was measured using a scintillation counter. B. The above mentioned strains were also used for extraction and measurement of the free intracellular serine as described in the materials and methods.

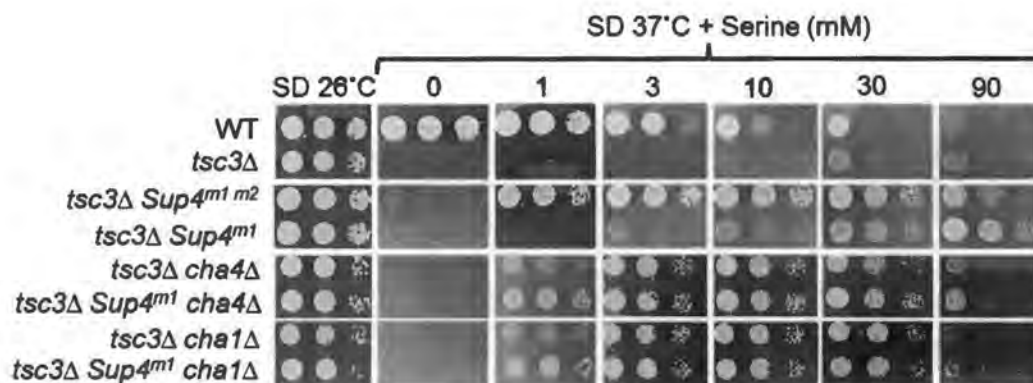


Figure 3-15. In the absence of the *Sup4^{m1}* mutation, deletion of *CHA1* also rescued the temperature sensitivity of *tsc3Δ* at 37 °C on minimal media at serine concentrations similar to *cha4Δtsc3Δ*.

The WT, *tsc3Δ*, *tsc3ΔSup4^{m1m2}ade2-101*, *tsc3ΔSup4^{m1}ade2-101*, *tsc3Δcha4Δ*, *tsc3ΔSup4^{m1}cha4Δade2-101*, *tsc3Δcha1Δ* and the *tsc3ΔSup4^{m1}cha1Δade2-101* mutants were tested for growth on SD at 26 °C and 37 °C, and on SD at 37 °C with increasing concentrations of serine. All strains were spotted at an initial OD₆₀₀ of 0.5 and then serially diluted 10 fold. Photographs were taken after 3 days.

Deletion of *CHA4* influences the *Sup4^{mi}* mutation and the Lcb1p-ΔTMD1 equivalently but loss of the *ORMs* is not similar to the *Sup^{mi}* mutation.

It was observed that the *tsc3ΔSup4^{mi}* mutant grows similarly to the *LCB1-ΔTMD1tsc3Δ* mutant on YPD at 37 °C (**Figure 3-16A, rows 4 and 6**). This invokes the hypothesis that deletion of TMD1 of Lcb1p is equivalent to *Sup4^{mi}* and even raises the possibility that the *Sup4^{mi}* mutation might alter the topology of Lcb1p-TMD1. To investigate the relationship between the Lcb1p-ΔTMD1 and *Sup4^{mi}* mutations, the effect of deleting *CHA4* in the *LCB1-ΔTMD1tsc3Δ* mutant was examined. The results showed that growth of the *LCB1-ΔTMD1tsc3Δ* mutant at 37 °C was enhanced by *CHA4* deletion comparably to the *tsc3ΔSup4^{mi}* mutant (**Figure 3-16A, rows 3 and 7**). Moreover, the *LCB1-ΔTMD1tsc3Δcha4Δ* mutant also exhibited high myriocin resistance similar to that of the *tsc3ΔSup4^{mi}cha4Δ* mutant (**Figure 3-16B, rows 3 and 7**). Thus, deletion of *CHA4* equivalently influences the *Sup4^{mi}* mutation and the Lcb1p-ΔTMD1. As discussed above, the Orms bind to TMD1 of Lcb1p and regulate SPT activity, but deletion of TMD1 results in better suppression of *tsc3Δ* than does deletion of the Orms. As the *CHA4* deletion influences the *Sup4^{mi}* mutation and the Lcb1p-ΔTMD1 equivalently, it was investigated whether the *Sup4^{mi}* mutation influences the topology of TMD1 of Lcb1p. For example, if the *Sup4^{mi}* mutation prevents insertion of TMD1 into the membrane, it might behave like the Lcb1p-ΔTMD1. To determine whether the N-terminus of Lcb1p resides in the ER lumen in the *Sup4^{mi}* mutant, a plasmid expressing N-terminally GC-tagged Lcb1p (GC @ 4th codon) was introduced into the mutant strain. The results show that GC cassette on the N-terminus of Lcb1p (30) is glycosylated to produce multiple bands with reduced electrophoretic mobility (**Figure 3-16C, lane 1**) whereas the same mutant strain expressing the Lcb1p plasmid without the GC cassette does not have any

multiple bands (**Figure 3-16C, lane 2**). These results indicate that the *Sup4^{mi}* mutation is not grossly altering the membrane topology of Lcb1p-TMD1.

As was mentioned earlier, the suppressor screen that identified *Sup4^{mi/m2}* was conducted in an *orm1Δorm2Δtsc3Δ* mutant. However, the Orms do not influence suppression (**Figure 3-16A, compare rows 3 and 9**). It is nonetheless possible that the *Sup4^{mi}* mutation prevents the Orms from regulating even when they are present. If this were the case, then deletion of *CHA4* would be expected to enhance suppression of the *orm1Δorm2Δtsc3Δ* mutant and allow it to grow similarly to the *tsc3ΔSup4^{mi}cha4Δ* mutant. Although deletion of *CHA4* does improve both growth at 37 °C and resistance to myriocin of the *orm1Δorm2Δtsc3Δ* mutant (**Figures 3-16A, lane 10; 3-16B, lane 10**), both phenotypes are less robust than the *tsc3ΔSup4^{mi}cha4Δ* mutant (**Figures 3-16A, lane 3 and 3-16B, lane 3**). Taken together, the data show that deletion of *CHA4* influences the *Sup4^{mi}* mutation and the Lcb1p-ΔTMD1 equivalently but that loss of the *ORMs* is not equivalent to the *Sup^{mi}* mutation and thus that the *Sup4^{mi}* is regulating sphingolipid biosynthesis through an *ORM* independent pathway.

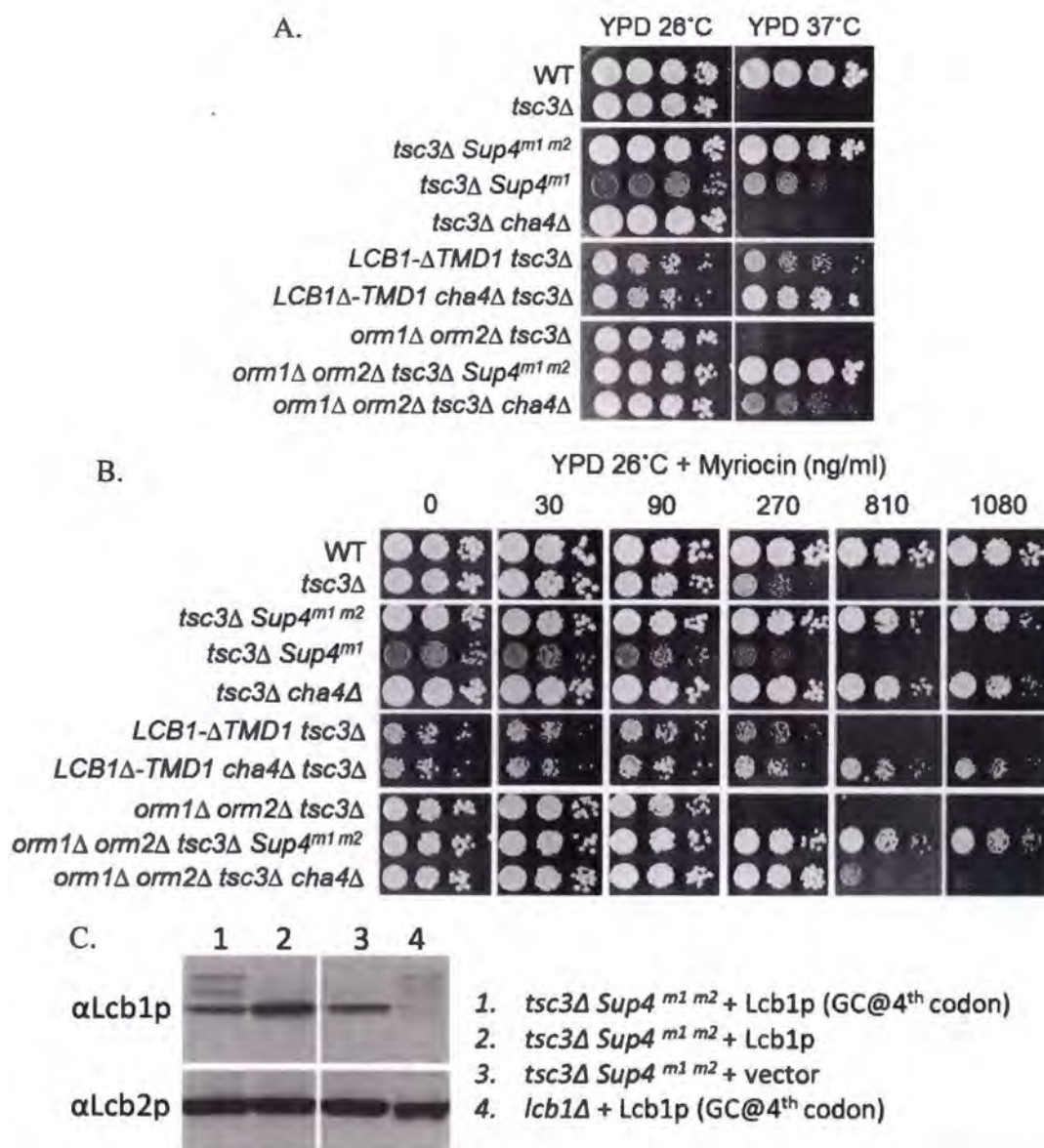


Figure 3-16. Deletion of *CHA4* influences the *Sup4^{m1}* mutation and the Lcb1p-ΔTMD1 equivalently but the *Sup^{m1}* mutation does not behave like an *orm1Δorm2Δ* mutant.

A. Deletion of either the TMD1 of Lcb1p or the *ORMs* rescued the growth defect of *cha4Δtsc3Δ* on YPD at 37 °C. **B.** Deletion of *CHA4* enhances the myriocin resistance of the *orm1Δorm2Δtsc3Δ* and the *LCB1-ΔTMD1tsc3Δ* mutant. The WT, *tsc3Δ*, *tsc3ΔSup4^{m1 m2}*, *tsc3ΔSup4^{m1}ade2-101*, *tsc3Δcha4Δ*, *LCB1-ΔTMD1tsc3Δ*, *LCB1-ΔTMD1cha4Δtsc3Δ*, *orm1Δorm2Δtsc3Δ*, *orm1Δorm2Δtsc3ΔSup4^{m1 m2}*, and the *orm1Δorm2Δtsc3Δcha4Δ* mutants were tested for growth on YPD at 26 °C and 37 °C, and also on YPD at 26 °C with increasing concentrations of myriocin. All strains for figure 3-16A

were spotted at an initial OD₆₀₀ of 0.5 whereas the strains for figure 3-16B were spotted at an initial OD₆₀₀ of 0.05 and then serially diluted 10 fold. Photographs were taken after 3 days. C. Lcb1p with the glycosylation reporter cassette (GC) at the 4th codon was expressed in the *tsc3ΔSup4^{m1m2}ade2-101* mutant. Note, the mutant also has endogenous Lcb1p protein which cannot get glycosylated. Hence, as control Lcb1p without any GC cassette (lane 2) or the empty vector (lane 3) was also expressed in the same strain to compare the percentage of glycosylated Lcb1p versus the non-glycosylated Lcb1p. The lane 4 contains microsomal proteins from *lcb1Δ* mutant expressing the same Lcb1p plasmid with the glycosylation reporter cassette (GC) at the 4th codon (30). All the strains were logarithmically grown and microsomal proteins were resolved by SDS-PAGE. Lcb1p and Lcb2p were detected by immunoblotting with their respective antibodies. The presence of multiple bands in the Lcb1p blot having the GC@4th codon (lane 1 as well as in lane 4, which has been characterized in previous studies) shows that the N – terminus of Lcb1p is glycosylated in the presence of *Sup4^{m1m2}* mutation.

Vma13p is needed for the *Sup4^{m1m2}* mediated regulation of sphingolipid biosynthesis.

A single nucleotide polymorphism was observed in the promoter region of the *VMA13* gene in 88% of the reads obtained from the *tsc3ΔSup4^{m1m2}* mutant and not in the reads from the *tsc3Δade2-101* mutants making it a candidate for the *Sup4^{m1}* mutation. The *VMA13* gene encodes a small subunit of the V1 peripheral membrane domain of the vacuolar H⁺-ATPase (V-ATPase) (39). V-ATPases are electrogenic proton pumps present throughout the endomembrane system that regulate vesicular transport and the function of various transporters directly or indirectly (23). Although the mutation was not in the *VMA13* ORF, it might affect its expression. Alternatively, this mutation might simply be linked to the actual *Sup4^{m1}* mutation and therefore be enriched in the reads obtained from the *tsc3ΔSup4^{m1m2}* mutant. To determine whether the *Sup4^{m1}* mutation is linked to *VMA13*, a *vma13Δ::KANtsc3Δ* strain was generated by replacing the *TSC3* gene with *URA3* in the *vma13Δ::KAN* mutant and crossed with the *tsc3ΔSup4^{m1m2}* for studying the linkage with *Sup4^{m1}*. Following sporulation and tetrad dissection, a high level of non-viable spores were observed. Detailed analysis of the spores revealed that most of the spores that failed to germinate were the *vma13Δtsc3ΔSup4^{m1m2}* mutants suggesting that deletion of *VMA13* compromises the ability of the *Sup4^{m1m2}* spores to germinate. Further investigation revealed that the *vma13Δtsc3ΔSup4^{m1m2}* (*VMA13* was replaced by the kanamycin cassette in the *tsc3ΔSup4^{m1m2}* mutant) fail to grow on YPD at 37 °C and that the effect is recessive, as it was rescued by expressing wild type Vma13p (Figure 3-17A). It was also found that the *vma13Δtsc3Δ* double mutant is more sensitive to myriocin than the *tsc3Δ* single mutant as well as that the *vma13Δ* mutant is more myriocin sensitive than wild-type. This suggests that Vma13p may be required for

normal activity of both the SPT heterodimer and heterotrimer (**Figure 3-17B**). Of course, we have not ruled out the possibility that optimal sphingolipids are required for viability of the *vma13Δ* mutant. Interestingly, the serine mediated rescue of temperature sensitivity of the *tsc3ΔSup4^{m1m2}* was impaired in the absence of *VMA13* (**Figure 3-18A**), raising the possibility that loss of *VMA13* inhibits serine uptake or utilization. However, a serine uptake assay showed no significant difference between the *tsc3ΔSup4^{m1m2}* and the *vma13Δtsc3ΔSup4^{m1m2}* mutants (**Figure 3-18B**). Moreover, the intracellular free serine levels were also high in the *vma13Δtsc3ΔSup4^{m1m2}* mutant compared to the *vma13Δtsc3Δ* mutant (**Figure 3-18C**). These data together indicate that serine uptake is not impaired in the *vma13Δtsc3ΔSup4^{m1m2}* mutant and show that *VMA13* plays some other role that is critical for growth of the *tsc3ΔSup4^{m1m2}* mutant at 37 °C.

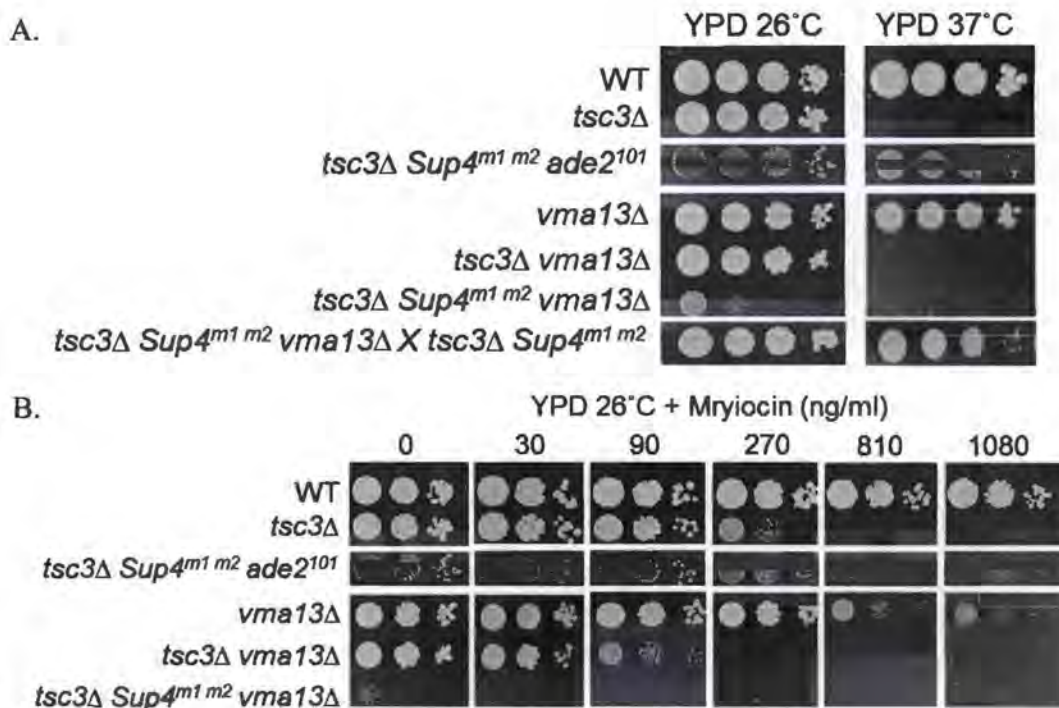
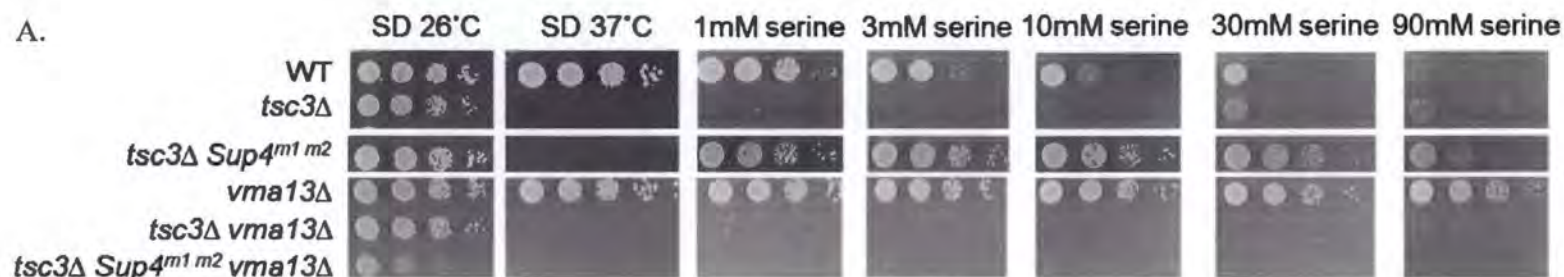
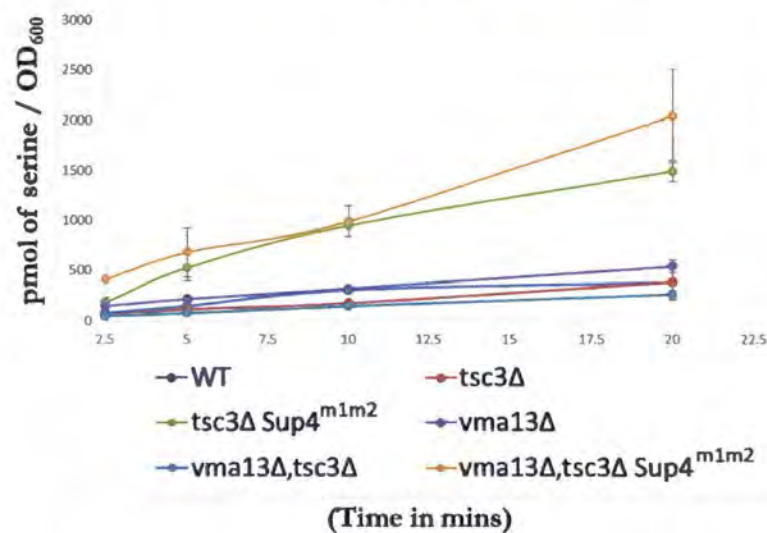


Figure 3-17. The *tsc3ΔSup4^{m1m2}vma13Δ* mutant failed to grow at 37 °C and the phenotype was reversed by wild type Vma13p.

A. Deletion of *VMA13* inhibited the growth of *tsc3ΔSup4^{m1m2}* at 37 °C. Expressing the wild type *VMA13* rescued the growth defect of *tsc3ΔSup4^{m1m2}vma13Δ* on YPD at 37 °C. The *tsc3ΔSup4^{m1m2}vma13Δ ade2-101* was crossed with the *tsc3ΔSup4^{m1m2}* and the diploid was tested for growth on YPD at 37 °C. The WT, *tsc3Δ*, *tsc3ΔSup4^{m1m2}ade2-101*, *vma13Δ*, *tsc3Δvma13Δ*, and the *tsc3ΔSup4^{m1m2}vma13Δade2-101* were tested for growth on YPD at 26 °C and 37 °C. All strains were spotted at an initial OD₆₀₀ of 0.5 and then serially diluted 10 fold. Photographs were taken after 3 days of growth. **B.** The *tsc3Δvma13Δ* mutant is more sensitive to myriocin compared to the *tsc3Δ* mutant. The WT, *tsc3Δ*, *tsc3ΔSup4^{m1m2}ade2-101*, *vma13Δ*, *tsc3Δvma13Δ*, and the *tsc3ΔSup4^{m1m2}vma13Δade2-101* were tested for growth on YPD with myriocin at 26 °C. All strains were spotted at an initial OD₆₀₀ of 0.05 and then serially diluted 10 fold. Photographs were taken after 3 days.



B. SERINE UPTAKE ASSAY



C.

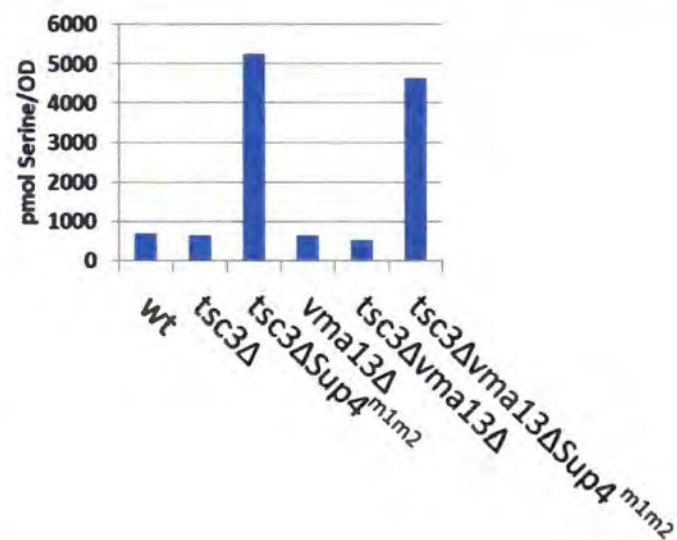


Figure 3-18. Deletion of the *VMA13* does not interfere with serine uptake of *tsc3ΔSup4^{m1m2}*.

A. Addition of serine did not rescue the growth defect of *tsc3ΔSup4^{m1m2}vma13Δade2-101* mutant at 37 °C. The WT, *tsc3Δ*, *tsc3ΔSup4^{m1m2}*, *vma13Δ*, *tsc3Δvma13Δ*, and the *tsc3ΔSup4^{m1m2}vma13Δade2-101* were tested for growth on SD at

26 °C and 37 °C, and also on SD at 37 °C with increasing concentrations of serine. All strains were spotted at an initial OD₆₀₀ of 0.5 and then serially diluted 10 fold. Photographs were taken after 3 days. **B.** The *tsc3ΔSup4^{m1m2}vma13Δ* mutant as well as the *tsc3ΔSup4^{m1m2}* mutant has similar serine uptake rates. 10 OD₆₀₀ units of logarithmically growing cells were harvested followed by washing with dH₂O and 50 mM sodium citrate (SC) buffer. Cells were suspended in the SC buffer at a concentration of 2 OD₆₀₀/ml and a mixture of cold and radioactive ³H serine (10 µCi/mL) was added. Equal amounts of culture were pipetted (at 2.5, 5, 10, and 20 min) onto filters and immediately washed 2 times with SC buffer. The filter papers were dried and the radioactivity was measured using scintillation counter. **C.** The above mentioned strains were also used for extraction and measurement of the free intracellular serine levels by following the protocol for measurement of intracellular amino acids as described in the materials and methods.

DISCUSSION:

The isolation and characterization of recessive suppressors of the temperature sensitivity of an *orm1Δorm2Δtsc3Δ* mutant revealed novel mechanisms involved in regulation of sphingolipid biosynthesis. In this study, intracellular levels of serine have been found to regulate sphingolipid biosynthesis independently of the Orm mediated regulation of SPT. The *tsc3ΔSup4^{m1m2}* exhibited high myriocin resistance because of increased levels of intracellular LCBs and ceramides, indicating loss of function of negative regulators of sphingolipid biosynthetic pathway other than the *ORMs*. Genetic analysis showed that the *tsc3ΔSup4^{m1m2}* mutant has two unlinked mutations, both of which are required for good growth at 37 °C. The *Sup4^{m1}* mutation by itself supported modest growth of *tsc3Δ* at 37 °C but provided only weak myriocin resistance very similar to that of the *tsc3Δ* mutant. On the other hand, the *tsc3ΔSup4^{m2}* mutation by itself did not allow growth of *tsc3Δ* at 37 °C but conferred strong myriocin resistance compared to the *tsc3Δ* mutant. This suggested that both the *Sup4^{m1}* and *Sup4^{m2}* may directly or indirectly regulate SPT. The role of *Sup4^{m2}* was confirmed once it was established as a mutation in the *CHA4* ORF resulting in highly elevated intracellular serine.

The expression of Lcb1p and Lcb2p was same in the *tsc3ΔSup4^{m1m2}* compared to WT and *tsc3Δ* indicating that neither *Sup4^{m1}* nor *CHA4* is involved in regulating Lcb1p or Lcb2p stability. Moreover, neither *Sup4^{m1}* nor the *CHA4* deletion increased *in vitro* SPT activity of the heterodimer unlike previously characterized dominant mutations in Lcb2p (60). It is important to note that the standard SPT assays are performed with saturating concentrations of serine; hence any changes in SPT activity caused from changes in serine affinity might not be apparent in the results from these assays.

However, the *Sup4^{m1m2}* mutations are not present in the Lcb1p or Lcb2p, thus ruling out the possibility that *Sup4^{m1}* is directly affecting affinity of the heterodimer for serine. Studies clearly show that *Sup4^{m2}* is a mutation in Cha4p, which breaks down serine in the mitochondria, and that the intracellular serine levels are high in the *tsc3ΔSup4^{m1m2}* mutant (**Figure 3-14B**) and raise the possibility that *Sup4^{m1}* is enabling the heterodimer to utilize the serine more efficiently.

The possibility that growth of the *tsc3ΔSup4^{m1m2}* mutant at 37 °C was due to decreased turnover of the LCBs was ruled out. In particular, since Lcb4p phosphorylates the LCBs and Dpl1p irreversibly cleaves the LCB-*Ps* (75) (62) and deletion of either of these genes allows modest growth of *tsc3Δ* at 37 °C, the possibility that the *Sup4^{m1}* mutation was in *LCB4* or *DPL1* was investigated. If these were the case, since the *Sup4^{m1}* mutation is recessive, introduction of the WT *LCB4* or *DPL1* would reverse the growth of *tsc3ΔSup4^{m1m2}* at 37 °C. Since expression of neither Lcb4p nor Dpl1p affected suppression, it suggests that the *Sup4^{m1}* is apparently not impairing sphingolipid degradation.

Cha4p is the DNA binding transcriptional activator of the catabolic L-serine deaminase Cha1p (43). It also activates transcription of *SRG1* which in turn imposes a transcriptional interference on the *SER3* gene, which encodes the serine biosynthetic enzyme 3-phosphoglycerate dehydrogenase (58). Thus, the mutation in *CHA4* causes elevated serine biosynthesis and reduced serine degradation. Presumably, given that SPT has a relatively low affinity for serine (K_M of ~4 mM) (13), the increased levels of intracellular L-serine (**Figure 3-14B**) result in increased *in vivo* SPT activity. In addition to regulating Cha1p and Ser3p, Cha4p is reported to transcriptionally regulate several

additional genes (89). However, deletion of *CHA1* confers the same level of myriocin resistance and growth at 37 °C to the *tsc3ΔSup4^{mi}* mutant as does the deletion of *CHA4*, and thus the loss of mitochondrial serine degradation is adequate to explain the effects of the *cha4Δ* on sphingolipid biosynthesis. Cowart et al. have shown that heat stress upregulates acute sphingolipid synthesis and that this acts as signal for up-regulation of *CHA1* expression (13, 61). Our finding is in accordance with this observation and indicates that deletion of *CHA4* disrupts the signaling pathway resulting in loss of the sensor and as a result Cha1p is not expressed resulting in increased serine levels and upregulated LCB production at elevated temperatures (37 °C). However, deletion of *CHA4* also results in increased serine uptake which is unexpected as the intracellular serine concentrations are already elevated because of loss of Cha1p expression. This data suggests that Cha4p may have some other unknown function(s) involving amino acid uptake. It is interesting to note that Gap1p, a general amino acid permease that takes up serine as one of the many substrates, is reported to have a positive genetic correlation with Lcb1p subunit of SPT (10, 11). Moreover, the observation that the increased serine uptake resulting from deletion of *CHA4* is dependent on Tsc3p, suggests that the cellular sphingolipid levels influence the rate of serine uptake.

Previous studies (13) have also shown that extracellular serine is needed for increased LCB and sphingolipid synthesis upon heat stress in WT yeast. In this study it has been confirmed that the same occurs in the *tsc3Δ* mutant at 37 °C and thus that the heterodimer (Lcb1p-Lcb2p), independently of Tsc3p, has the capability to utilize increased extracellular serine upon heat stress. Moreover, the *CHA4* deletion enhanced the growth rescue of *tsc3Δ* on 1 mM serine at 37 °C (**Figure 3-13 row 2 and 6**)

indicating that the level of serine available in the growth media is not sufficient for increasing sphingolipid biosynthesis in absence of Tsc3p. Rather, coupling of extracellular serine availability with inhibition of intracellular serine degradation is important for increased LCB and sphingolipid production in a *tsc3Δ* mutant upon heat stress.

The *CHA4* deletion is not sufficient to rescue the temperature sensitivity of *tsc3Δ* without the *Sup4^{ml}* mutation or serine supplementation. This suggests that serine supplementation can eliminate the need of the *Sup4^{ml}* mutation raising the possibility that the *Sup4^{ml}* mutation is also involved in serine uptake. However, our data show that the *Sup4^{ml}* mutation is not involved in serine uptake and further corroborates the possibility that the *Sup4^{ml}* mutation somehow results in better utilization of the intracellular serine generated because of *CHA4* deletion.

The *tsc3ΔSup4^{ml}* mutant as well as the *LCB1-ΔTMD1tsc3Δ* mutant has similar growth rates at 37 °C. Moreover deletion of *CHA4* was additive to both the mutant strains in terms of myriocin resistance and growth at 37 °C. This suggested that may be having the *Sup4^{ml}* mutation might be equivalent to deletion of TMD1 of Lcb1p. However, the *orm1Δorm2Δcha4Δtsc3Δ* have poor growth compared to *tsc3ΔSup4^{ml}cha4Δ* at 37 °C indicating that the mechanism of regulation of sphingolipid biosynthesis by the *Sup4^{ml}* is different from the known Orm mediated regulation even though the TMD1 of Lcb1p might be playing a common role. It also indicates that the *Sup4^{ml}* mutation is not upstream of the Orms. This was further supported by the result that an *orm1Δorm2Δtsc3ΔSup4^{mlm2}* has a growth rate similar to *tsc3ΔSup4^{mlm2}*.

Previous studies showed that amino acid uptake in yeast proceeds by proton co-transport according to potential across the plasma membrane (13, 83). It was observed that the deletion of *VMA13* inhibited growth of the *tsc3ΔSup4^{m1m2}* at 37 °C, and it can be reverted by expressing the wild type Vma13p. This suggested that functional Vma13p is essential for *Sup4^{m1m2}* mediated growth rescue of *tsc3Δ* at 37 °C. It was observed that *vma13Δtsc3Δ* is myriocin sensitive compared to *tsc3Δ* and addition of serine did not rescue the temperature sensitivity of the *vma13Δtsc3Δ* or the *vma13Δtsc3ΔSup4^{m1m2}* suggesting that in the absence of Vma13p, the *Sup4^{m1m2}* mediated growth rescue of *tsc3Δ* is abolished. However, the serine uptake was unaffected in the *vma13Δtsc3ΔSup4^{m1m2}* mutant indicating that deletion of *VMA13* is not interrupting amino acid (serine) uptake, rather loss of Vma13p is affecting *Sup4^{m1m2}* mediated growth rescue of *tsc3Δ* by some other means.

Altogether these data confirm that other than the *ORMs*, *Sup4^{m1}* and *CHA4* are involved in regulation of sphingolipid biosynthesis by modulating the intracellular serine concentrations. It can be speculated that *Sup4^{m1}* have a direct role which is mediated by TMD1 of Lcb1p and is separate from Orm mediated regulation. However, it will be important to identify the gene having the *Sup4^{m1}* mutation for further characterization. This can be achieved by performing paired end whole genome sequencing and analysis. Failure to locate the *Sup4^{m1}* mutation, though the sequencing was deep enough to identify the control mutation in the *ADE2* gene and *Sup4^{m2}/CHA4*, may be because unpaired end sequencing does not identify the ends of the reads. As a result, it is not possible to identify regions having insertions and deletions of more than 4 base pairs which can be the *Sup4^{m1}* mutation.

Table 2. List of strains used in chapter 3.

NAME	STRAINS	GENOTYPE
TDY4B	WT	<i>Mata his3Δ leu2Δ ura3Δ lys2Δ</i>
TDY4071	<i>tsc3Δ</i>	<i>Mata tsc3Δ::clonNATr his3Δ leu2Δ ura3Δ lys2Δ</i>
SUR2Δ	<i>sur2Δ</i>	<i>Mata sur2Δ::KAN his3Δ leu2Δ ura3Δ met15Δ</i>
KGY1108	<i>sur2Δtsc3Δ</i>	<i>Mata sur2Δ::KAN tsc3Δ::URA3 his3Δ leu2Δ ura3Δ met15Δ</i>
KGY1001	<i>orm1Δorm2Δ</i>	<i>Mata orm1Δ::clonNATr orm2Δ::HIS3 ura3Δ leu2Δ lys2Δ</i>
KGY1105	<i>orm1Δorm2Δ tsc3Δ</i>	<i>Mata tsc3Δ::URA3^{mut} orm1Δ::clonNATr orm2Δ::HIS3 ura3Δ leu2Δ met15Δ his3Δ</i>
NSY30D	<i>orm1Δorm2Δ tsc3ΔSup4^{m1 m2}</i>	<i>Mata met15Δ leu2Δ ura3Δ his3Δ orm1Δ::clonNATr orm2Δ::HIS3 tsc3Δ::URA3 Sup4^{m1 m2}</i>
NSYA6c	<i>orm1Δorm2Δ tsc3Δcha4Δ</i>	<i>met15Δ leu2Δ ura3Δ orm1Δ::clonNATr orm2Δ::HIS3 tsc3Δ::URA3^{mut} cha4Δ::KAN</i>
TDY1120	<i>LCB1-ΔTMD1</i>	<i>Mata his3Δ leu2Δ ura3Δ met15Δ lys2Δ lcb1Δ::LCB1-ΔTMD1</i>
TDY1126	<i>LCB1-ΔTMD1 tsc3Δ</i>	<i>Mata his3Δ leu2Δ ura3Δ met15Δ lys2Δ tsc3Δ::URA3 lcb1Δ::LCB1-ΔTMD1</i>
NSY1126	<i>LCB1-ΔTMD1 tsc3Δcha4Δ</i>	<i>Mata his3Δ leu2Δ ura3Δ met15Δ lys2Δ tsc3Δ::URA3 cha4Δ::KAN lcb1Δ::LCB1-ΔTMD1</i>
TDY9113	<i>lcb1Δtsc3Δ</i>	<i>Mata ura3Δ leu2Δ trp1Δ lcb1Δ::KAN tsc3Δ::clonNATr</i>
NSY45B-1	<i>lcb1Δtsc3Δ Sup4^{m1m2}</i>	<i>Mata ura3Δ his3Δ leu2Δ met15Δ tsc3Δ::URA3 lcb1Δ::KAN Sup4^{m1 m2}</i>
NSY45B	<i>tsc3ΔSup4^{m1m2}</i>	<i>Mata ura3Δ his3Δ leu2Δ met15Δ tsc3Δ::URA3 Sup4^{m1 m2}</i>
NSYI-12b	<i>tsc3ΔSup4^{m1m2}</i>	<i>Mata ura3Δ lys2Δ his3Δ leu2Δ tsc3Δ::clonNATr Sup4^{m1 m2}</i>
NSY45B-2	<i>sur2Δtsc3Δ Sup4^{m1m2}</i>	<i>Mata ura3Δ his3Δ leu2Δ met15Δ tsc3Δ::URA3 sur2Δ::KAN Sup4^{m1 m2}</i>
NSY11a2 ade2 ^{mut} A	<i>tsc3ΔSup4^{m1m2} ade2-101</i>	<i>Mata ura3Δ his3Δ leu2Δ met15Δ ade2-101 tsc3Δ::URA3 Sup4^{m1 m2}</i>
NSYD7c	<i>tsc3ΔSup4^{m1}</i>	<i>Mata lys2Δ ura3Δ his3Δ leu2Δ met15Δ ade2-101 tsc3Δ::URA3 Sup4^{m1}</i>
NSYD7b	<i>tsc3ΔSup4^{m2}</i>	<i>Mata ura3Δ his3Δ leu2Δ met15Δ tsc3Δ::URA3 Sup4^{m2}</i>
CHA4Δ	<i>cha4Δ</i>	<i>Mata cha4Δ::KAN his3Δ leu2Δ ura3Δ met15Δ</i>
NSY40717 -1	<i>cha4Δtsc3Δ</i>	<i>Mata cha4Δ::KAN tsc3Δ::clonNATr his3Δ leu2Δ ura3Δ lys2Δ</i>

NSYD7c- cha4Δ	<i>cha4Δtsc3Δ</i> <i>Sup4^{m1}</i>	<i>Mata lys2Δ ura3Δ his3Δ leu2Δ met15Δ ade2-101</i> <i>cha4Δ::KAN tsc3Δ::URA3 Sup4^{m1}</i>
CHA1Δ	<i>cha1Δ</i>	<i>Mata cha1Δ::KAN his3Δ leu2Δ ura3Δ met15Δ</i>
NSY1	<i>cha1Δtsc3Δ</i>	<i>Mata cha1Δ::KAN tsc3Δ:: clonNATr his3Δ leu2Δ</i> <i>ura3Δ met15Δ</i>
NSYD7c- cha1Δ	<i>cha1Δtsc3Δ</i> <i>Sup4^{m1}</i>	<i>Mata lys2Δ ura3Δ his3Δ leu2Δ met15Δ ade2-101</i> <i>cha1Δ::KAN tsc3Δ::URA3 Sup4^{m1}</i>
VMA13Δ	<i>vma13Δ</i>	<i>Mata vma13Δ::KAN his3Δ leu2Δ ura3Δ met15Δ</i>
NSY2	<i>vma13Δtsc3Δ</i>	<i>Mata vma13Δ::KAN tsc3Δ::URA his3Δ leu2Δ</i> <i>ura3Δmet15Δ</i>
NSY11a2 ade2 ^{mut} A vma13Δ	<i>vma13Δtsc3Δ</i> <i>Sup4^{m1 m2}</i>	<i>Mata ura3Δ his3Δ leu2Δ met15Δ ade2-101</i> <i>vma13Δ::KAN tsc3Δ::URA3 Sup4^{m1 m2}</i>

Table 3. List of primers used in chapter 3.

NAME	PRIMER SEQUENCE
2TSC3	5'-GGGCCCCTCGAGGGCAAGTAGTGCATCCAG-3'
1TSC3	5'-GGGCCC GGATCCTTTATGTATTGTGTGTA-3'
AD2F	5'-GTAACGCCGTATCGTGATTAA-3'
AD2R	5'-GTACAGTCACTGGAATCGAAT-3'
SUR2F	5'-GGCCGTCGACCGACCTCCTGTTTCCTATTGTCTT-3'
SUR2R	5'-GGCCTCTAGAATGTTTCGTGTATCCAGGCAAACCT-3'
CHA4F	5'-AAGGAAAAA AgggccgcCTGATCGCTAGAGATCCGAT-3'
CHA4R	5'-TTTTCCTTTTgcggccgcTCCAGAATCCAGCAGGGTTG-3'
CHA4F1	5'-GGGACATTACCTTTT-3'
CHA1F	5'-AAGGAAAAA AgggccgcCCGTGATATCCTCTAGGGCT-3'
CHA1R	5'-TTTTCCTTTTgcggccgcCTAATAGAACGATATCTGGT-3'
L1XF	5'-GAATTCCTCGAGATAGGGGCATATTGCTGCGGT-3'
L1XR	5'-GGCCGGATCCTCGAGCGCATTCTCTGGGCGCCGTG-3'
VMA13F	5'-cgcggatccTCATAAGCATAATACAATGGTGC-3'
VMA13R	5'-cggcctcgagTGACAACGATTGATCACGCAGAT-3'
DPL1F	5'-GCCGGATCCAATACCCCTAATTAC-3'
DPL1R	5'-GGCCCTCGAGCAGGCAAGTTAGATTTCCC-3'
LCB4F	5'-GCGGCCGCATTTCTCTGTATACAGGC-3'
LCB4R	5'-CTCGAGTGAATAGAATAGTTAGCT-3'

Table 4. List of candidate mutations identified in the *tsc3ΔSup4^{m1m2}* and not in the *tsc3Δade2-101* by next generation sequencing and linkage analysis with *Sup4^{m1}* and *Sup4^{m2}*.

Location	% Score	Linkage analysis with nearby gene marked with Kanamycin	Linkage with <i>sup4^{m1}</i>	Linkage with <i>sup4^{m2}</i>	Kanamycin marker verified
Chr II (38728)	98.4	ATP1 (YBL099W)	No	No	Yes
Chr II (774430)	100	YBR285W	No	No	No
Chr III (92480)	100	DCC1 (YCL016C)	No	No	No
Chr IV (569994)	100	UBC5 (YDR059C)	No	No	No
Chr IV (688074)	91.7	VBA4 (YDR119W)	No	No	No
Chr IV (1117110)	100	YSP2 (YDR326C)	No	No	No
Chr XI (610650)	100	PXL1 (YKR090W)	No	No	No
Chr XII (338672)	>90	CHA4 (YLR098C)	Not verified	Yes	Yes
Chr XV (35765)	99.8	FRE7 (YOL152W)	No	No	No
Chr XVI (643579)	88.2	VMA13 (YPR036W)	No	No	Yes
Chr XII (784382)	>90	TMA10	No	No	No
ChrXIV (439397)	>90	OCA1	No	No	No

The linkage analysis for the candidate mutations was performed with the nearby non-essential genes (listed in the column 3 of the table above). All the genes selected for linkage analysis were within the range of 100% linkage with the respective candidate mutations (listed in column 1). The column 2 shows the percent of reads from that region which showed the candidate mutation. The haploid knock-out strain collection contains all the non-essential genes replaced with the kanamycin cassette individually. The respective strains, for the genes selected for linkage analysis, were taken from this haploid knockout collection so that all the candidate

mutations get marked with the kanamycin cassette for linkage analysis. The *TSC3* was knocked out using the *URA3* marker only in the following strains to generate the double knock-out: *tsc3ΔURAtp1ΔKAN*, *tsc3ΔURAvma13ΔKAN*, *tsc3ΔURAtma10ΔKAN*, *tsc3ΔURAoca1ΔKAN* mutants. The *CHA4* however was knocked out in the *tsc3ΔSup4^{m1}* mutant to generate the *tsc3ΔSup4^{m1}cha4ΔKAN* mutant, by replacing the *CHA4* with the kanamycin cassette. The remaining *ybr285wΔKAN*, *dcc1ΔKAN*, *ubc5ΔKAN*, *vba4ΔKAN*, *ysp2ΔKAN*, *pxl1ΔKAN*, and *fre7ΔKAN* strains contained the wild type *TSC3* gene. All the kanamycin marked strains were crossed with the *tsc3ΔNATRSup4^{m1m2}* to generate the diploid. The diploids were sporulated and the tetrads were analyzed for linkage. Other than the linkage analysis with the *cha4ΔKAN*, the expected result for the rest of the candidate genes is, if the candidate mutation is linked to *Sup4^{m1}* then none of the *tsc3Δ* kanamycin resistant spores will be growing at 37 °C. If the candidate mutation is linked to *Sup4^{m2}* then none of the *tsc3Δ* kanamycin resistant spores will be strongly growing at 37 °C. It was observed that all the diploids yielded spores which were kanamycin resistant and also growing at 37 °C in the expected ratio. However, in case of the *tsc3Δvma13ΔKAN* X *tsc3ΔNATRSup4^{m1m2}* diploid, none of the kanamycin resistant spores grew at 37 °C, but the percent of 4 spore tetrads was really poor. Further analysis revealed that the spores which failed to germinate are all *vma13Δtsc3ΔSup4^{m1m2}* suggesting that the deletion of *VMA13* compromises the ability of the *Sup4^{m1m2}* spores to germinate and is not because of linkage between *VMA13* locus and *Sup4^{m1}* mutation. In case of the *tsc3ΔSup4^{m1}cha4ΔKAN* X *tsc3ΔNATRSup4^{m1m2}* diploid all the spores were growing at 37 °C including the kanamycin resistant spores indicating that the *CHA4* is allelic to *Sup4^{m2}*.

Table 5. Table showing list of genes not linked to *Sup4^{m1}* and *Sup4^{m2}*.

Linkage analysis with gene	Linkage with <i>sup4^{m1}</i>	Linkage with <i>sup4^{m2}</i>
ADE2	No	No
MET15	No	No
LYS2	No	No
MAT α	No	No
MAT α	No	No

Table 6. List of precursors/products ion mass/charge (m/z) ratio's, associated collision energy, and dwell time used for MRM detection of individual molecular species of free LCBs and LCB-Ps.

Sphingoid bases	Precursor/product ion (m/z)	Collision energy (eV)	Dwell time in (msec)
C16DHS	274.3/60	35	25
C18DHS	302.3/60	38	25
C20DHS	330.3/60	26	25
C16PHS	290.3/60	35	25
C18PHS	318.3/60	43	25
C20PHS	346.3/60	41	25
anhyC18PHS	300.3/60	43	25
anyhC20PHS	328.4/60	43	25
C16DHS-P	354.3/238.3	19	25
C18DHS-P	382.3/266.3	19	25
C20DHS-P	410.3/294.3	25	25
C16PHS-P	370.3/272.3	22	25
C18PHS-P	398.3/300.3	20	25
C20PHS-P	426.3/328.3	20	25
16KDS	272.4/242.3	28	25
18KDS	300.7/270.2	28	25
20KDS	328.4/298.3	28	25
C12-SM	647.7/184.4	40	25
C12-Cer	482.6/264.4	35	25

Sphingoid bases	Precursor/product ion (m/z)	Collision energy (eV)	Dwell time in (msec)
C12-GlcCer	644.6/264.4	42.5	25
C12-Cer1P	562.6/264.4	45	25
C12-LacCer	806.6/264.4	55	25
d17:0	288.4/60	40	25
D17:0P	368.4/270.3	20	25
d17:1	286.3/268.3	19	25
d17:1P	366.2/250.3	23	25

CHAPTER 4: Topological characterization of the small subunits of human SPT.

ABSTRACT:

The small subunits of human SPT localize in the ER along with the LCB1-LCB2 heterodimers and increase the catalytic activity several fold. Topological studies reveal that the N-terminus of the ssSPTs is in the cytosol whereas the C-terminus is in the ER lumen. This topological orientation is retained with the truncated ssSPTs which consist of only a 33-amino acid core domain all that is needed for heterodimer activation. A split-ubiquitin based two-hybrid screen identified several candidate ssSPT-interacting proteins. Further characterization of these proteins will establish which of these interactions are physiologically significant and thereby increase understanding of regulation of human SPT.

BACKGROUND:

Two human functional orthologs of Tsc3p, ssSPTa and ssSPTb, were identified by functional screening of a human cDNA library. The ssSPTs (ssSPTa and ssSPTb) are small proteins, encoded by distinct genes, which are stably expressed in the absence of human SPT heterodimer and localize to the ER membrane. Like Tsc3p, they interact directly with the human LCB1-LCB2 heterodimers and enhance activity several fold (31). The ssSPTa subunit confers a preference for C16-CoA while ssSPTb confers a preference for C18-CoA with the LCB1-LCB2a heterodimer whereas with LCB1-LCB2b, neither the ssSPTa nor the ssSPTb show any strong chain length preference for the acyl-CoA substrate (31). Recent studies have shown that a single residue in the ssSPTs is responsible for the acyl-CoA substrate specificity. However, the exact

mechanism of SPT activation and substrate selection by the ssSPTs is yet to be determined.

An important step in understanding the mechanism by which the ssSPTs activate the LCB1-LCB2 heterodimers will be to determine their membrane topology. Moreover, the distinct acyl-CoA preferences and increased enzymatic activity conferred by the ssSPTs make these small proteins attractive candidates for regulation of SPT. Preliminary experiments in our laboratory (Dr. S. Gupta, unpublished) have shown that deletion of 9 and 14 amino acid residues from the C-terminus of the ssSPTa and ssSPTb respectively, activates the catalytic activity of the LCB1-LCB2a/b heterodimer better than the full length subunits. Moreover by bioinformatics analysis it has been shown that the C-termini are highly conserved within, but divergent between, the ssSPTa and ssSPTb subfamilies (other vertebrates) suggesting that the conserved residues at the C-terminus of the ssSPTs may be important in mediating negative regulation of SPT, perhaps by acting as binding sites for negative regulators. Hence, the goal of these studies was to determine the topology of the small subunits and to screen for interacting partners of the ssSPTs which might be involved in the regulation of sphingolipid biosynthesis.

MATERIALS AND METHODS:

Strains:

All strains are in the BY4741 background. The strains used in this study are listed in Table 9.

Growth media:

The media used in this study, YPD or SD supplemented with the indicated concentrations of 3-amino-1,2,4-triazole (3-AT), were prepared according to standard protocols (79).

Plasmids:

Cub-ssSPTa-pGH316, Cub-ssSPTb-pGH316, HA-ssSPTa-pGH316, and HA-ssSPTb-pGH316 - The yeast expression vector, pGH316, was constructed by cloning a fragment containing the yeast *LCB2* gene, along with 680 bp of upstream and 345 bp of downstream flanking sequence into pRS316. The *LCB2* ORF was then replaced with a *NheI* site by site-directed mutagenesis to generate the pGH316 (31). The ssSPTa or ssSPTb ORFs with N-terminal *NheI* and C-terminal *AvrII* ends were PCR amplified and cloned into the pGH316 and plasmids having the inserts oriented for expression from the *LCB2* promoter were identified and named ssSPTa/b-pGH316. *SpeI*-ended “LexA-Cub” or “HA” cassettes were ligated into *NheI*-linearized ssSPTa/b-pGH316 to generate the N-terminally tagged ssSPTs.

ssSPTa-HA-pGH316 and ssSPTb-HA-pGH316 – For construction of the C-terminally tagged ssSPTs, N-terminal *AvrII* and C-terminal *NheI* ended ssSPTa or ssSPTb was cloned into pGH316. A *SpeI*-ended HA cassette was ligated into *NheI*-linearized ssSPTa/b-pGH316.

***LCB1-Cub*-pGH316** –The human *LCB1* PCR fragment was inserted into the *NheI* site of pGH316. An *XbaI* site was introduced before the stop codon of the *LCB1* by site-directed mutagenesis. N-terminal *XbaI* and C-terminal *SpeI* ended - Cub-LexA-VP16 -

cassette was inserted in-frame into the *XbaI* site before the stop codon of *LCB1* in pGH316. The *URA3* marker of this construct was replaced with the *LEU2* marker.

LCB2a-Cub-pGH316 – The human *LCB2a* PCR fragment with *AvrII* at the N-terminus and *NheI* at the C-terminus was cloned into the *NheI* site of pGH316. An N-terminal *XbaI* and C-terminal *SpeI* ended - Cub-LexA-VP16 - cassette was inserted in-frame into the C-terminal *NheI* site before the stop codon of *LCB2a*. The *URA3* marker of this construct was replaced with the *TRP1* marker.

LCB2b-Cub-pGH316 – The human *LCB2b* PCR fragment was cloned into the *NheI* site of pGH316. An N-terminal *XbaI* and C-terminal *SpeI* ended - Cub-LexA-VP16 - cassette was inserted in-frame into an *AvrII* site before the stop codon of *LCB2b*. The *URA3* marker of this construct was replaced with the *TRP1* marker.

HA-ssSPTa CΔ21/25-Myc-pPR3-N – 21 or 25 amino acids were deleted from the C-terminus of the ssSPTa by introducing a stop codon by site-directed mutagenesis into the NubG-HA-ssSPTa- pPR3 plasmid (31). A *SpeI*-ended 3XMyC cassette was ligated into a *NheI* site placed immediately upstream of the stop codon in this plasmid to generate the HA-ssSPTa CΔ21/25-Myc.

ELO3-Cub-pRS315 – The *ELO3*-pRS315 was constructed by cloning a fragment of the yeast *ELO3* gene with *BamHI* ends, which includes 280 bp of upstream and 180 bp of downstream flanking sequence, into the *BamHI* site in the pRS315. An *AvrII* site was introduced by site directed mutagenesis just before the stop codon of *ELO3*. The *SpeI*-ended “Cub-LexA” cassette was amplified by PCR and ligated into the *AvrII*-linearized *ELO3*-pRS315.

Primers:

Primers used in this study are listed in Table 10.

Yeast transformation:

All yeast transformations were done using the standard yeast transformation protocol (79).

Yeast plasmid and genomic preparation:

Yeast plasmid and genomic DNA were isolated using the Zymoprep I™ Kit (Zymo Research, Inc) according to the manufacturer's protocol.

Site-directed mutagenesis:

All the site-directed mutagenesis was performed using the QuikChange II Site-directed mutagenesis kit (Agilent Technologies) according to the manufacturer's protocol.

Microsome preparation:

As described in the materials and methods, chapter 2.

Western blot:

As described in the materials and methods, chapter 2.

Split-ubiquitin yeast two-hybrid assay:

The L-40 (46) strain having the engineered split-ubiquitin yeast two-hybrid reporter system was used to detect interaction between membrane proteins. In the split-ubiquitin membrane based yeast two-hybrid (SU2H) assay, the N-terminal (Nub) half of ubiquitin is fused to one protein and the C-terminal (Cub) half of ubiquitin, followed by

the LexA transcription factor, is fused to its potential interacting partner. If the candidate partners interact, the Nub and Cub-LexA domains associate to generate a substrate for ubiquitin protease, which thus cleaves and releases the LexA transcription factor. The free LexA transcription factor enters the nucleus and activates transcription of the '*HIS3*' reporter gene, thereby allowing growth on – *his* media (46). 3-amino-1,2,4-triazole (3-AT) is a heterocyclic organic compound which is a competitive inhibitor of the product of the *HIS3* gene. Addition of 3-AT into media thus imposes an increased level of selection by requiring increased *HIS3* expression for growth. This is a useful system for identifying high affinity *in vivo* binding between two proteins. It should be noted that the ubiquitin protease is cytosolic, and thus the topology of potentially interacting proteins must be considered when deciding where to append the Nub and Cub-LexA domains (46).

Right-side-out vesicle preparation:

Yeast strains were grown overnight in the appropriate medium to an OD₆₀₀ of approximately 1. 100 OD₆₀₀ of cells were harvested, washed with dH₂O, with spheroplasting buffer (1.2 M sorbitol, 50 mM potassium acetate, 20 mM Tris-HCl at pH 7.5, 0.5 mM β-mercaptoethanol, and 10 mM sodium azide) and suspended in 10 ml of spheroplasting buffer containing 1 mg/ml of zymolyase and incubated at 37 °C for 30 min. The zymolyase-treated cell suspension was layered on a cushion of 2 M sorbitol (at a ratio of 1:2) and centrifuged at 500 x g for 10 min at 4 °C. The supernatant was discarded and the pellet was resuspended in 10 ml of lysis buffer (0.1 M sorbitol, 50 mM potassium acetate, 20 mM Tris-HCl at pH 7.5, and 1 mM β-mercaptoethanol) containing PMSF and protease inhibitors and slowly homogenized on ice to prevent frothing. The

homogenate was centrifuged at 1000 x g for 5 min at 4 °C; the supernatant was transferred to a fresh ultracentrifuge tube and centrifuged at 100000 x g twice for 30 min at 4 °C. The final pellet was suspended in storage buffer (250 mM sorbitol, 50 mM potassium acetate, 20 mM Tris-HCl at pH 7.5 and 1 mM β -mercaptoethanol) and flash frozen in liquid nitrogen before storing at – 80 °C (67).

Protease protection assay:

100 μ g of right-side-out vesicles were resuspended in 40 μ l of TEGM buffer and treated with 0.3 μ g/ μ l of proteinase K in the presence and absence of 0.4% Triton X-100 on ice for 2 hrs. 5 μ l of 40 mM PMSF and 10 μ l of 50% TCA were added to the tubes and incubated on ice for 20 min to stop the reaction. The vesicles were pelleted at 10600 x g for 10 min at 4 °C and washed with 400 μ l of acetone. 25 μ l of 4X SDS sample buffer (Life Technologies) with 10 μ l of 10X reducing agent (Life Technologies) were added to the pellet and heated at 70 °C for 10 min and then either store at -20 °C or immediately run on SDS-PAGE (67).

RESULTS:

The ssSPTs have single TMD with the N-termini in the cytosol and the C-termini in the ER lumen.

Protease protection assays were performed to determine the location of the N and C-termini of ssSPTa and b. N or C-terminally HA-tagged ssSPTa and b were inserted into pGH316 for expression from the yeast LCB2 promoter. The constructs were expressed along with the human LCB1-LCB2a/b heterodimers in an *lcb1 Δ lcb2 Δ tsc3 Δ* mutant strain. Right-side-out vesicles were prepared from the transformants and expression of the ssSPTs was confirmed by immunoblotting. Integrity and sidedness of

the vesicles was confirmed by affirming that the luminal ER protein, Kar2p, was inaccessible to protease unless the vesicles were treated with detergent (**Figure 4B, lanes 2 and 4**) (85). The results showed that the N-termini of the HA-ssSPTs were accessible to proteinase K with or without detergent whereas the C-termini of the ssSPTs-HA were protease-resistant unless the vesicles were detergent-solubilized. Thus, when expressed in *S. cerevisiae*, the ssSPTs are oriented with their N-termini in the cytosol and their C-termini in the ER lumen (**Figure 4B**). Two TMDs were predicted to be present in the ssSPTs by hydropathy analysis (**Figure 4A**). However as the ends of the ssSPTs were found to be on the opposite sides of the ER membrane, the data indicate an odd number of TMDs. In a series of deletion studies, it was observed that a CA21 and CA25 truncation in ssSPTa retained the ability to significantly activate the human SPT heterodimer indicating that a core region of 33 amino acid residues is sufficient for the activity and acyl-CoA selectivity (37) and suggests the presence of a single TMD. Moreover the *Drosophila* and *Arabidopsis* ssSPTs have a single predicted TMD and the *Arabidopsis* ssSPTb has been confirmed to have single TMD (49). To investigate this further, a protease protection assay was performed with the C-terminally truncated ssSPTa Δ 21/25 having a Myc-tag at the C-terminus, and it was found that the original orientation was preserved even in the C-terminally truncated subunits (**Figure 4C**). As the C-terminal truncations extend into the distal predicted TMD the data also support the conclusion that the ssSPTs contain a single TMD.

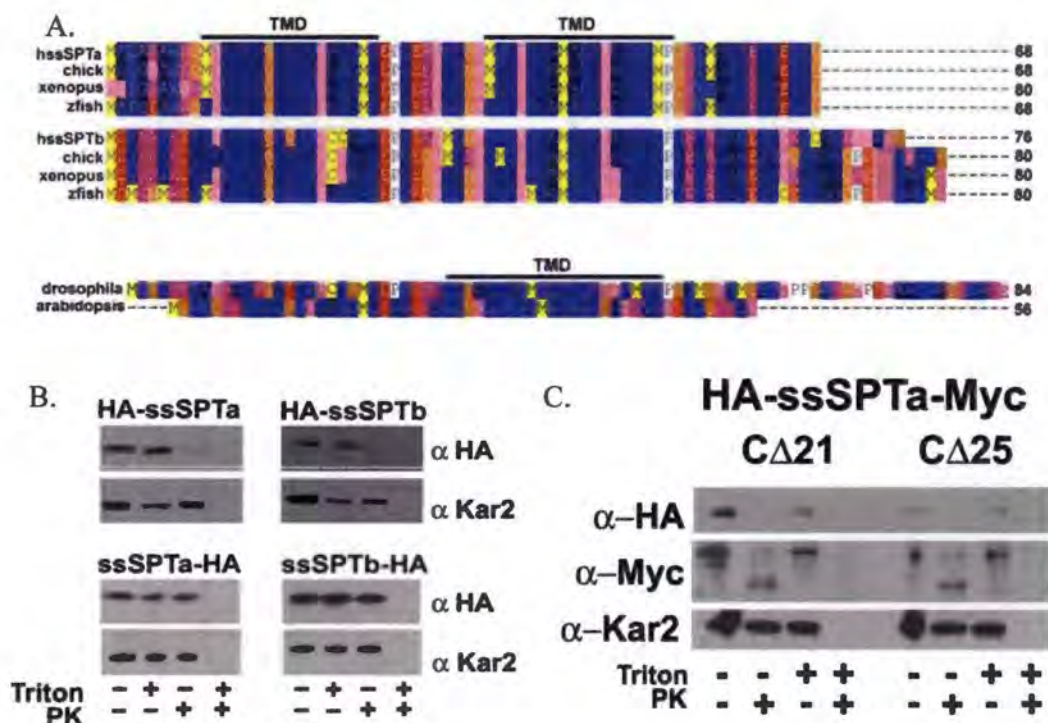


Figure 4. The ssSPTs have a single TMD and are oriented with their N-termini in the cytosol.

A. Alignment of vertebrate and invertebrate candidate ssSPTs showing the two TMDs predicted by hydropathy analysis. The alignment includes the ssSPTa and ssSPTb subfamilies from *Homo sapiens*, (hssSPTa or hssSPTb), *Gallus domesticus* (chick), *Xenopus laevis* (xenopus) and *Danio rerio* (zebrafish). hssSPTa is aligned and numbered without its three amino terminal residues (MAG) which are absent in the other vertebrate ssSPTa subunits. B. Right-side-out microsomal vesicles were prepared from yeast expressing N- or C-terminally HA-tagged ssSPTa or ssSPTb, along with LCB1 and LCB2a. The microsomes were either mock digested or digested with proteinase K (PK) in the absence and presence of Triton X-100. The luminal ER protein, Kar2p, served as a control for vesicle integrity. C. Right-side-out vesicles were prepared from yeast expressing LCB1, LCB2a, and N-terminally HA-tagged ssSPTa with either the C-terminal 21 or 25 amino acids replaced by a Myc tag. The right-side-out microsomes were either mock digested or digested with proteinase K (PK) in the absence and presence of Triton X-100. The luminal ER protein, Kar2p, served as a control for vesicle integrity.

Candidate ssSPT interacting proteins were identified using the split-ubiquitin yeast two-hybrid system.

An N-terminally Nub-tagged human cDNA library (31) was screened to identify candidate proteins interacting with the ssSPTs. As mentioned in the materials and methods, the Nub and Cub domains must be appended to cytosolic domains of the potentially interacting partners. Since the ssSPTs are stably expressed in the absence of the human SPT heterodimers, accordingly, N-terminally Cub-LexA tagged ssSPTa was used as the bait and co-transformed along with the N-terminally Nub-tagged human cDNA library in the L-40 (46) reporter strain and plated on SD *-ura -trp*. Among the 3000 transformants, 25 were recovered as histidine prototrophs.

The 25 colonies growing on *-his* + 25 mM 3-AT were further tested for a positive interaction between Cub-ssSPTa and a Nub-tagged partner on *-his* + 50 mM 3-AT plates. Out of the 25 Nub-tagged candidates, 10 were identified as strong interactors by their ability to grow on *-his* + 50 mM 3-AT and are listed in Table 7. The 10 candidate plasmids were recovered from yeast by plasmid extraction and passaged through *E. coli* before sequencing to identify the interacting proteins. As the ssSPTs interact with the SPT heterodimer, whether the 10 candidates can also interact with the SPT heterodimer was investigated. Using split-ubiquitin yeast two-hybrid assay, all 10 candidate proteins were found to interact with LCB1-Cub, but differential interaction with LCB2 were observed. Five candidates interacted with both LCB2a-Cub and LCB2b-Cub, three only interacted with LCB2b-Cub but not with LCB2a-Cub and two did not interact with either LCB2 subunits (Table 8). The 10 candidates did not show positive interaction with the Elo3-Cub, negative control, confirming that growth on the 50 mM 3-

AT plates reflects a specific interaction between the candidate proteins and the human SPT subunits.

Table 7. List of candidates found in split-ubiquitin based two-hybrid screen using LexA-Cub-ssSPTa as bait.

Sl. No.	Abbreviation	Gene Name
1	BCAP31	B-cell receptor-associated protein 31
2	PLP2	Human proteolipid protein 2
3	ARL6IP5	ADP-ribosylation like factor 6 interacting protein 5
4	STAT6	Signal transducer and activator of transcription 6
5	AIG1	Androgen induced 1
6	VAMP	Vesicle associated membrane protein associated
7	NAPG	N-ethyl maleimide – sensitive factor attachment protein
8	EBP	Emopamil binding protein
9	SERP1	Stress associated endoplasmic reticulum protein 1
10	OK/SW-CL.16	Putative ORF

Table 8. Interaction of the 10 candidate proteins with either LCB1, LCB2a, LCB2b, ssSPTa, ssSPTb, or Elo3 as determined by split-ubiquitin yeast two-hybrid assay.

Nub-Gene	LCB1-Cub	LCB2a-Cub	LCB2b-Cub	Cub-ssSPTa	Cub-ssSPTb	Elo3-Cub
BCAP31	+++	+++	+++	+++	+++	-
PLP2	+++	-	+	+++	+++	-
ARL6IP5	+++	-	+++	+++	+++	-
STAT6	+++	+++	+++	+++	+++	-
AIG1	+++	-	-	+++	+++	-
VAMP2	+++	+++	+++	+++	+++	-
NAPG	+++	-	-	+++	+++	-
EBP	+++	+	+	+++	+++	-
SERP-1	+++	+++	+++	+++	+++	-
Unknown	+++	-	+++	+++	+++	-

DISCUSSION:

The ssSPTs enhance SPT activity and confer distinct substrate preferences. By hydropathy analysis, two TMDs were predicted in the human ssSPTs (**Figure 4a**). However, protease protection assays of the exogenously expressed ssSPTs in yeast, revealed that the N-termini of the ssSPTs are in the cytosol whereas the C-termini are in the lumen, indicating the presence of odd number of TMD(s) (**Figure 4b**). Bioinformatic analysis has shown that putative ssSPT homologs are present in many eukaryotic organisms and several of these putative ssSPT homologs have been shown to be bonafide ssSPTs (49). These homologs share a central core domain with several conserved amino acid residues whereas the N and C-terminal domains are more divergent. This suggested that the divergent N and C-terminal domains may be responsible for the determination of the acyl-CoA preference and that the conserved core domain for enhancement of SPT activity. However, it was observed that the core domain consisting of only 33 amino acid residues, not only activates the heterodimer but also confers acyl-CoA selectivity. Moreover the conserved core domain of 33 amino acids also retained the same membrane topology as the full length ssSPTs (**Figure 4c**). As the maximal C-terminal truncations (CA21 and CA25 in ssSPTa) extend into the distal predicted TMD, the data also support the conclusion that the ssSPTs contain a single TMD. Since the truncated small subunits behave like their full length counterparts, it will be of interest to investigate, how the ssSPTs are targeted to the membrane.

Proteins interacting with the ssSPTa and b were identified (Table 7) and it was shown that all the candidate proteins interacted with both ssSPTa and ssSPTb, whereas they interacted differently with the SPT heterodimer (Table 8). The 10 candidates were identified by screening only 3000 colonies whereas the entire human genome consists of

20051 genes other than pseudogenes, microRNA genes, small nuclear RNA, and small nucleolar RNA. It seems unlikely that such a high percentage (0.33%) of the human proteome specifically interacts with the ssSPTs, and that many of these interactions are false positives. However, in a separate co-immunoprecipitation experiment proteins that co-immunopurified with the human fusion SPT LCB2a-ssSPTa-LCB1-FLAG from HEK cells were identified by mass spectrometry. 4 of the same candidate proteins (BCAP31, PLP2, STAT6, VAMP2) were identified. This suggests that at least some of the candidate interacting proteins will prove to be physiologically relevant interacting partners of ssSPTs. Moreover, the human cDNA library used for the split-ubiquitin yeast two-hybrid screen, was not normalized and hence there is the possibility that the highly expressed genes are over represented, further suggesting that may be some of the interactions can be significant. It is plausible that some of these proteins act as chaperones for directing the ssSPTs to the ER. Understanding the roles played by these proteins alone and in association with the ssSPTs, will likely increase understanding of the regulation of SPT and should these proteins regulate SPT activity, they may be potential therapeutic targets for developing drugs to cure some of the many diseases associated with sphingolipid biosynthetic pathway.

Table 9. List of strains used in chapter 4.

NAME	STRAIN	GENOTYPE
L-40	WT	<i>Mata, trp1-901 leu2-3,112 his3Δ200 lys2-801 ade2Δ ura3Δ LYS2::lexA-HIS3 ura3::lexA-lacZ</i>
TDY9103	<i>lcb1Δlcb2Δtsc3Δ</i>	<i>Mata lcb1Δ::KAN lcb2Δ::KAN tsc3Δ::NATR his3Δ leu2Δ ura3Δ lys2Δ trpΔ::HIS3</i>

Table 10. List of primers used in chapter 4.

NAME	PRIMER SEQUENCE
H3AF	5'-GGCCGTCGACATGGCTAGCATGGCGGGGATGGCGCTGGCG-3'
H3AR	5'-GCGCCTCGAGTCTAGATCATTGTACGATTTCAAAGTA-3'
H3BF	5'-GGCCACTAGTATGGCTAGCATGGATTTGAGGCGTGTGAAG-3'
H3BR	5'-GCGCCTCGAGTCTAGATCAATTAGAAATTGTACTGTG-3'
ODB90F	5'-GGGATGGCACTATACACATAGGGATACGTCTTCATGCCC-3'
ODB91R	5'-GGGCATGAAGACGTATCCCTATGTGTATAGTGCCATCCC-3'
ODB94F	5'-CTGGTTTCCATTGTGGGGTAGATGGCACTATACACAGGA-3'
ODB95R	5'-TCCTGTGTATAGTGCCATCTACCCCAACAATGGAAACCAG-3'
ODB145F	5'-GGGATGGCACTATACACAGCTAGCTAGGGATACGTCTTCATGCC-3'
ODB146R	5'-GGGCATGAAGACGTATCCCTAGCTAGCTGTGTATAGTGCCATCCC-3'
ODB147F	5'-CTGGTTTCCATTGTGGGGGCTAGCTAGATGGCACTATACACAGGA-3'
ODB148R	5'-TCCTGTGTATAGTGCCATCTAGCTAGCCCCCAACAATGGAAACCAG-3'
ELO3MF	5'-GGCCGGATCCGTATCACTACTCCTCACTGT-3'
ELO3PR	5'-GGCCGGATCCTCCAGACTGTGAATAAAC-3'
ADWE3F	5'-TCTTCCAGGAAAGCTCCTAGGTAAATAGGAAGCGAG-3'
ADWE3R	5'-CTCGCTTCCTATTTACCTAGGAGCTTTCCTGGAAGA-3'
340F	5' TCTTCCAGGAAAGCTGCTAGCTAAATAGGAAGCGAG-3'
341R	5'-CTCGCTTCCTATTTAGCTAGCAGCTTTCCTGGAAGA-3'

REFERENCES

1. Aerts JM, Ottenhoff R, Powlson AS, Grefhorst A, van Eijk M, et al. 2007. Pharmacological inhibition of glucosylceramide synthase enhances insulin sensitivity. *Diabetes* 56: 1341-9
2. Alexeev D, Alexeeva M, Baxter RL, Campopiano DJ, Webster SP, Sawyer L. 1998. The crystal structure of 8-amino-7-oxononanoate synthase: a bacterial PLP-dependent, acyl-CoA-condensing enzyme. *J Mol Biol* 284: 401-19
3. Anderson N, Borlak J. 2006. Drug-induced phospholipidosis. *FEBS Lett* 580: 5533-40
4. Bartke N, Hannun YA. 2009. Bioactive sphingolipids: metabolism and function. *J Lipid Res* 50 Suppl: S91-6
5. Bornaes C, Ignjatovic MW, Schjerling P, Kielland-Brandt MC, Holmberg S. 1993. A regulatory element in the CHA1 promoter which confers inducibility by serine and threonine on *Saccharomyces cerevisiae* genes. *Mol Cell Biol* 13: 7604-11
6. Boven LA, van Meurs M, Boot RG, Mehta A, Boon L, et al. 2004. Gaucher cells demonstrate a distinct macrophage phenotype and resemble alternatively activated macrophages. *Am J Clin Pathol* 122: 359-69
7. Breslow DK, Collins SR, Bodenmiller B, Aebersold R, Simons K, et al. Orm family proteins mediate sphingolipid homeostasis. *Nature* 463: 1048-53
8. Buede R, Rinker-Schaffer C, Pinto WJ, Lester RL, Dickson RC. 1991. Cloning and characterization of LCB1, a *Saccharomyces* gene required for biosynthesis of the long-chain base component of sphingolipids. *J Bacteriol* 173: 4325-32
9. Chavez JA, Summers SA. Lipid oversupply, selective insulin resistance, and lipotoxicity: molecular mechanisms. *Biochim Biophys Acta* 1801: 252-65
10. Chen EJ, Kaiser CA. 2002. Amino acids regulate the intracellular trafficking of the general amino acid permease of *Saccharomyces cerevisiae*. *Proc Natl Acad Sci USA* 99: 14837-42
11. Costanzo M, Baryshnikova A, Bellay J, Kim Y, Spear ED, et al. The genetic landscape of a cell. *Science* 327: 425-31
12. Cowart LA. 2009. Sphingolipids: players in the pathology of metabolic disease. *Trends Endocrinol Metab* 20: 34-42

13. Cowart LA, Hannun YA. 2007. Selective substrate supply in the regulation of yeast de novo sphingolipid synthesis. *J Biol Chem* 282: 12330-40
14. Cowart LA, Obeid LM. 2007. Yeast sphingolipids: recent developments in understanding biosynthesis, regulation, and function. *Biochim Biophys Acta* 1771: 421-31
15. D'Angelo G, Polishchuk E, Di Tullio G, Santoro M, Di Campli A, et al. 2007. Glycosphingolipid synthesis requires FAPP2 transfer of glucosylceramide. *Nature* 449: 62-7
16. Dawkins JL, Hulme DJ, Brahmabhatt SB, Auer-Grumbach M, Nicholson GA. 2001. Mutations in SPTLC1, encoding serine palmitoyltransferase, long chain base subunit-1, cause hereditary sensory neuropathy type I. *Nat Genet* 27: 309-12
17. de Duve C. 1983. Lysosomes revisited. *Eur J Biochem* 137: 391-7
18. Degroote S, Wolthoorn J, van Meer G. 2004. The cell biology of glycosphingolipids. *Semin Cell Dev Biol* 15: 375-87
19. Dickson RC, Sumanasekera C, Lester RL. 2006. Functions and metabolism of sphingolipids in *Saccharomyces cerevisiae*. *Prog Lipid Res* 45: 447-65
20. Duan RD, Nilsson A. 2009. Metabolism of sphingolipids in the gut and its relation to inflammation and cancer development. *Prog Lipid Res* 48: 62-72
21. Edvardson S, Hama H, Shaag A, Gomori JM, Berger I, et al. 2008. Mutations in the fatty acid 2-hydroxylase gene are associated with leukodystrophy with spastic paraparesis and dystonia. *Am J Hum Genet* 83: 643-8
22. Eggeling C, Ringemann C, Medda R, Schwarzmann G, Sandhoff K, et al. 2009. Direct observation of the nanoscale dynamics of membrane lipids in a living cell. *Nature* 457: 1159-62
23. Forgac M. 1999. Structure and properties of the vacuolar (H⁺)-ATPases. *J Biol Chem* 274: 12951-4
24. Fyrst H, Saba JD. An update on sphingosine-1-phosphate and other sphingolipid mediators. *Nat Chem Biol* 6: 489-97
25. Gable K, Gupta SD, Han G, Niranjanakumari S, Harmon JM, Dunn TM. A disease-causing mutation in the active site of serine palmitoyltransferase causes catalytic promiscuity. *J Biol Chem* 285: 22846-52
26. Gable K, Slife H, Bacikova D, Monaghan E, Dunn TM. 2000. Tsc3p is an 80-amino acid protein associated with serine palmitoyltransferase and required for optimal enzyme activity. *J Biol Chem* 275: 7597-603

27. Gai X VD. 2005. Personal communication to SGD regarding sequence of the ade2-101 allele.: Saccharomyces Genome Database
28. Haak D, Gable K, Beeler T, Dunn T. 1997. Hydroxylation of *Saccharomyces cerevisiae* ceramides requires Sur2p and Scs7p. *J Biol Chem* 272: 29704-10
29. Han G, Gable K, Yan L, Allen MJ, Wilson WH, et al. 2006. Expression of a novel marine viral single-chain serine palmitoyltransferase and construction of yeast and mammalian single-chain chimera. *J Biol Chem* 281: 39935-42
30. Han G, Gable K, Yan L, Natarajan M, Krishnamurthy J, et al. 2004. The topology of the Lcb1p subunit of yeast serine palmitoyltransferase. *J Biol Chem* 279: 53707-16
31. Han G, Gupta SD, Gable K, Niranjanakumari S, Moitra P, et al. 2009. Identification of small subunits of mammalian serine palmitoyltransferase that confer distinct acyl-CoA substrate specificities. *Proc Natl Acad Sci U S A* 106: 8186-91
32. Han S, Lone MA, Schneiter R, Chang A. Orm1 and Orm2 are conserved endoplasmic reticulum membrane proteins regulating lipid homeostasis and protein quality control. *Proc Natl Acad Sci U S A* 107: 5851-6
33. Hanada K. 2003. Serine palmitoyltransferase, a key enzyme of sphingolipid metabolism. *Biochim Biophys Acta* 1632: 16-30
34. Hanada K, Hara T, Nishijima M. 2000. Purification of the serine palmitoyltransferase complex responsible for sphingoid base synthesis by using affinity peptide chromatography techniques. *J Biol Chem* 275: 8409-15
35. Hanada K, Kumagai K, Yasuda S, Miura Y, Kawano M, et al. 2003. Molecular machinery for non-vesicular trafficking of ceramide. *Nature* 426: 803-9
36. Hannun YA, Luberto C, Argraves KM. 2001. Enzymes of sphingolipid metabolism: from modular to integrative signaling. *Biochemistry* 40: 4893-903
37. Harmon JM, Bacikova D, Gable K, Gupta SD, Han G, et al. Topological and functional characterization of the ssSPTs, small activating subunits of serine palmitoyltransferase. *J Biol Chem* 288: 10144-53
38. Hauck CR, Grassme H, Bock J, Jendrossek V, Ferlinz K, et al. 2000. Acid sphingomyelinase is involved in CEACAM receptor-mediated phagocytosis of *Neisseria gonorrhoeae*. *FEBS Lett* 478: 260-6
39. Ho MN, Hirata R, Umemoto N, Ohya Y, Takatsuki A, et al. 1993. VMA13 encodes a 54-kDa vacuolar H(+)-ATPase subunit required for activity but not assembly of the enzyme complex in *Saccharomyces cerevisiae*. *J Biol Chem* 268: 18286-92

40. Hollak CE, Evers L, Aerts JM, van Oers MH. 1997. Elevated levels of M-CSF, sCD14 and IL8 in type 1 Gaucher disease. *Blood Cells Mol Dis* 23: 201-12
41. Holland WL, Brozinick JT, Wang LP, Hawkins ED, Sargent KM, et al. 2007. Inhibition of ceramide synthesis ameliorates glucocorticoid-, saturated-fat-, and obesity-induced insulin resistance. *Cell Metab* 5: 167-79
42. Holleran WM, Takagi Y, Uchida Y. 2006. Epidermal sphingolipids: metabolism, function, and roles in skin disorders. *FEBS Lett* 580: 5456-66
43. Holmberg S, Schjerling P. 1996. Cha4p of *Saccharomyces cerevisiae* activates transcription via serine/threonine response elements. *Genetics* 144: 467-78
44. Hurwitz R, Ferlinz K, Sandhoff K. 1994. The tricyclic antidepressant desipramine causes proteolytic degradation of lysosomal sphingomyelinase in human fibroblasts. *Biol Chem Hoppe Seyler* 375: 447-50
45. Ishii M, Egen JG, Klauschen F, Meier-Schellersheim M, Saeki Y, et al. 2009. Sphingosine-1-phosphate mobilizes osteoclast precursors and regulates bone homeostasis. *Nature* 458: 524-8
46. Johnsson N, Varshavsky A. 1994. Split ubiquitin as a sensor of protein interactions in vivo. *Proc Natl Acad Sci U S A* 91: 10340-4
47. Kaida K, Kusunoki S. Antibodies to gangliosides and ganglioside complexes in Guillain-Barre syndrome and Fisher syndrome: mini-review. *J Neuroimmunol* 223: 5-12
48. Kim RH, Takabe K, Milstien S, Spiegel S. 2009. Export and functions of sphingosine-1-phosphate. *Biochim Biophys Acta* 1791: 692-6
49. Kimberlin AN, Majumder S, Han G, Chen M, Cahoon RE, et al. Arabidopsis 56-Amino Acid Serine Palmitoyltransferase-Interacting Proteins Stimulate Sphingolipid Synthesis, Are Essential, and Affect Mycotoxin Sensitivity. *Plant Cell*
50. Kolzer M, Werth N, Sandhoff K. 2004. Interactions of acid sphingomyelinase and lipid bilayers in the presence of the tricyclic antidepressant desipramine. *FEBS Lett* 559: 96-8
51. Korkotian E, Schwarz A, Pelled D, Schwarzmann G, Segal M, Futerman AH. 1999. Elevation of intracellular glucosylceramide levels results in an increase in endoplasmic reticulum density and in functional calcium stores in cultured neurons. *J Biol Chem* 274: 21673-8
52. Kruer MC, Paisan-Ruiz C, Boddaert N, Yoon MY, Hama H, et al. Defective FA2H leads to a novel form of neurodegeneration with brain iron accumulation (NBIA). *Ann Neurol* 68: 611-8

53. Kumagai K, Kawano M, Shinkai-Ouchi F, Nishijima M, Hanada K. 2007. Interorganelle trafficking of ceramide is regulated by phosphorylation-dependent cooperativity between the PH and START domains of CERT. *J Biol Chem* 282: 17758-66
54. Lahiri S, Futerman AH. 2007. The metabolism and function of sphingolipids and glycosphingolipids. *Cell Mol Life Sci* 64: 2270-84
55. Lester RL, Wells GB, Oxford G, Dickson RC. 1993. Mutant strains of *Saccharomyces cerevisiae* lacking sphingolipids synthesize novel inositol glycerophospholipids that mimic sphingolipid structures. *J Biol Chem* 268: 845-56
56. Lingwood D, Simons K. Lipid rafts as a membrane-organizing principle. *Science* 327: 46-50
57. Mandala SM, Thornton R, Tu Z, Kurtz MB, Nickels J, et al. 1998. Sphingoid base 1-phosphate phosphatase: a key regulator of sphingolipid metabolism and stress response. *Proc Natl Acad Sci U S A* 95: 150-5
58. Martens JA, Wu PY, Winston F. 2005. Regulation of an intergenic transcript controls adjacent gene transcription in *Saccharomyces cerevisiae*. *Genes Dev* 19: 2695-704
59. Merrill AH, Jr., Sullards MC, Allegood JC, Kelly S, Wang E. 2005. Sphingolipidomics: high-throughput, structure-specific, and quantitative analysis of sphingolipids by liquid chromatography tandem mass spectrometry. *Methods* 36: 207-24
60. Monaghan E, Gable K, Dunn T. 2002. Mutations in the Lcb2p subunit of serine palmitoyltransferase eliminate the requirement for the TSC3 gene in *Saccharomyces cerevisiae*. *Yeast* 19: 659-70
61. Montefusco DJ, Newcomb B, Gandy JL, Brice SE, Matmati N, et al. Sphingoid bases and the serine catabolic enzyme CHA1 define a novel feedforward/feedback mechanism in the response to serine availability. *J Biol Chem* 287: 9280-9
62. Nagiec MM, Skrzypek M, Nagiec EE, Lester RL, Dickson RC. 1998. The LCB4 (YOR171c) and LCB5 (YLR260w) genes of *Saccharomyces* encode sphingoid long chain base kinases. *J Biol Chem* 273: 19437-42
63. Nikolova-Karakashian MN, Rozenova KA. Ceramide in stress response. *Adv Exp Med Biol* 688: 86-108
64. Nixon RA, Yang DS, Lee JH. 2008. Neurodegenerative lysosomal disorders: a continuum from development to late age. *Autophagy* 4: 590-9

65. O'Neill SM, Olympia DK, Fox TE, Brown JT, Stover TC, et al. 2008. C(6)-Ceramide-Coated Catheters Promote Re-Endothelialization of Stretch-Injured Arteries. *Vasc Dis Prev* 5: 200-10
66. Park TS, Hu Y, Noh HL, Drosatos K, Okajima K, et al. 2008. Ceramide is a cardiotoxin in lipotoxic cardiomyopathy. *J Lipid Res* 49: 2101-12
67. Paul S, Gable K, Dunn TM. 2007. A six-membrane-spanning topology for yeast and Arabidopsis Tsc13p, the enoyl reductases of the microsomal fatty acid elongating system. *J Biol Chem* 282: 19237-46
68. Pavoine C, Pecker F. 2009. Sphingomyelinases: their regulation and roles in cardiovascular pathophysiology. *Cardiovasc Res* 82: 175-83
69. Penno A, Reilly MM, Houlden H, Laura M, Rentsch K, et al. Hereditary sensory neuropathy type 1 is caused by the accumulation of two neurotoxic sphingolipids. *J Biol Chem* 285: 11178-87
70. Podrez EA. Anti-oxidant properties of high-density lipoprotein and atherosclerosis. *Clin Exp Pharmacol Physiol* 37: 719-25
71. Posse de Chaves E, Sipione S. Sphingolipids and gangliosides of the nervous system in membrane function and dysfunction. *FEBS Lett* 584: 1748-59
72. Qin J, Berdyshev E, Goya J, Natarajan V, Dawson G. Neurons and oligodendrocytes recycle sphingosine 1-phosphate to ceramide: significance for apoptosis and multiple sclerosis. *J Biol Chem* 285: 14134-43
73. Roelants FM, Breslow DK, Muir A, Weissman JS, Thorner J. Protein kinase Ypk1 phosphorylates regulatory proteins Orm1 and Orm2 to control sphingolipid homeostasis in *Saccharomyces cerevisiae*. *Proc Natl Acad Sci U S A* 108: 19222-7
74. Rosen H, Gonzalez-Cabrera PJ, Sanna MG, Brown S. 2009. Sphingosine 1-phosphate receptor signaling. *Annu Rev Biochem* 78: 743-68
75. Saba JD, Nara F, Bielawska A, Garrett S, Hannun YA. 1997. The BST1 gene of *Saccharomyces cerevisiae* is the sphingosine-1-phosphate lyase. *J Biol Chem* 272: 26087-90
76. Schiller J, Zschornig O, Petkovic M, Muller M, Arnhold J, Arnold K. 2001. Lipid analysis of human HDL and LDL by MALDI-TOF mass spectrometry and (31)P-NMR. *J Lipid Res* 42: 1501-8
77. Schnaar RL. Brain gangliosides in axon-myelin stability and axon regeneration. *FEBS Lett* 584: 1741-7

78. Seelan RS, Qian C, Yokomizo A, Bostwick DG, Smith DI, Liu W. 2000. Human acid ceramidase is overexpressed but not mutated in prostate cancer. *Genes Chromosomes Cancer* 29: 137-46
79. Sherman F FGRaHJB. 1986. *Methods in Yeast Genetics*. Cold Spring Harbor, New York: Cold Spring Harbor Laboratory
80. Shimabukuro M, Higa M, Zhou YT, Wang MY, Newgard CB, Unger RH. 1998. Lipoapoptosis in beta-cells of obese prediabetic fa/fa rats. Role of serine palmitoyltransferase overexpression. *J Biol Chem* 273: 32487-90
81. Shimobayashi M, Oppliger W, Moes S, Jenö P, Hall MN. TORC1-regulated protein kinase Npr1 phosphorylates Orm to stimulate complex sphingolipid synthesis. *Mol Biol Cell* 24: 870-81
82. Simpson MA, Cross H, Proukakis C, Priestman DA, Neville DC, et al. 2004. Infantile-onset symptomatic epilepsy syndrome caused by a homozygous loss-of-function mutation of GM3 synthase. *Nat Genet* 36: 1225-9
83. Sophianopoulou V, Dhalluin G. 1995. Amino acid transporters of lower eukaryotes: regulation, structure and topogenesis. *FEMS Microbiol Rev* 16: 53-75
84. Staretz-Chacham O, Lang TC, LaMarca ME, Krasnewich D, Sidransky E. 2009. Lysosomal storage disorders in the newborn. *Pediatrics* 123: 1191-207
85. Tokunaga M, Kawamura A, Kohno K. 1992. Purification and characterization of BiP/Kar2 protein from *Saccharomyces cerevisiae*. *J Biol Chem* 267: 17553-9
86. van Echten G, Sandhoff K. 1989. Modulation of ganglioside biosynthesis in primary cultured neurons. *J Neurochem* 52: 207-14
87. van Meer G, Hoetzl S. Sphingolipid topology and the dynamic organization and function of membrane proteins. *FEBS Lett* 584: 1800-5
88. Varki NM, Varki A. 2007. Diversity in cell surface sialic acid presentations: implications for biology and disease. *Lab Invest* 87: 851-7
89. Venters BJ, Wachi S, Mavrich TN, Andersen BE, Jena P, et al. A comprehensive genomic binding map of gene and chromatin regulatory proteins in *Saccharomyces*. *Mol Cell* 41: 480-92
90. Vieira CR, Muñoz-Olaya JM, Sot J, Jiménez-Baranda S, Izquierdo-Useros N, et al. Dihydrosphingomyelin impairs HIV-1 infection by rigidifying liquid-ordered membrane domains. *Chem Biol* 17: 766-75
91. Vitner EB, Platt FM, Futerman AH. Common and uncommon pathogenic cascades in lysosomal storage diseases. *J Biol Chem* 285: 20423-7

92. Walkley SU, Vanier MT. 2009. Secondary lipid accumulation in lysosomal disease. *Biochim Biophys Acta* 1793: 726-36
93. Walter S, Fassbender K. Sphingolipids in Multiple Sclerosis. *Cell Physiol Biochem* 26: 49-56
94. Yard BA, Carter LG, Johnson KA, Overton IM, Dorward M, et al. 2007. The structure of serine palmitoyltransferase; gateway to sphingolipid biosynthesis. *J Mol Biol* 370: 870-86